

Meeting Environmental Challenges with Remote Sensing Imagery

AGI Environmental Awareness Series

Meeting Environmental Challenges with Remote Sensing Imagery

Rebecca L. Dodge
Russell G. Congalton

American Geosciences Institute

In cooperation with

AmericaView, American Society for Photogrammetry and Remote Sensing (ASPRS) and the U.S. Geological Survey

ISBN: 978-0-922152-94-0

Published in the United States of America. All rights reserved. No part of this work may be reproduced or transmitted in any form or by any means, electronic or mechanical, recording, or any information storage and retrieval system without the expressed written consent of the publisher.

The views and opinions expressed herein are those of the authors and do not necessarily represent the views of the American Geosciences Institute, its member societies or its employees.

Design by Brenna S. Tobler
Illustration by Kathleen Cantner

© 2013 American Geosciences Institute
Printed in the United States of America.

To purchase additional copies of this book, please contact AGI Publications at (703) 379-2480 x 0, at pubs@agiweb.org, or at <http://www.agiweb.org/pubs>.

American Geosciences Institute

4220 King Street, Alexandria, VA 22302, U.S.A.
(703) 379-2480, www.agiweb.org



The American Geosciences Institute is a nonprofit federation of geoscientific and professional associations that represents more than 250,000 geologists, geophysicists, and other earth scientists. Founded in 1948, AGI provides information services to geoscientists, serves as a voice of shared interests in our profession, plays a major role in strengthening geoscience education, and strives to increase public awareness of the vital role the geosciences play in society's use of resources, resilience to natural hazards, and the health of the environment.

AGI Environmental Awareness Series

Groundwater Primer

Sustaining Our Soils and Society

Metal Mining and the Environment

Living with Karst: A Fragile Foundation

Water and the Environment

Petroleum and the Environment

Meeting Challenges with Geologic Maps

Aggregate and the Environment

Soils, Society, and the Environment

Coal and the Environment

Living with Unstable Ground

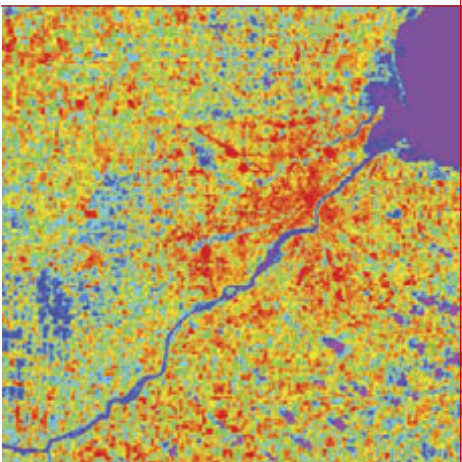
About the Authors

**Rebecca L. Dodge, Ph.D., Associate Professor,
Department of Geosciences, Midwestern State University**

Dr. Dodge graduated from U.T. Arlington with a B.S. in Geology in 1975. She received her Master's and Ph.D. from the Colorado School of Mines; her research concerned the mapping and dating of active faults in northwestern Nevada. Her early professional career continued this focus, and involved airborne and spaceborne photography and imagery. She spent over two decades in the oil exploration business, applying remote sensing technology for both exploration and environmental purposes. Since joining academia 15 years ago she has been researching and teaching the uses of remote sensing from satellite platforms, for resource and environmental management applications. She currently teaches geology and environmental science courses at Midwestern State University. Dr. Dodge is also the Chairman of the Board of AmericaView. In addition, she is deeply committed to training and educating future K-12 science teachers in geosciences, earth system science, and environmental observations techniques, with an emphasis on the integration of field observations and geospatial technology.

**Russell G. Congalton, Ph.D., Professor, Department of
Natural Resources and the Environment, University of
New Hampshire**

Russell G. Congalton is a professor in the Department of Natural Resources and the Environment at the University of New Hampshire and has over 30 years of research and teaching experience in remote sensing, GIS, and other geospatial technologies. His research in spatial data uncertainty, accuracy assessment, and validation of geospatial data is internationally known and recognized. Currently, he serves as Editor-in-Chief of *Photogrammetric Engineering and Remote Sensing*, is the Vice Chair of the Board of Directors for America View, and is a member of the USGS Powell Center Working Group on Global Croplands and Food Security. Dr. Congalton has authored or coauthored more than 150 papers and conference proceedings and another dozen books/book chapters. He received his B.S. in Natural Resource Management from Rutgers University in 1979 and an M.S. (1981) and Ph.D. (1984) in remote sensing and forest biometrics from Virginia Tech.



Publishing Partners

AmericaView

AmericaView (AV) is a nationwide 501(C)(3) non-profit organization that supports the use and application of remote sensing data and related technologies for applied research, K-16 education, workforce development, and geospatial science and technology outreach. AV's networks, facilities, and capabilities are used for sharing and applying remotely sensed data in a wide range of civilian applications ranging from urbanization to natural disaster response to biodiversity conservation. The AmericaView Consortium is funded by a grant from the U.S. Geological Survey (USGS) Land Remote Sensing Program and is currently comprised of 39 university-led, state-based consortia



(called StateViews) working together to maintain and expand a network of state and local remote sensing scientists and specialists. More than 350 universities, non-profits, corporate and governmental entities are members of AmericaView. With expertise in applied remote sensing and geospatial science and technology, our members support the USGS Land Remote Sensing Program through annual projects that involve their partners in the sciences, education and outreach. In 2012, our partners completed over 400 individual projects involving applied remote sensing, education and outreach, and data archiving.

USGS Land Remote Sensing Program

The Nation's economic, environmental, and national security rely on continual observations of the Earth's land surface to understand changes to the landscape at local, regional, national, and global scales. The USGS acquires land-surface data through the placement of sensors onboard satellites, piloted aircraft, and unmanned aerial systems or by obtaining such data from other operators of such systems. The Department of the Interior (DOI), through USGS, provides a comprehensive, permanent, and impartial record of the Earth's surface that is freely available to a wide range of users.



The USGS, on behalf of DOI, shares responsibility for Landsat Program Management with the National Aeronautics and Space Administration (NASA). Under this highly successful partnership, NASA develops and launches Landsat-class satellites while the USGS develops the associated ground systems, operates the satellites, and manages and distributes Landsat imagery. Since 1972, Landsats have provided the only continuous, authoritative record of changes to the Earth's land surfaces at a scale allowing us to differentiate between natural and human-induced change.

American Society for Photogrammetry and Remote Sensing (ASPRS)

Founded in 1934, the American Society for Photogrammetry and Remote Sensing (ASPRS) is a scientific association serving over 7,000 professional members around the world. Our mission is to advance knowledge and improve understanding of mapping



sciences to promote the responsible applications of photogrammetry, remote sensing, geographic information systems (GIS) and supporting technologies.

Contents

- 1 What is Remote Sensing**
Rebecca L. Dodge and Russell G. Congalton
- 30 Remote Sensing Enables Assessing Hurricane Damage**
Rebecca L. Dodge
- 32 Remote Sensing Supports Emergency Management Response to Tornadoes**
Sam Batzli
- 34 Remote Sensing Enables Forest Ice Storm Damage Detection**
Christine E. Emrich and Jeffrey L. Lewis
- 36 Remote Sensing Identifies Hail Damage to Crops**
Cheryl Reese, Mary O'Neill, Pravara Thanapura and Ryan Patterson
- 38 Remote Sensing Identifies Hazards at Anatahan Volcano, Northern Mariana Islands**
Rebecca L. Dodge
- 40 Remote Sensing Enables Lava Flow Hazard Assessment**
Robert Wright
- 42 Remote Sensing Reveals Vertical Coastline Displacements Caused by Earthquakes**
Rebecca L. Dodge
- 44 Remote Sensing Determines Urban Heat Island Effects**
Kevin Czajkowski, Teresa Benko and Timothy Ault
- 46 Remote Sensing is Essential for Suppressing Alaska Wildfires**
Thomas Heinrichs
- 48 Remote Sensing identifies Agricultural Problem Areas**
Cheryl Reese, Sharon Clay, David Clay, and Gregg Carlson
- 50 Remote Sensing Enables Census of Lake Water Quality**
Marvin Bauer and Leif Olmanson
- 54 Remote Sensing Enables Modeling of Groundwater Pollution Risk**
James W. Merchant and Patti R. Dappen
- 58 Remote Sensing Monitors Vegetation Changes Over Time**
Demetrio P. Zourarakis
- 62 Remote Sensing Enables Watershed Analysis For Land Use Assessment And Planning**
Brian D. Lee, Corey L. Wilson and Angela Schörgendorfer
- 66 Remote Sensing Reveals Relationships Among Whitebark Pine, Bark Beetles and Climate Variability**
Rick L. Lawrence and Jeffrey Jewett
- 68 Remote Sensing Identifies Impacts of Climate Variability on Reservoirs**
James W. Merchant and Milda R. Vaitkus
- 70 Remote Sensing Assesses Flooding at Devils Lake, North Dakota**
Bradley C. Rundquist and Paul E. Todhunter
- 72 Remote Sensing Maps Co-Produced Water from Natural Gas Extraction**
Ramesh Sivanpillai and Scott N. Miller
- 74 Remote Sensing Enables Modeling of Soil Loss Susceptibility**
Jackie Reed, John Congleton and Rebecca L. Dodge
- 76 Remote Sensing Enables Mapping of Understory Invasive Plants**
Songlin Fei and Michael Shouse
- 78 Remote Sensing Helps Protect Hemlock in an Invasion Crisis**
Songlin Fei and Ningning Kong
- 80 Remote Sensing Enables Space Shuttle Columbia Recovery**
Paul R. Blackwell
- 82 Image credits**



Preface



Recognizing environmental change and its human and ecological impacts is critical to sustainable continued economic and social development. The identification and tracking of environmental change has become more effective over the last 50 years as increasingly detailed remote sensing imagery has become available. Such imagery, both photographic and digital, has enabled the monitoring, and more importantly, the analysis of natural and human-induced changes to the global environment.

The first airborne remotely-sensed image was acquired barely 150 years ago from a balloon and, less than 50 years later, newspapers across the globe documented the effects of the 1906 San Francisco earthquake with a photograph taken by a camera suspended from a kite. Photographic images of deadly floods in China, taken by Charles Lindbergh during the 1930s, aided natural disaster relief operations. Photographs of Earth's atmosphere, taken during 1940s-era experimental rocket launches, enabled scientists to envision monitoring weather and mapping the entire Earth from satellites.

When the United States finally launched operational civilian satellites in the early 1960s, weather was the focus of the first digital images from orbit. Every manned mission into space dedicated time to photographic observations of Earth. By the mid-1960s the United States began planning the launch of dedicated earth observation satellites to digitally image the Earth's land and ocean surfaces. Today, manned and unmanned satellites from more than ten nations monitor Earth's atmosphere and surface environments across a wide range of the electromagnetic spectrum, producing critical image data used in the monitoring and analysis of environmental change.

While the intensity or pace of some environmental changes are not influenced by humans, those changes which are affected by human activities are increasingly evident. The interactions between natural events and human activities are expanding in scope and frequency as humans expand the "surface area" of human interaction with the natural landscape. Repeated coverage by satellite-imaging systems enables both short-term and long-term environmental

change detection, which is critical for protecting natural and human environments. This book starts with an overview of how remote sensing imagery is enabling scientists, engineers, policymakers, and others to meet the environmental challenges resulting from interactions between environmental change and human activities. Some of those interactions include:

- ◇ Weather hazards
- ◇ Geological hazards
- ◇ Land use/land cover changes
- ◇ Water resource changes
- ◇ Climate variability
- ◇ Resource development
- ◇ Environmental restoration

In particular, the first section examines how satellite images are able to detect features at the Earth's surface (such as plants, rocks, soil, water, fire, ice and snow) and in the Earth's atmosphere (such as clouds, ozone, carbon monoxide, smoke, dust, ash and other particulate matter). Some of these observations can only be made in parts of the electromagnetic spectrum that are not visible to the human eye.

The book concludes with selected applications of satellite imagery on issues that affect the environment and human society. These examples cover the range of environmental challenges listed above and have been provided by applied scientists in diverse disciplines who work for organizations including academic partner universities in the AmericaView Consortium, the U.S. Geological Survey, and the National Aeronautic and Space Administration.



Acknowledgments

The authors gratefully acknowledge

NASA scientists and the NASA Earth Observatory for their efforts to enable educators, the general public, and policy makers to explore the causes and effects of climatic and environmental change through the use of real satellite data. Through the Earth Observatory web site (<http://earthobservatory.nasa.gov>), we are able to see our Earth through the eyes of multiple satellite sensors, and learn with scientists as they analyze imagery, discover change, monitor natural and human activities that influence the environment, and apply the results.



What is Remote Sensing

Every organism remotely senses as it observes its surrounding environment on Planet Earth. We locate ourselves spatially, monitor our surroundings, and observe how our surroundings change. For example, when we see heavy rain we know flooding may follow; we see a fire and we know that structures or vegetation may burn; we see ice accumulated on vegetation and structures and we know that they may break and fall; we feel the ground shake and we know that structures and hillsides may collapse. Remote sensing is learning something about an object without touching it. As human beings, we remotely sense objects with a number of our senses using our eyes, our noses, and our ears.

Fifty Years of Remote Sensing Observations from Space

Observing the Earth from above has provided an advantage for millennia. Climbing the tallest tree or hill to observe surroundings eventually led to observations from towers. The view went higher and higher: from balloons, to kites, to aircraft, and then to rockets. Permanent recording of these observations (using cameras) began barely 150 years ago; remote sensing images from aircraft and space platforms are now commonplace. These images provide the base maps used for our weather reports as well as the maps you download from the Internet to send to friends visiting your home.

Inspired by photographs taken from V-2 rocket test flights in 1946, early space-age scientists quickly recognized that Earth observations from space were a valuable way to map changes in the Earth's environment. Clyde Holliday, the engineer who developed the camera launched on these rockets, wrote in *National Geographic* in 1950 that a V-2 photo (Figure 1) showed for the first time "how our Earth would look to visitors from another planet coming in on a space ship." He said

"Results of these tests now are pointing to a time when cameras may be mounted on guided missiles for ...mapping inaccessible regions of the earth in peacetime, and even photographing cloud formations, storm fronts, and overcast areas over an entire continent in a few hours the entire

land area of the globe might be mapped in this way."

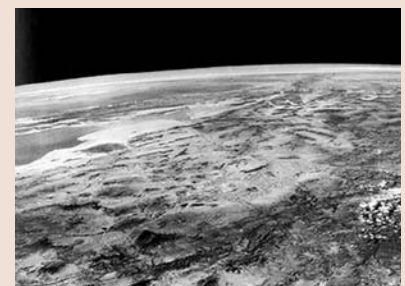


Figure 1. View northwest across northern Mexico toward the Gulf of California; California, Arizona, and New Mexico appear on the right side in this photograph taken from a V-2 rocket fired from White Sands, New Mexico in 1950.

Figure 2a. Photograph taken by John Glenn from Mercury Program flight Friendship 7, 1962.



A little over a decade later, the United States began developing the first satellites designed to observe Earth's weather from orbit. TIROS-1 was launched in 1960. By 1962, when the unmanned TIROS system began continuous observations, the mission confirmed that satellite imagery could help understanding of Earth's changing weather systems. Its success also led to the recognition of the need to observe and map Earth's land and water surfaces, for which photographic missions aboard manned spacecraft began in 1962.

Astronauts began using hand-held cameras to develop an extensive archive of photographs, now numbering over 800,000, with John Glenn's Mercury Program flight on Friendship 7 in 1962. Glenn purchased a 35-millimeter Ansco Autoset camera prior to the flight to include as part of his allowed two pounds of personal effects; one photograph (Figure 2a) revealed the potential of oblique photography for making observations of both clouds and the Earth's atmosphere. A photograph taken by astronauts Frank Borman and James A. Lovell (Figure 2b) during the Gemini 7 mission (1965), looking south from Northern Bolivia across the Andes, provided further evidence of the promise of oblique imagery for atmospheric and meteorological applications.

Gemini astronauts also participated in the Synoptic Terrain Photography and Synoptic Weather Photography experiments,

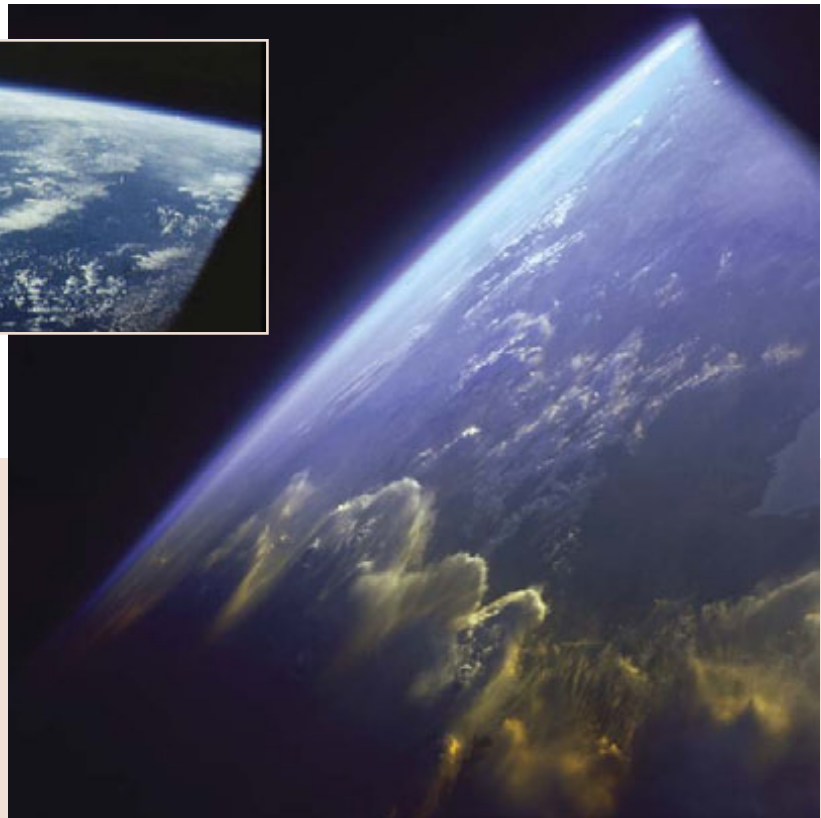


Figure 2b. A storm front formation, Andes Mountains, seen from Gemini 7 on December 5, 1965.

the results of which led to the identification and validation of numerous capabilities for remote sensing imagery. Although the weather photographs were designed to supplement observations from unmanned weather satellites, the Terrain Photography Experiment was designed to obtain new higher-resolution coverage of poorly mapped land areas, and to provide observations to assist geologic investigations of specific areas. For example, Gemini astronauts photographed the Red Sea Rift (Figure 3a) and other tectonic zones (Figure 3b) in support of scientists who were developing the theory of plate tectonics.

In 1966 the United States announced Project EROS — the Earth Resources Observations Satellite — which culminated in

the launch of the Earth Resources Technology Satellite (ERTS, later renamed Landsat) in 1972. At the time of its launch, scientists in diverse disciplines had been using aerial photography for 50 years to inventory and monitor Earth resources and natural hazards, and to monitor environmental changes. These scientists had high expectations concerning the utility of remote sensing imagery taken from satellites. The advantages offered by a continuously orbiting satellite observation platform included repeat coverage on a regular basis. This advantage enables monitoring of seasonal change, of short-term changes such as floodwater advance and retreat, and of long-term changes such as coastline retreat, desert advance, urban sprawl, and land cover change. A second advantage was the broad area



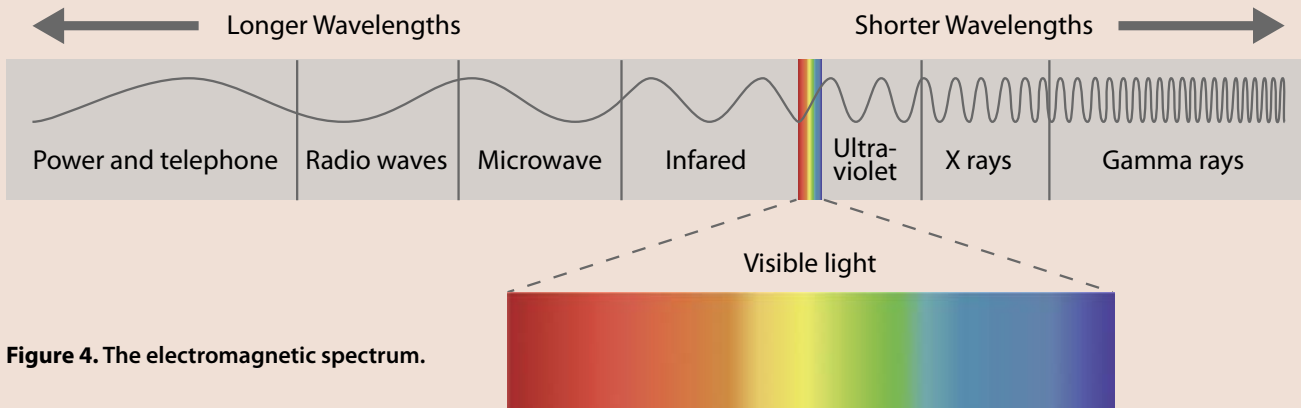
Figure 3a. View looking east across the Nile Delta of Egypt toward the Red Sea oceanic rift zone; the Mediterranean Sea is on the left (June 1965, Gemini 4).

Figure 3b. (below) View looking northeast across the Imperial Valley and Salton Sea of California into the Basin and Range of Nevada (August 1965, Gemini 5).

a single image could cover, facilitating rapid analysis of large areas and recognition of previously unidentified features including earthquake-generating faults, active volcanoes, deteriorating ecosystems, and land conversions related to human development.

Landsat observes the Earth in multiple discrete wavelengths of light, some outside of the visible range, which enables new analyses of surface features not possible with photographic imagery. The early application expectations for Landsat products were rapidly exceeded. Ensuing remote sensing satellites launched by more than a dozen countries over the last 40 years have mapped the entire globe many times over using diverse imaging systems on numerous platforms.





What is “Sensed”

Remote sensing sensors record the interactions of electromagnetic radiation with an object that the energy strikes. To understand how these sensors work a basic understanding of electromagnetic (EM) radiation and the EM spectrum (Figure 4), as well as how EM radiation interacts with Earth’s surface and atmosphere is needed.

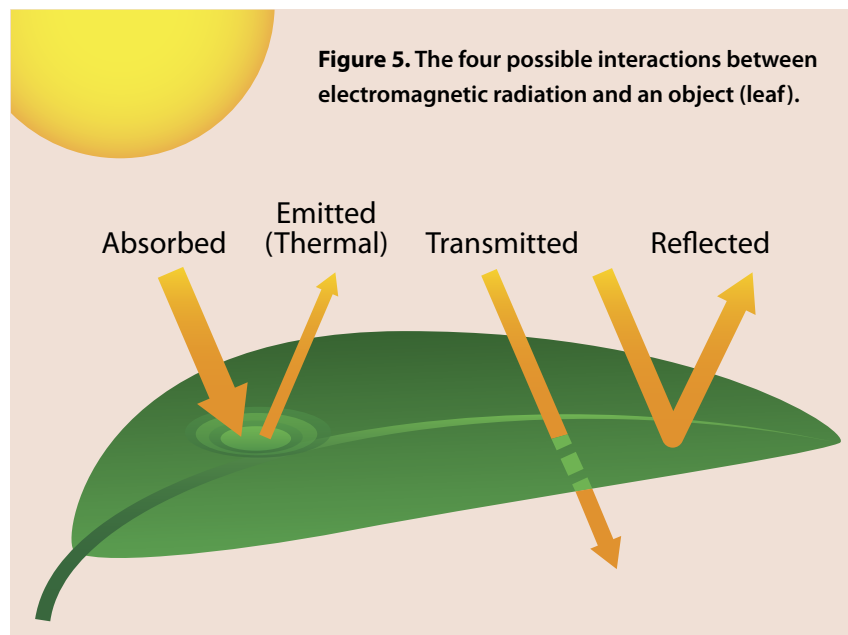
EM radiation forms in numerous ways but the most important to humans are the nuclear reactions within the sun that produce a complete spectrum of EM radiation. The part of the EM spectrum that we experience daily is visible light; however, most of the EM spectrum falls outside the range of the relatively narrow portion that we can see with our eyes.

Many regions of the EM spectrum, including X-rays, radio waves, and microwaves, have specific uses. Some wavelengths of the EM spectrum are absorbed by gases in the atmosphere before reaching Earth’s surface, including gamma rays, X-rays, and most wavelengths of ultraviolet (UV) light. Wavelengths of the EM spectrum that pass through the atmosphere without being absorbed are said to pass through atmospheric windows.

There are four major interactions that can occur when EM radiation strikes an object (Figure 5). These interactions include the radiation being (1) absorbed, (2) converted to thermal (heat) energy then emitted, (3) transmitted through the object, and (4) reflected by the object. Most remote sensing systems record reflected electromagnetic radiation, typically reflected sunlight. Other systems record wavelengths of light emitted by Earth’s surface, typically thermal wavelengths.

How images are acquired

As previously discussed, remote sensing imagery can either be photographic or digital. Photographic, or analog, remote sensing uses film to record reflected electromagnetic (EM) radiation to produce an image of the scene. Images are reproduced as photographic prints or transparencies for interpretation, and subsequent



processing options such as brightness and contrast corrections are somewhat limited. Digital remote sensing instruments record the reflected or emitted EM radiation that impacts the sensor and record the data as numerical values that can then be displayed on a computer monitor as an image. The digital nature of the product allows numerous processing options. Photo-interpretation of analog images involves visual inspection and annotation; interpretation of digital imagery expands on this to include complex computer-based numerical processing as well.

Sensors, either analog or digital, which simply record the reflected or emitted radiation from the environment are termed passive sensors. However, some sensors generate their own EM radiation and measure the reflection of that energy, and are called active sensors. A camera becomes an active sensor when a flash attachment is used; the camera is no longer dependent on sunlight for a source of electromagnetic radiation to illuminate a scene. Other active sensors illuminate target scenes with visible and short-wave (reflected) infrared wavelengths (LIDAR sensors) or with microwave wavelengths (Radar sensors).

Accurate Spatial Location

A remotely sensed image is a type of map, but it contains distortions caused by variations in object height. Such distortions render measured spatial (geographic) distances between objects on the image inaccurate, but they can be removed through various numerical processing steps, thereby making the image an accurate map. Achieving this level of geographic accuracy in “corrected” imagery is critical for repeated observations of environmental change.

Temporal Resolution

Temporal resolution is defined by how frequently a specific area of interest can be imaged. Aircraft borne sensors can acquire imagery of an area as needed for as long as atmospheric conditions allow flight operations and do not obscure the target. Sensors on satellites are in a fixed orbit and can image only a selected area on a set schedule. Landsat satellites operate with vertical-viewing sensors,

recording images that are perpendicular to Earth’s surface relative to the satellite’s orbit. This is why Landsat can sense the same place only every 16 days, when its orbit brings it back over the same geographic area. Other sensors can be actively pointed at targets and can acquire imagery to the side of their orbits. This increases the revisit frequency (temporal resolution) of that sensor. However, the geometric and spectral response complications from oblique imagery require additional processing, and can experience absolute limits past which the data is unusable.

When repeated monitoring of a location is required, the temporal resolution is a major factor in whether a specific system can be used. For example, Landsat cannot be used to daily monitor river flooding in the Midwestern United States as a given location is only imaged every 16 days.

Spatial Resolution

Spatial resolution refers to the size of the smallest objects that can be distinguished in an image. In digital imagery, spatial resolution is limited by the pixel size of the imagery. A pixel is the smallest two-dimensional area sensed by the remote sensing device. In an image with coarse

What Information Images Provide

- ◇ With modern remote sensing systems covering the globe almost continuously, the opportunities to genuinely analyze a specific issue are greatly increased — an image is “a picture worth a thousand words.” Even more importantly, different imaging systems enable scientists to examine areas of interest using different technical constraints that might shed critical information on a problem. In addition to different levels of spatial location accuracy,
- ◇ separate systems offer variable temporal resolution (length of time between repeat coverage of features being monitored)
- ◇ Spatial resolution with respect to size of objects recorded
- ◇ EM spectral resolution (number of separate wavelength bands recorded)
- ◇ Radiometric resolution
- ◇ Extent of geographic coverage

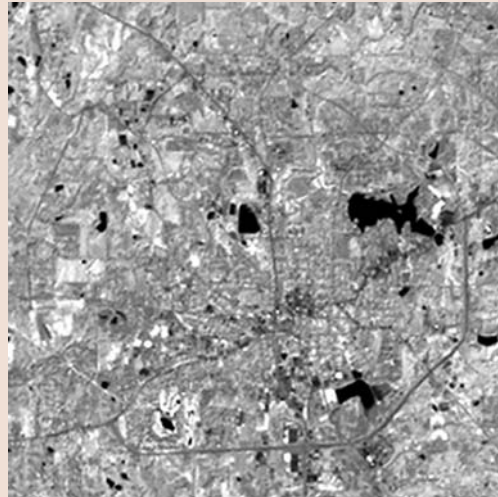


Figure 6. Paris, France. The upper image has 10-m resolution; the lower image has 30-m resolution.

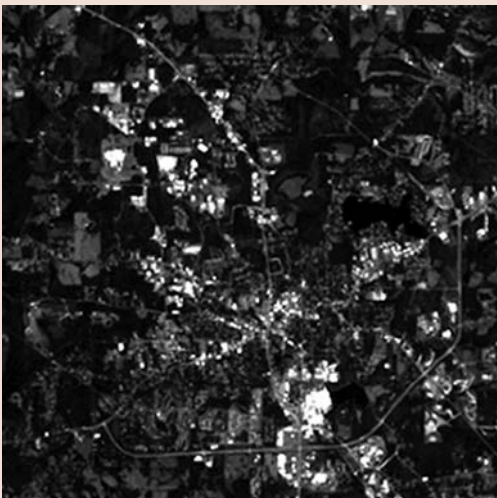
**Band 1
Reflected
Blue**



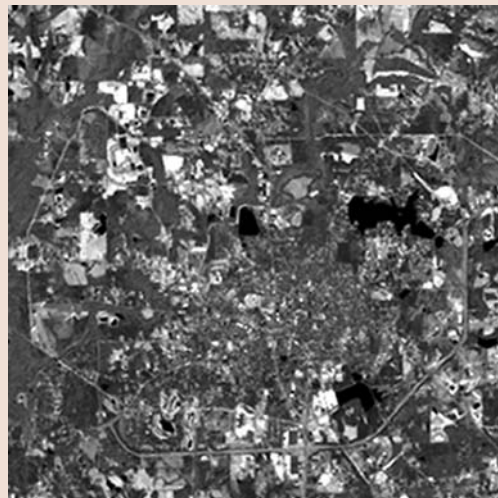
**Band 4
Reflected
Infrared**



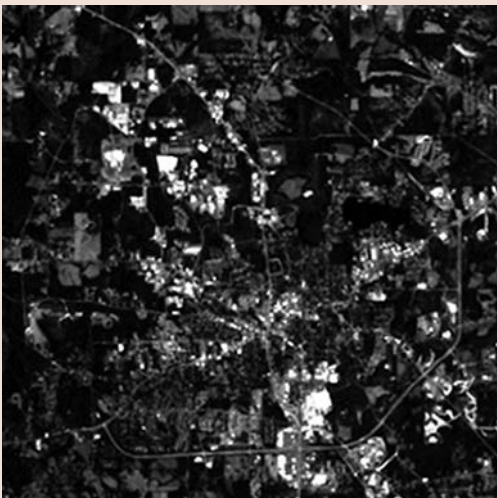
**Band 2
Reflected
Green**



**Band 5
Reflected
Infrared**



**Band 3
Reflected
Red**



**Band 7
Reflected
Infrared**



Figure 7. Six separate wavelength bands of reflected sunlight are recorded by the Landsat 5 satellite, ranging from visible wavelengths into the reflected infrared wavelengths. This 1999 image of the Carroll County area of western Georgia has heavy forest cover. Vegetation absorbs sunlight strongly in the visible wavelengths (bands 1, 2, and 3) and reflects sunlight most strongly in the near infrared (band 4). Absorption by vegetation increases slightly in bands 5 and 7, which record mid-infrared reflected wavelengths.

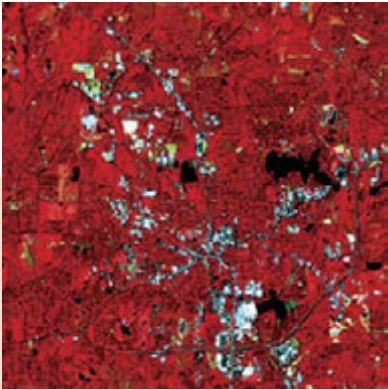


Figure 8. A false-color infrared composite (Landsat bands 2, 3, and 4 in Figure 7) of Carroll County, Georgia, shows the short-wave infrared reflected wavelengths (band 4) in red. Vegetation reflects sunlight very strongly in that wavelength region and appears red in this composite. Developed areas appear bluish grey and water appears black.

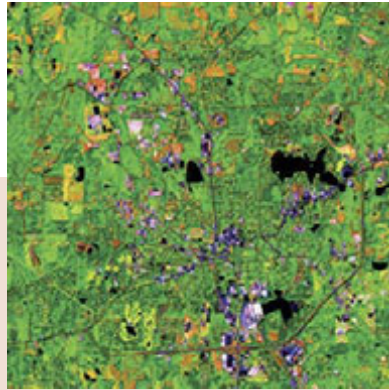


Figure 9. A false natural-color composite (Landsat bands 2, 4, and 5 in Figure 7) of Carroll County, Georgia, shows the short-wave infrared reflected wavelengths (band 4) in green. Vegetation reflects sunlight very strongly in that wavelength region and appears green in this composite. Developed areas appear purplish and water appears black.

spatial resolution, each pixel may be as large as 1 kilometer x 1 kilometer in size. The Landsat Thematic Mapper (TM) imagery has a pixel size of 30 meters x 30 meters (moderate resolution). Figure 6 shows part of the city of Paris in an image with 30-meter pixels, compared to the same area in an image with 10-meter pixels.

Spectral Resolution

Spectral resolution of a remote sensing device is one of the central properties of the platform. Spectral resolution is a measure of the separate portions of the electromagnetic spectrum that are sensed by the remote sensing device. Each portion is called a “band.” A second factor important in spectral resolution is the width of the bands, particularly if the sensor is panchromatic, or captures only one band of imagery. Panchromatic images, whether from a sensor that only images in a single band, or just the data from one band of a multispectral device, are black

and white, regardless of the portion of the spectrum sensed. Many remote sensing platforms utilize sensors that can detect in multiple bands, some of which are quite wide, commonly covering an entire color such as the red or the blue portions of the spectrum. For example, the first Landsat multispectral scanners recorded four separate, relatively wide bands in the green, red, and two shortwave infrared wavelength bands.

Scenes from Landsats 4, 5, and 7 (Landsat 6 was lost at launch) include seven separate but relatively wide bands that comprise a single image, including (Figure 7) the visible bands (1-3), three bands in the reflected infrared region (4, 5, and 7), and one band in the thermal infrared region (6).

Spectral bands of imagery can be rendered as computer images. Computer monitors are constructed to display the three primary colors in visible light (red, green and blue), and thus can display three bands of digital imagery simultaneously.

If panchromatic imagery is displayed, then that single band is displayed through all three components of the computer monitor (red, green, and blue) and the image will appear in shades of gray. However, if a multispectral image is displayed, it is possible to choose which bands to display through the three available color components of the monitor. To display an image similar to a typical photograph (called a natural color composite), each color band is displayed through its corresponding monitor color (for example, the blue band is displayed through the blue component of the monitor). However, many other composite images (called false color composites) can be generated.

For example, one kind of false color composite would display the reflected infrared band 4 through the red component, the red band 3 through the green component, and the green band 2 through the blue component of the monitor. (Figure 8). Figure 9 shows another kind of false color composite that displays the infrared band 5 through the red component, the infrared band 4 through the green component, and the green band (2) through the blue component of the monitor.

Even though only three bands can be displayed simultaneously on a computer monitor, many different composite images are possible. The choice of bands to be placed in each color component produces images that are useful for different applications. By leveraging how specific features reflect in different wavelengths, different band combinations can be used to improve interpretation ability of the image. The examples above illustrate the way interpretation of vegetation is enhanced in images that use the reflected infrared wavelength bands. Water bodies are also enhanced in color

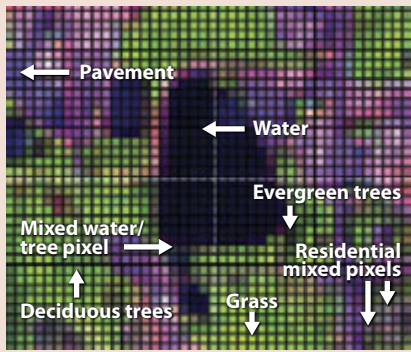


Figure 10. This false color composite has been enlarged to the point where the individual pixels are visible in order to focus more on the spectral detail rather than the spatial detail. Each pixel is a 30m by 30m area.

composites that use the reflected infrared bands because water does not tend to reflect infrared radiation and thus appears black. Whether an interpreter chooses to highlight vegetation in the red band or the green band is a personal choice. Many interpreters prefer the natural color composites for interpretation of human-built infrastructure and bare ground.

A second way to view spectral bands is on a pixel-by-pixel basis, using a graph format. Figure 10 zooms in on the lake in the center of Figures 8 and 9. The color composite shows only three of the six bands from the visible and reflected infrared spectrum. However, the image is made up of a matrix of pixels, with one “layer” for each individual spectral band. The digital remote sensing device records a spectral response — a measure of the intensity of energy sensed — for each pixel in each band. This response is called the brightness value (BV) or the digital number (DN).

Single-band layers for this scene are shown in Figure 7. Note that the lakes (water) are dark in each wavelength band shown in Figure 7. However, vegetation is dark on bands 1–3, brightest in band 4 (shown in green in Figures 9 and 10 composites), and progressively darker in bands 5 and 7. Therefore, a water or vegetation pixel has a distinctive spectral response pattern across wavelength bands related to how well it reflects and absorbs light in different bands. The same is true for many other types of surface cover. When responses are graphed to show digital number (DN)

values in each band, similar cover types show similar spectral response patterns (Figure 11). If a pixel covers an area with a homogeneous type of surface cover, then the spectral response recorded for that pixel will be purely that type. Pixels in the middle of the lake will have similar responses as long as the entire pixel is covering water (Figure 11a). However, if the pixel is recorded for an area that has a mixture of types, then the spectral response will be an average of all the pixel encompasses. For example, pixels on the edge of the lake likely cover both water and land surfaces will distinctly differ from purely open-water pixels. Single pixels over pure stands of evergreen or deciduous trees will have yet another distinctive spectral response patterns (Figure 11b, c). Pixels with a mixture of evergreen and deciduous trees will have an intermediate green color, and pixels that mix trees, paved areas, houses, and grass — like the pixels that cover residential areas in the lower right-hand corner of Figure 10 — appear in other distinctive and variable colors.

Radiometric Resolution

Recall that an image is a matrix of pixels, with one “layer” for each spectral band. The digital remote sensing device records a spectral response for each pixel in each band — its digital number (DN). A pixel with a low DN in a given band would indicate very low EM radiation from the surface covering that pixel. For example, water in the reflected infrared wavelengths

(bands 4 and 5) or the visible wavelengths (bands 1–3) for tree pixels. Yet tree pixels have relatively high values in reflected infrared EM radiation (band 4).

The numeric range of the DN for each pixel is determined by the character of the digital remote sensing device. The sensitivity of the device to the level of EM radiation is called the device’s radiometric resolution. The greater its radiometric resolution, the greater the range of numeric values for spectral response the device can record. The Landsat TM imagery of Carrollton, Georgia, has a DN range from 0 to 255 (or 8 bits). Earlier remote sensing imagery tended to have lower levels of radiometric resolution, while some more recent platforms have even higher radiometric resolution.

Geographic Extent

Extent is the size of the area covered by a single scene and typically, the larger the area a pixel represents on the ground, the larger the extent of the scene. Historically, digital satellite imagery covered large extents and had large- to moderately large-sized pixels. A single Landsat scene covers approximately 32,000 square kilometers of Earth’s surface (185km wide by 172 km along the ground track), with a moderate resolution pixel size of 30 meters. More recent, high spatial resolution digital sensors flown on both satellites and airplanes have much smaller geographic extents.

Figure 11a. Spectral response pattern of a single pure water pixel showing a low DN value (~30) in the visible blue wavelength (TM band 1). DN values decrease continuously at longer wavelengths.

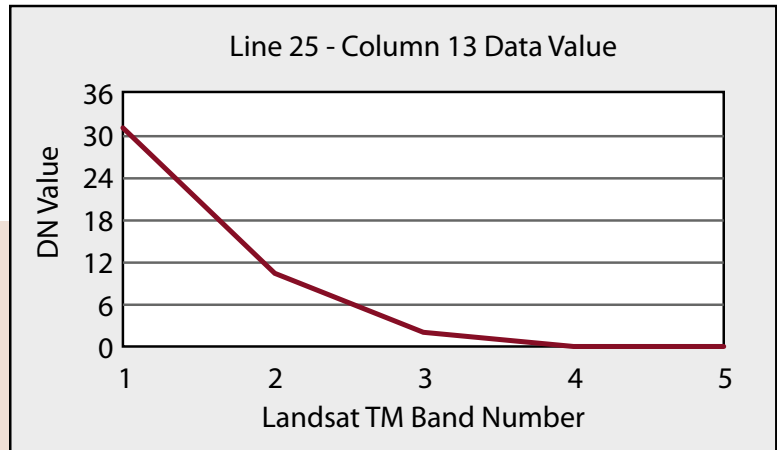


Figure 11b. Spectral response pattern of pure evergreen tree cover; absorption dominates in the visible TM bands 1–3 and the maximum DN value of ~125 occurs in the first reflected infrared TM band (4).

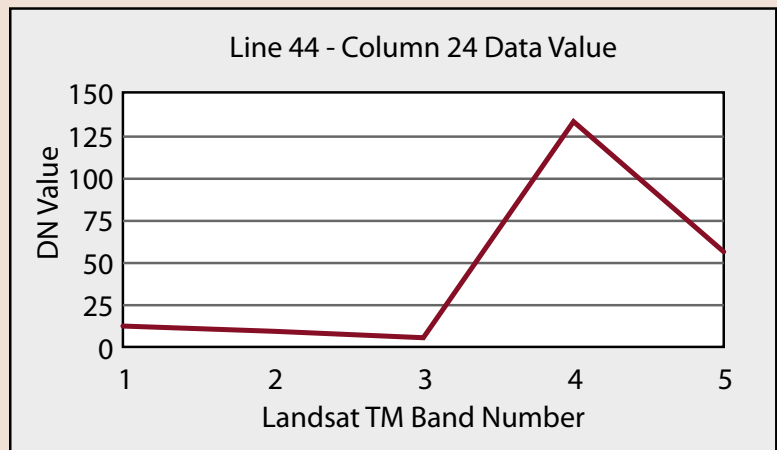
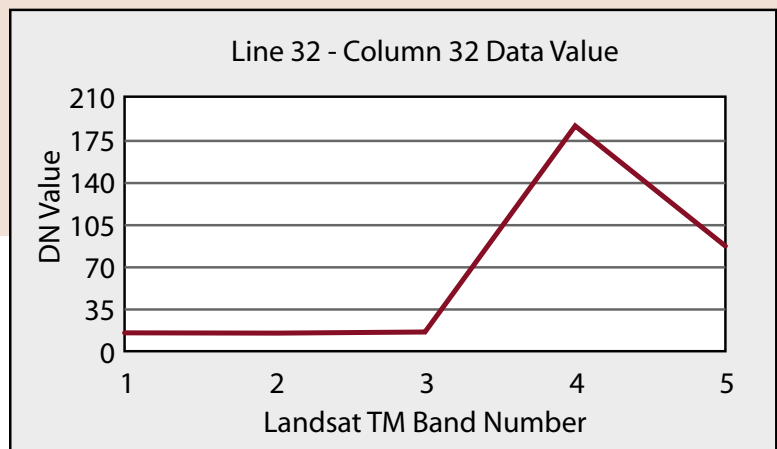


Figure 11c. Spectral response pattern of pure deciduous tree cover; absorption dominates in the visible bands 1–3 and the maximum DN value of ~180 occurs in the first reflected infrared band (4).



Selecting Imagery

A project's objective and budget will determine the selection or acquisition of the appropriate remotely sensed data. Image selection considers each of the choices explained above. For example, when identifying forested areas versus grass-covered areas in a large geographic region, imagery such as Landsat TM imagery, which has moderate spatial resolution and covers a large

area, probably has appropriate extent, as well as appropriate spectral, spatial, radiometric and temporal resolution. Differentiating between, for example, individual deciduous and evergreen trees in a small mixed stand of forest would require higher spatial and spectral resolution. Similarly, differentiating

specific crops in an agricultural setting could require higher resolutions of all kinds, and smaller geographic extent. If monitoring a flood event across a region area were the objective, Landsat's spatial resolution and extent might be adequate, but its typical temporal resolution might not meet the project needs.

How Digital Images are Analyzed

Analysis in digital remote sensing is analogous to photo interpretation. The process takes selected imagery and converts it into more useful information in the form of a map. Digital image analysis is usually a multi-step process: (1) image selection (above), (2) pre-processing including image enhancement, (3) classification, and (4) accuracy assessment. To detect changes in an area, similarly processed images of the same area acquired at different times are required.

Pre-processing

Pre-processing comprises any technique performed on the image prior to classification. There are many possible pre-processing techniques. The three most important techniques include: geometric registration, radiometric and atmospheric correction, and numerous forms of image enhancement.

Geometric registration is typically performed to adjust the imagery to accurately coincide spatially to another image, spatial data layer or to the ground surface. The significant advances in GIS (geographic information systems) have made the use of geometric registration an integral part of digital remote sensing.

Radiometric and atmospheric correction is performed to remove the effects of spectral variations caused by atmospheric conditions. For example, Earth's atmosphere reflects some EM radiation back toward a sensor before that radiation interacts with the ground surface. This effect varies seasonally and with changing weather conditions. This interference needs to be removed so that multiple dates or multiple scenes of imagery can be analyzed together, or so the imagery can be compared with ground data.

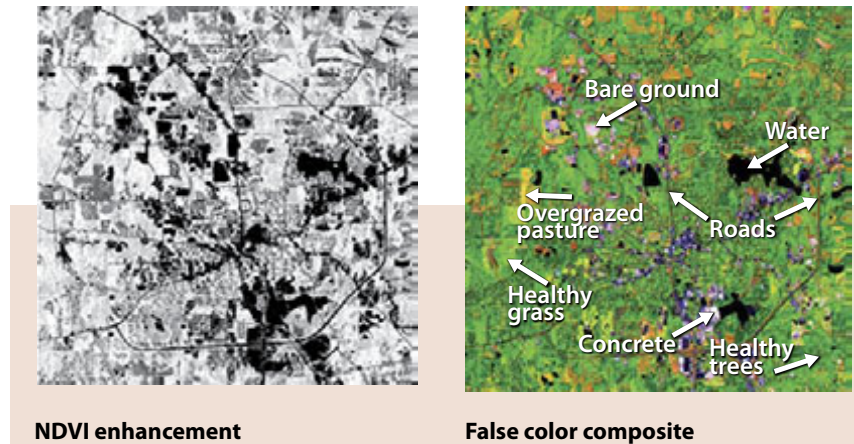


Figure 12. In an NDVI enhancement, vegetation appears relatively bright and non-vegetated areas are very dark. Surface areas with stressed vegetation (overgrazed pasture) appear brownish-green in the image on the right, and are medium to dark gray on the NDVI enhancement. Bare ground, pink in the false color composite, appears very dark in the NDVI image, as do roads and other paved areas.

Historically, computers that made these corrections required the collection of information about the atmospheric conditions at the time of the image acquisition. Obtained from ground-based observations, this information was used to remove the atmospheric effects. More recently, methods have been developed that use information gained directly from the imagery itself to provide the required data to accomplish the atmospheric corrections.

Many types of digital image processing enhancements can be applied to remotely sensed data. Enhancements to digital imagery are mathematical procedures that are applied to the digital numbers (DNs) in the image on a pixel-by-pixel basis. Some of these enhancements, such as Principal Components Analysis (PCA), can be applied to individual bands of imagery or to all pixels in all bands of the imagery. PCA is a sequential mathematical procedure that identifies specific sets of bands in

multi-band imagery that show the greatest spectral differences among surface features; there are multiple PCA images possible for a single image. For example, one PCA of an image over an actively burning fire might emphasize the extent of the smoke from the fire. Another PCA image in the sequence might show the already-burned area, and another might show the actively burning (hottest) area.

Another common mathematical procedure can transform any two bands of image data into numerical ratio indices. An example is the Normalized Difference Vegetation Index or NDVI. Figure 12 is an NDVI image of the Carroll County scene compared with the false color composite from Figure 9. The NDVI ratio image was created by comparing the DN values in the visible red wavelengths (band 3, where vegetation DN values are low) with the DN values in the first reflected infrared wavelength (band 4, where vegetation DN values are highest). This

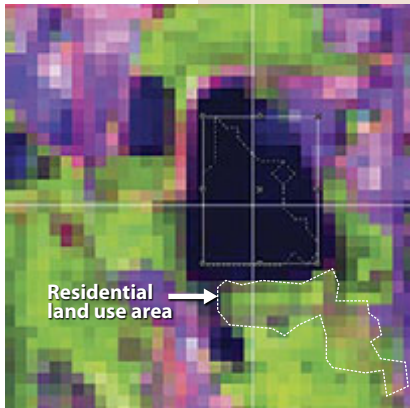


Figure 13. Dashed lines within the white rectangle surround pure “water” pixels identified by an analyst and used to train the image processing software to identify pixels with similar spectral response elsewhere in the image. The software uses this response to compare each pixel in each band of the image in the supervised classification process. A residential area southeast of the lake has a heterogeneous spectral response; it is much harder to define a training area for this type of land use class and many training areas may be required to distinguish important features.

enhancement produces very bright tones for the most vigorous vegetation and dark tones for non-vegetated areas (such as water and roads).

Classification

Image classification groups pixels within an image into categories with similar pixel characteristics, these are called classes or themes. The resulting “thematic map” typically reflects land cover or land use. Classes may be broad, such as vegetation and water, or more specific, such as deciduous trees, pine trees, shallow water, and deep water.

Digital image classification has historically been limited to separating classes based on spectral response differences among different types of land cover or land use. Because digital imagery is a collection of numbers (DNs) that represent the spectral response for each pixel in each wavelength band of EM radiation, computers can process an image pixel-by-pixel in each band to separate and group pixels according to their spectral response patterns.

The earliest digital image processing techniques relied on input from human

interpreters, who would provide general guidance based on analog image interpretation before the digital process began. This method is called supervised classification. Later methods involved statistical clustering routines that are called unsupervised classification techniques.

Supervised vs. Unsupervised Classification

To begin a supervised classification, the analyst must identify areas of the image with a known surface cover type and create a training area (grouping of pixels) from which the computer generates a statistics file. Informational types that are homogeneous and distinct (e.g., water or sand) require only a few training areas. Figure 13 shows “water” pixels from the Carroll County Landsat scene selected to train the image processing software to recognize pixels that have the spectral response of water (Figure 11a). Complex, heterogeneous informational types (e.g., mixed forests, residential areas) require more training areas to “train” the computer to identify these cover types.

In an unsupervised classification, the analyst begins by selecting the number

of unique, separate classes that will be derived from the spectral response data contained in the image. The computer process applies a statistical clustering algorithm to group the pixels in the image into spectral classes. These classes are spectrally unique, but a single cluster may be a combination of a number of land cover or land use types.

Figure 14 shows a second Landsat image of Carroll County taken in 1989 on the left, covering the southeast portion of the Carrollton area shown in Figure 9b. On the right, an unsupervised classification is shown in which the analyst has set at 20 the number of classes for the clustering algorithm to identify. In the unclassified image, the water in a lake in the lower right quadrant shows two shades of blue, indicating different water depths, but the classification algorithm placed all of the pixels in the lake into the same class. Paved areas and bare ground appear in several shades of purple and pink in both images, and the analyst must decide how to combine different spectral classes to create a usable thematic map. For example, the analyst could choose to combine all classes that represent roads into a single “transportation” class, and all classes that contain houses into a single “residential” class. Using the unsupervised approach, the analyst typically defines a

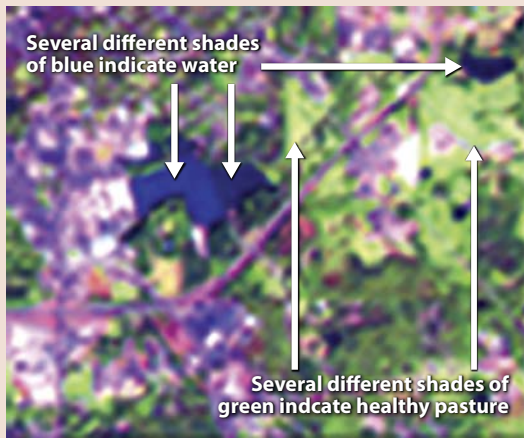
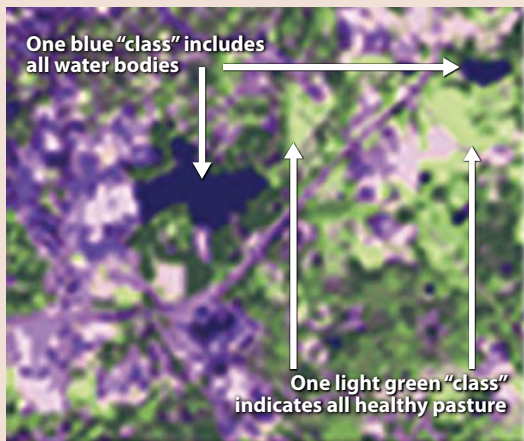


Figure 14. 1989 Landsat image of Carroll County showing the unclassified image at the top and the 20-cluster unsupervised classification at the bottom. The images have been zoomed in sufficiently to focus on the spectral detail necessary for effective classification.



larger number of classes at the beginning with the knowledge that classes will be combined at the end of the process.

Both supervised and unsupervised classification techniques are useful for producing maps, and both require input from trained image analysts. The techniques are commonly used in sequence: An unsupervised classification highlights spectrally separate classes within the image coverage area, then the analyst selects

training areas for use in a supervised classification. This enables the analyst to apply local knowledge and input information beyond the spectral data derived from pixels. Such information may include textural qualities specific to certain land cover types as well as associations among land cover types, such as those between wetlands near water bodies. Emerging image processing techniques are enabling digital processing to use such non-spectral image characteristics.

Accuracy Assessment

Once a thematic map has been created from the remotely sensed imagery, it is important to know how accurate the map is. There are two components to map accuracy: positional accuracy and thematic accuracy. Positional accuracy is a measure of the distances between points on a map compared with the distances between the same on the ground. Thematic accuracy is a measure of whether the classes shown on the thematic map produced from the imagery are accurately identified. Positional accuracy is measured in distances while thematic accuracy uses a table called an error matrix to show errors in labeling. Usually, field observations are used for assessing the accuracy of a thematic map.

Figure 15 shows the effect of an accuracy assessment performed on a supervised classification of the 1999 Carroll County Landsat image. The original thematic map of land cover on the left shows specific inaccuracies in separating pavement (red, 67% accurate), residential areas (pink, 56% accurate) and commercial development (yellow, 63% accurate). Following field inspection of areas with known ground cover types, new training areas were submitted to the supervised classification algorithm and the classification was run again, with significantly higher accuracy achieved in the thematic map shown on the right. Accuracy levels for roads, development, and residential land cover types improved to over 90%.

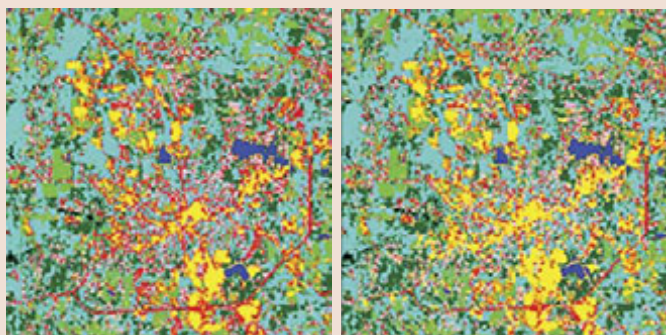


Figure 15. An initial supervised classification thematic map of 1999 land cover in Carroll County indicated confusion among land cover types. An accuracy assessment shows particular problems in distinguishing among developed land cover types. Retraining following field observations in confused areas improved the accuracy of the thematic map.

Detecting Change to Solve Problems

One of the most important and common uses of remotely sensed data is to identify changes in an area through time. Images can be used to simply identify “change versus no-change” or “from-to change” where the change from one land cover category to another is carefully recorded and mapped.

Figure 16 shows both the 1989 and 1999 Landsat images of Carroll County, as well as a change detection overlay highlighting areas with significant decrease in reflectance (red) and significant increases in reflectance (green). There are a significant number of methods for detecting changes. However, no matter which method is selected, the goal is the same: to show how land cover or vegetation or some other attribute has changed over time.

It is difficult to imagine humans carrying out any kind of development activity — settling on an island, building a city, planting a field, establishing a port, or harvesting any type of resource — in a location entirely free of the potential for natural environmental change. It is also difficult to imagine human development

activities such as these occurring without changing those natural environments. Human populations will continue to grow, requiring more development and more resources and quite literally interacting with more of Earth’s ecosystems.

Although environmental change can’t be avoided, we can use observations from remotely sensed imagery to sustainably manage human development.

About Environmental Change

Monitoring changes resulting from interactions between the environment and human activities relies on a growing record of satellite remote sensing observations that now spans over 50 years. Environmental scientists in multiple disciplines ranging from geology, oceanography, and meteorology to ecology, agriculture, forestry and epidemiology are using remotely sensed imagery to balance — and manage — the interactions

between the environment and human development. Advances in remotely sensed imagery, including acquisition, processing, and analysis, continue to advance our understanding and ability to meet the challenges associated with environmental change.

Imagery today not only provides early warning for meteorological hazards globally, but also supports real-time monitoring, rescue, response, and reconstruction. Remotely sensed imagery also supports such efforts for monitoring geologic change including volcanic eruptions, earthquakes, and tsunamis. Any changes to the natural or human-built landscape leave a signature that can be observed from orbit across a range of electromagnetic wavelengths, in support of real-time response and disaster relief.

Remote sensing imagery is also widely used to monitor land use and land cover change, both human-induced and natural. Because human-induced land use and land cover changes profoundly affect water resources, negative water resource impacts are often the first changes that

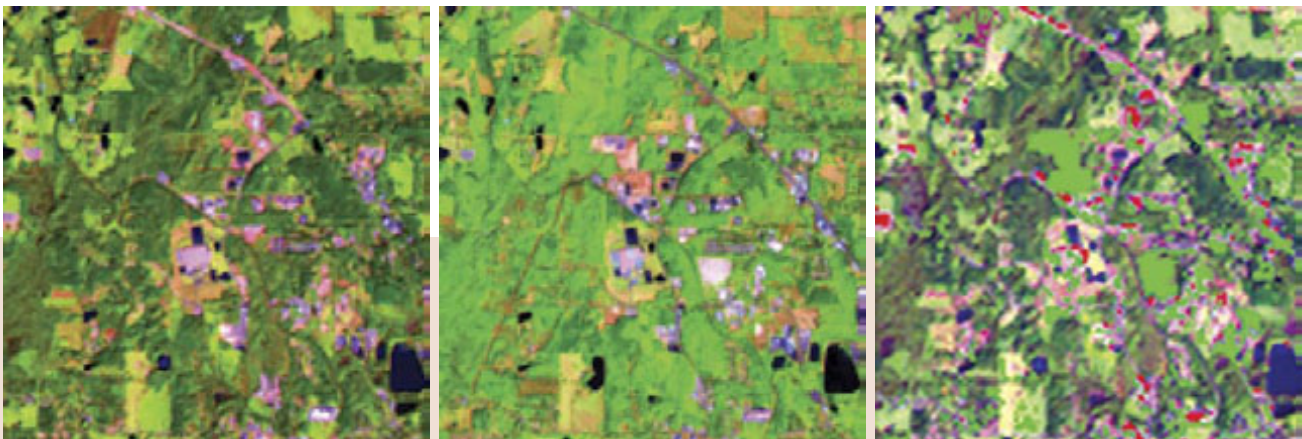


Figure 16. Carroll County, as shown in the 1989 image on the left above, had undergone significant land cover change by 1999, as shown in the image in the center. On the right, a change detection algorithm highlights in green areas where forest cover had been removed by 1999, leaving bare ground that has much higher reflectance. Areas that were bare ground in 1989 and had regrown vegetation by 1999 have much lower reflectance and are highlighted in red on the right.

Figure 17a. Almost surrounded by mountains, the level land at Gila Bend, Arizona makes an excellent catch basin for excess rainfall.



Figure 17b. In flood stage, Utah's Sevier River reclaims part of its floodplain.

result from expanding human development. Climate variability impacts are also increasing, with negative impacts not only on water resource availability, but also on natural ecosystems. Resource development also contributes to many types of measurable changes to the land surface and the ecologic and hydrologic systems. Finally, remote-sensing imagery taken in the wake of environmental changes enables scientists to develop predictive models to better plan for the future and to monitor environmental restoration efforts.

human infrastructure in the United States. A prime example of the confluence of natural hazards and human development

is the expansion of development onto floodplains. Floodplains exist naturally to accommodate runoff that exceeds the

Meteorological Hazards

Meteorological hazards cause some of the most devastating impacts on natural ecosystems and human settlements. Intense rainfall events that lead to flooding are the most costly natural disasters affecting

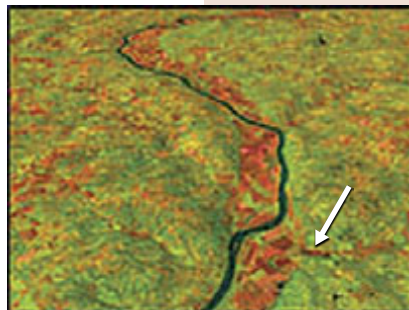


Figure 18a. Agricultural fields in the floodplain of the Missouri River are brown and pink on Landsat imagery from September of 1992.



Figure 18b. The floodplains of the Missouri River and several tributaries are inundated in this Landsat image, taken in September of 1993. Arrows mark matching features.

Assessing damage from meteorological hazards uses remotely sensed images in many other ways.

◇ Satellite imagery can detect and map the extent of inundation and consequent damage to ecosystems and human infrastructure following hurricanes. Take, for example, Hurricane Ike's landfall in Texas in 2008. Remediation efforts, including coastal restoration and vegetation replanting, were monitored with imagery.

◇ Emergency managers relied on maps generated from remotely sensed imagery for near-real-time response to tornado events in Wisconsin in 2001 and 2005.

◇ Following damage to forests during the 2003 ice storms in Kentucky, resource managers used satellite imagery to detect and map damage and to plan remediation efforts.

◇ Both farmers and crop insurance investigators rely on satellite imagery to map the extent and impact of hail storms on crops.

capacity of stream channels, but floodplains are often extensively developed for agriculture, housing, and industry because of their level surfaces and often fertile soils. Between June and September of 1993 a major flood affected most of the Mississippi River and its tributaries. Record rainfall events in several states flooded 150 major rivers and tributaries including the Missouri River; 75 towns were submerged and over 10,000 homes were destroyed. When levees were breached or overtopped, flooded areas frequently remained submerged for months (Figure 17).

As floodwaters worked their way downstream over several weeks, emergency workers needed accurate maps of flooding extent. Imagery accurately revealed the extent of flooding (Figure 18). This information was used to develop more accurate floodplain maps for developing recovery plans and better models for predicting the extent of future floods.

Geological Change

Although geological change may be a slow process often associated with erosion and deposition over long periods of time, when it occurs in human time scales it represents a clear hazard. Landslides can be one of the most dramatic and dangerous examples of geologic change. Earthquakes are a significant geological trigger for landslides as seen by the magnitude-7.6 earthquake that jolted a remote area of Kashmir in early October of 2005, killing nearly 75,000 inhabitants and destroying over 3 million homes. Landslides triggered by the earthquake's shaking killed tens of thousands of people. Mapping the earthquake damage for remote, relatively inaccessible areas is a challenge that can be met by using satellite imagery. Landslides affect not only buildings but also transportation infrastructure which needs to be rapidly mapped to aid rescue and recovery

Figure 19a. November 2000 ASTER image of Muzaffarabad, Kashmir and the Neelum River prior to the earthquake and landslides.

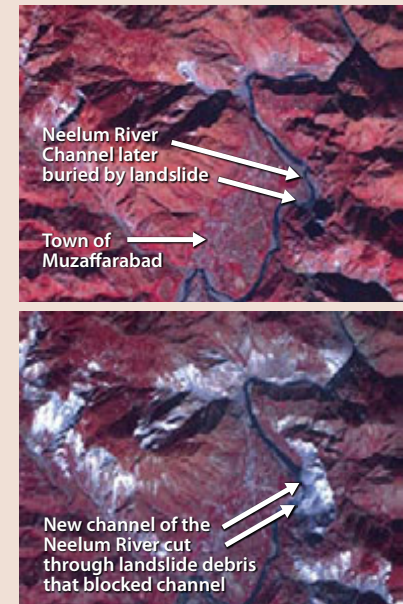


Figure 19b. By October 27, 2005 the Neelum River has cut through landslide debris and re-established flow.

efforts. Before-and-after images of one of the hardest-hit towns, Muzaffarabad, show how landslides blocked the Neelum River and forced it to cut a new channel through the landslide debris (Figure 19).

Heavily vegetated hillsides across the surrounding region are red in the “before” picture from November 2000 (Figure 19a). Hillsides where landslides have occurred are deforested and appear in light gray in the “after” image (Figure 19b).

Geologic hazards associated with earthquakes can also change the environment over very large areas, especially when an earthquake generates a tsunami. Tsunamis spread out in all directions from the epicenter of an offshore earthquake, and can travel for thousands of kilometers. One of the most deadly tsunamis in recent history took place on December 26, 2004. The damage zone encompassed the rim of the entire Indian Ocean basin;



Figure 20a. (left) ASTER imagery from November of 2002 showing beachfront development along the coast of Phang-Nga province, Thailand prior to the tsunami. Vegetation is red in this image.

Figure 20b. (right) ASTER imagery from December 2004 shows de-vegetated (gray) areas extending 1.5 km inland following the tsunami.

satellite imagery provided the most accurate appraisal of damage, enabling fast and focused response, providing needs assessments, and guiding recovery and remediation planning.

Both human settlements and natural ecosystems were profoundly altered by the tsunami. Tourist-centered waterfront development on the western coast of Thailand was particularly devastated. Figure 20 shows the coastline in Phang-Nga province, where development had extended right up to the beachfront and wave heights had exceeded four meters.

The impact of earthquakes on coastal regions can go far beyond tsunami effects. Vertical ground motion can cause ground

elevations to either raise up the sea floor, destroying coral reefs, or to submerge the land, drowning ecosystems critical

to shoreline protection. Remotely sensed imagery enables rapid and accurate mapping of such effects over broad areas.

Other applications:

- ◇ Volcanic activity can be monitored by satellite for ash clouds that might impact aircraft or people, as well as lava flows that might impact human infrastructure.
- ◇ The vertical ground motion resulting from an earthquake

can devastate coastal ecosystems and increase the vulnerability of coastal communities can be accurately mapped by satellite quickly in the aftermath of a major earthquake and assist rescue personnel and restoration efforts.



Figure 21a.
August 1984
Landsat TM
imagery of the
Plano, Texas area.

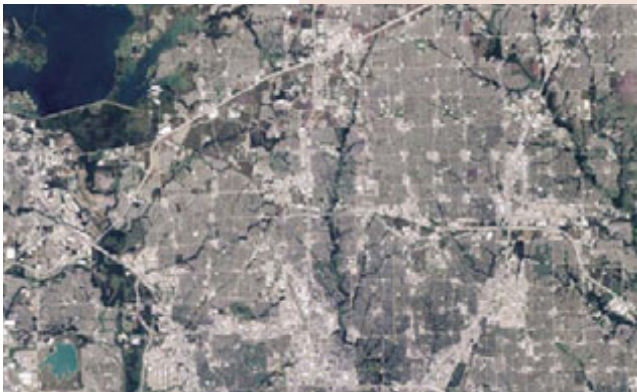


Figure 21b.
August 2009
Landsat TM
imagery of the
Plano, Texas area

Changes in land use and land cover

Although meteorological and geologic hazards can transform landscapes, human development is now the main driving force behind changes in land use and land cover. Land use and cover include natural vegetation, other surface features such as water bodies, and human-controlled cover such as pavement and crops. Changes in land use and cover occur as a result of both natural and human-induced processes and can impact soil and water resources negatively. Soil and hydrological systems sustain vegetative land cover, which in turn protects soil from erosion. Vegetation cover plays an important role in the water cycle by returning soil moisture to the atmosphere, where it can form clouds and precipitation. Whether land use and cover change is natural or human induced, monitoring change with imagery from space is an increasingly

effective method for assessing and managing impacts.

More than 40 years of Landsat space-based imagery is available to study land use and cover change globally. Landsat, first launched in 1972, has a specific focus on Earth observations. During this time period the human population of the Earth nearly doubled, from approximately 3.7 billion to over 7 billion. Land use and cover change mapping is now a basic element in planning for, and monitoring, development, as humans seek to balance their growth needs with the requirements for sustainable ecosystems. The impacts of development-induced change, particularly urbanization, can be observed from the perspective of their impacts on hydrological systems (including precipitation) and on soils and vegetation adjacent to cities.

Development around growing urban areas often extends significant distances

from urban centers. Housing for city workers may be tens of miles from urban centers, covering productive soil needed for crops to feed growing populations. In fact, most existing U.S. cities and towns are on, or expanding onto, the most productive farmland in the country. The booming suburbs peripheral to Dallas, Texas, clearly demonstrate the impact of “sprawl” on agriculture and water resources. Figure 21 shows the suburbs of Carrollton and Plano expanding toward the north and west during the 25 years between 1984 and 2009. Cultivated land has been covered by housing and related development as the population in these suburbs has more than tripled. Even more profoundly, the development has surrounded numerous streams that carry runoff into Lake Lewisville, which is one of the main sources of drinking water for Plano, Carrollton, and Dallas to the south. Underlying groundwater zones were depleted decades earlier by urban water demands within the Dallas area, and surface water serves as the only source for these cities for residential and industrial uses. Suburban runoff places a heavy contaminant load from streets, parking lots, and stormwater both on the lake and on streams that feed into the lake. As clearing for development encroached on the lake, soil became a common component of runoff; soil transmitted into drinking water reservoirs such as Lake Lewisville shortens the useful lifespan of the reservoir by displacing water-storage capacity with sediment fill.

As urbanization advances and covers farmland, agriculture is pushed outward and further displaces natural land cover. Urban growth that covers farmland often pushes agriculture development toward forested areas. Deforestation is one of the most significant land cover events occurring globally. The Amazonian rainforest is regularly mapped using data from multiple satellites to monitor loss of forest cover.



Figure 22a. MODIS imagery of the Rio Jaciparana area of Brazil, 2000. More than one-half of the area shown is still covered with uninterrupted tropical rainforest, shown in green. Brown rectilinear patterns indicate areas cleared for agriculture.



Figure 22b. MODIS imagery of the Rio Jaciparana area, Brazil, 2010. Less than one-third of the rainforest remains, replaced by agricultural clearings.

Brazil, where over 60% of the Earth's remaining rainforest is found, is committed to reducing deforestation and uses imagery to monitor land clearing related to both forestry and agricultural development.

In the state of Rondonia, over one-third of the original forest cover has been removed in the past three decades. Most

was originally removed by small landowners, who clear new areas every few years as the soil quickly loses its fertility due to heavy rainfall and soil erosion. In recent years large landowners have taken over the depleted agricultural lands for livestock pasture. Industrial-scale agriculture has also moved in to use cleared land for large-scale agriculture projects including food crops, grazing

and biofuels. Figure 22 shows the extent of deforestation around Rio Jaciparana in 2000 (22a) and in 2010 (22b).

Not all deforestation is caused by humans. Drought can create conditions that promote growth of invasive species or widespread forest fires. Gypsy moths and other pest species are also deforestation factors. During their larval stage, gypsy moths defoliate trees. While trees may re-grow leaves following such outbreaks, successive defoliation can kill trees. Landsat and MODIS satellite imagery are both applied to map defoliation and guide control efforts (Figure 23).

Trees are not the only targets of defoliation, though. Mapping the effects of plant and animal pests on agriculture was one of the earliest applications for aerial imagery. Figure 24 shows agricultural management at the level of individual fields.

Applications of remotely sensed imagery for land use and cover mapping are diverse. As the human footprint expands, changes in use and cover are increasingly the focus. Detecting these changes involves classification of remotely sensed imagery, which subdivides the landscape into different uses and cover types at a given point in time.

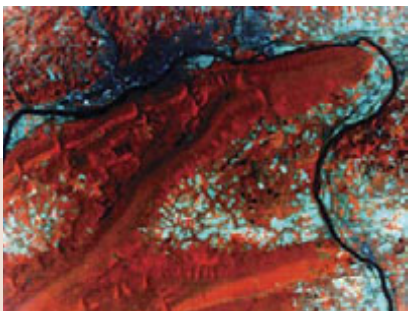


Figure 23a. Forested slopes in Pennsylvania's Appalachian Mountains are red in this Landsat MSS image from May of 1977. Unvegetated areas are blue.

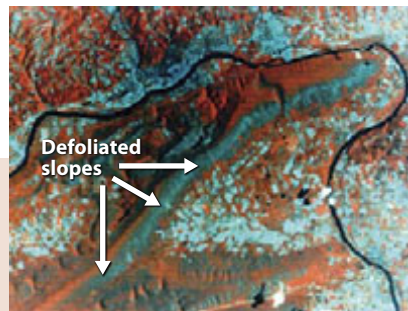


Figure 23b. Defoliated slopes appear blue in July of 1977, following the hatch of gypsy moth larvae.



Figure 23c. Gypsy moth (*Lymantria dispar*) caterpillars hatch and feed on leaves of many tree species, damaging and sometimes killing the host trees.

Other Applications:

- ◇ Comparative analyses can then be done between images captured on different dates.
- ◇ Changes in land use and land cover surrounding urban areas affect soil and water resources and even local temperature patterns.
- ◇ State and national firefighters use remotely sensed imagery at varying scales to fight fires and preserve forest ecosystems.
- ◇ Remotely sensed imagery is also applied to mapping agricultural land cover impacted by plant and animal pests.



Figure 24a. Airborne imagery from NASA's ADAR 5500 sensor uses green, red, and near-infrared light to show vegetation vigor; healthiest vegetation has the brightest red color in this false-color image. In California grape vineyards shown on the left, stressed vines appear blue in a diagonal strip through the lower field.

Figure 24b. An image derived by comparing just red and infrared light highlights the stressed vines and enables effective crop management.

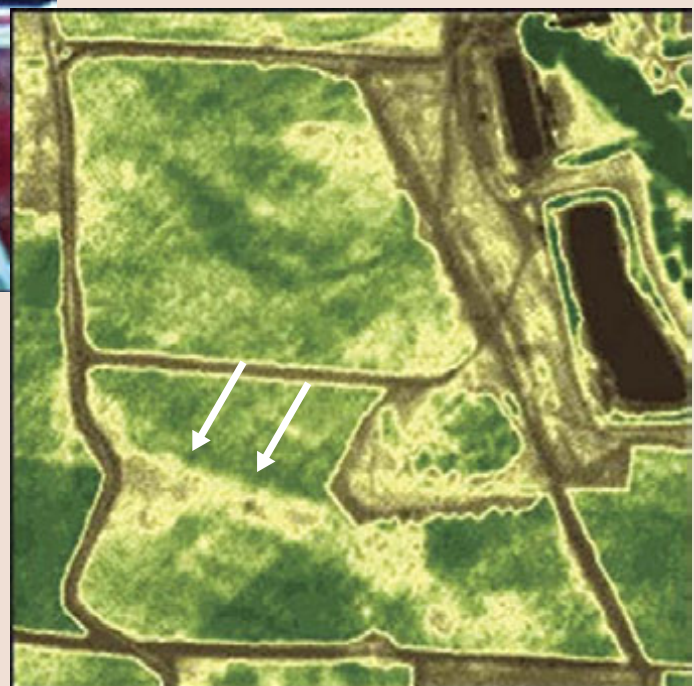




Figure 25a. May 2008 MODIS image delineates snow pack in the San Juan Mountains of Colorado. Such images guide snow melt and runoff predictions.

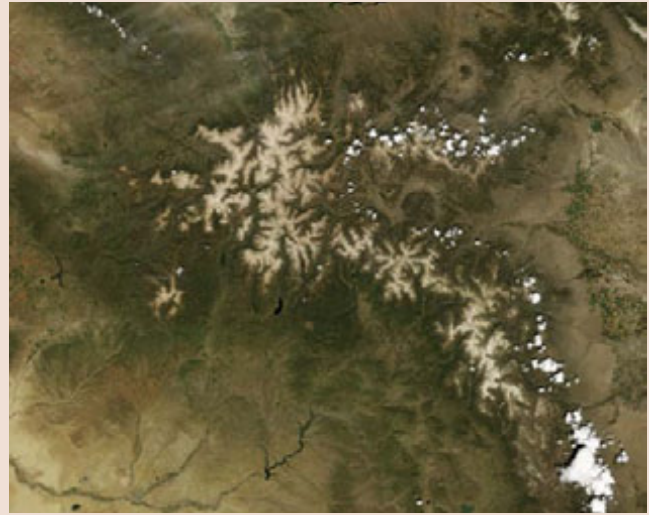


Figure 25b. May 2009 MODIS image indicates lesser extent of snow pack with consequences for spring runoff and water availability.

Water Resources

When external factors impact water resources, changes in water quality and water availability are often observed. Water must be available not only for human needs, such as agriculture, but also for ecosystem needs, such as base-flow for aquatic life or sufficient soil moisture to support complex ecosystems. Where snow melt is a critical water source, satellite imagery enables regional-scale snow pack monitoring. Tracking changes in snow cover without imagery uses, at best, selected field measurements; satellite imagery improves coverage and increases the accuracy of predictions about water availability (Figure 25). This capability improves ecosystem management, fire risk prediction, and irrigation management.

Irrigation is a major stress on water availability for ecosystems. In Kazakhstan in the 1960's, surface waters from the Amu Darya and Syr Darya rivers, which sustain the Aral Sea, were diverted

for irrigation for cotton and other agriculture. Once the fourth largest body of fresh water in the world, the Aral Sea has decreased in size by over 85% as now almost no fresh water enters the lake (Figure 26a and b). The result is that a once thriving freshwater ecosystem has been destroyed. As the lake dried, its salinity increased and salts accumulated in the lake-bottom sediments along with agricultural chemicals. Sediments now exposed on the dried lake bottom are easily mobilized by winds that spread toxic dust into surrounding areas, damaging both natural and agricultural vegetation (Figure 26c).

Water quality observations include water clarity measurements, which can be made from remotely sensed images based on how well sunlight penetrates water. Sunlight penetrates clear, clean water well, while more light is reflected from waters polluted by sediment or algal growth. Field measurements indicate clarity at individual observation points; satellite imagery measures the same parameter

over large areas quickly, and with accuracies similar to field measurements.

There is a direct correlation between water quality and changes in land cover and land use. Agricultural runoff containing fertilizers and soil supplies nutrients to the lakes, which can promote eutrophication. Eutrophication occurs when excess nutrients wash into water bodies and promote the growth of algae that can choke drinking water reservoirs with slimy, often toxic algal blooms. These blooms deplete oxygen, killing fish and making the water hazardous to humans and other animals. Lakes fed by urban and industrial runoff in areas without wastewater treatment can be contaminated by sewage as well; this contamination is another strong promoter of eutrophication (Figure 27).

Monitoring water quality goes beyond ecological and agricultural applications to include recreational and drinking water quality assessments; land use and cover is often a major factor in water quality.



Figure 26a. (left) 1989 Landsat TM mosaic showing the northern and southern Aral Sea. White areas are sea bottom exposed by a steady decrease in water levels that began in the 1960s.



Figure 26b. (right) 2003 MODIS image showing continued drop in water levels and exposure of sea bottom.

Figure 26c. 2008 MODIS image showing massive dust plumes rising from the desiccated floor of the Aral Sea. Further retreat of the water levels is also evident. The remaining lake is restricted to small northern and western parts of the original lake (Figure 26a).

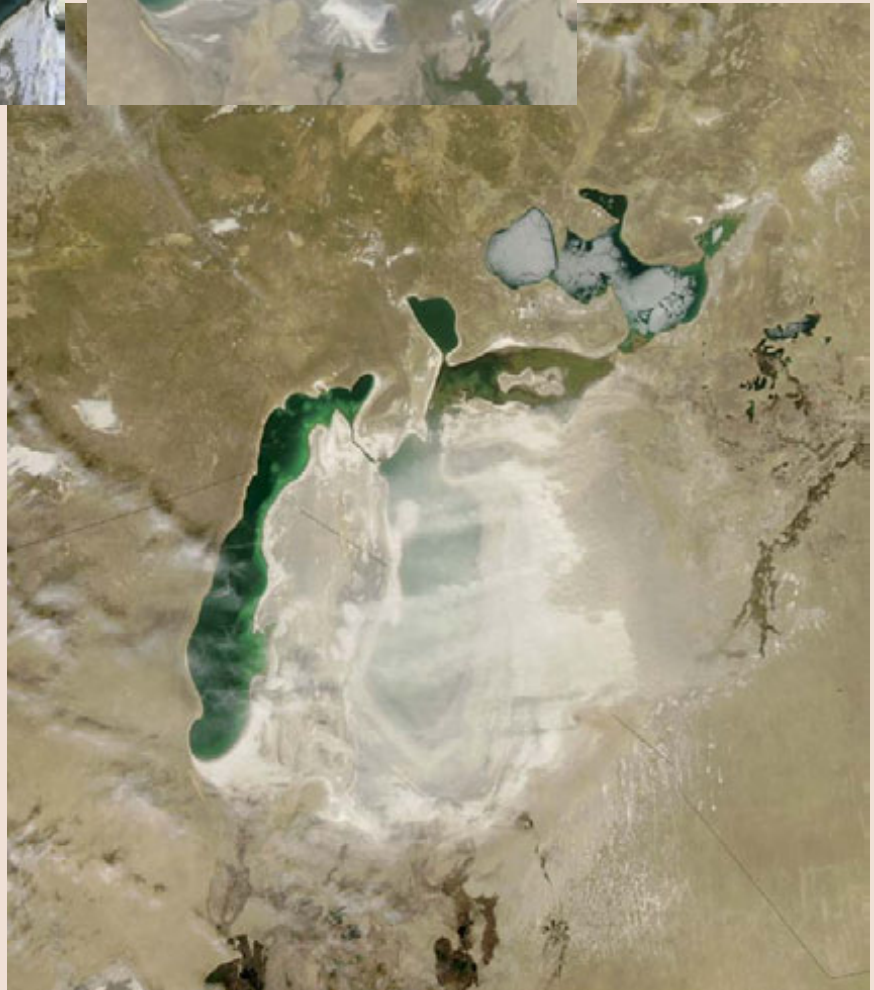




Figure 27. Lake Valencia, Venezuela, is impacted by untreated urban sewage runoff from the city of Maracay and agricultural runoff from surrounding agricultural areas. Swirling patterns of green within the lake are algal blooms that contribute to severe eutrophication, limiting both recreational use and the quality of drinking water.

Other Applications:

- ◇ In Minnesota, boating and fishing on lakes is important to the economy, and lake quality can be monitored accurately using remotely sensed images.
- ◇ Maps of land use and cover are used in analyses that model potential pollution of groundwater resources in Nebraska.
- ◇ Resource managers analyze the impacts of urbanization-induced land use and cover change on watersheds in Alabama and Kentucky, using the results to plan future development in a way that protects water resources and to design remediation projects that repair damage induced by past development.

Climate Variability Impacts

Change to climate occurs globally and can have regional and larger-scale impacts and sometimes occur with a specific frequency. Such change can impact the intensity, frequency, and spatial scope of events such as El Niño, tropical cyclones, or monsoons. One of the climate changes being measured is an increase in atmospheric temperature, which is contributing to the retreat of glaciers. As glaciers retreat, meltwater lakes commonly

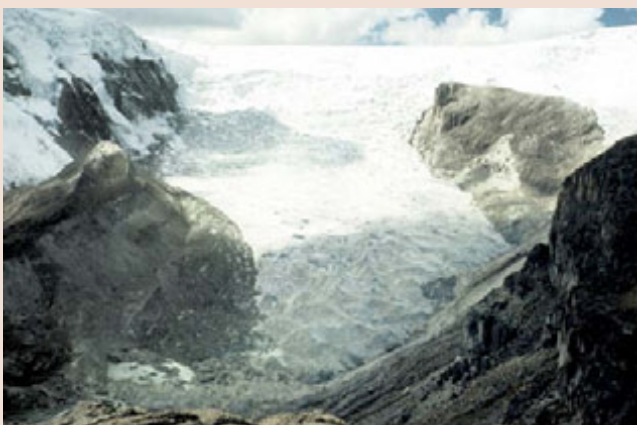


Figure 28a. The front of the Qori Kalis glacier in Peru in July of 1978.

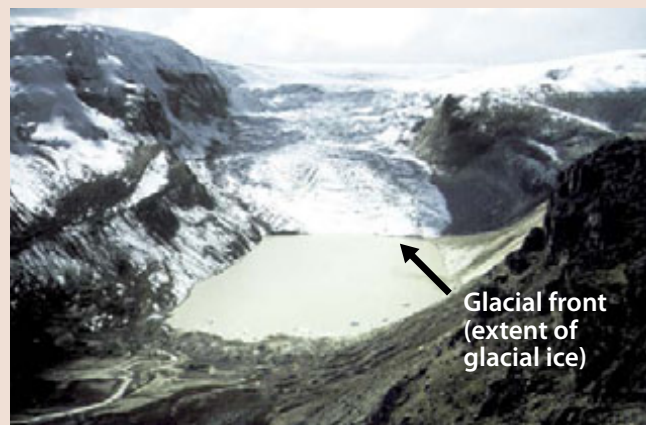


Figure 28b. By July of 2004, the glacial front had receded several hundred meters and a large meltwater lake had formed.

form in glacier-front valleys (Figure 28). Sometimes the glacial fronts collapse catastrophically and disintegrate, releasing large masses of ice into glacial front lakes or the ocean, often with a major flooding impact on the surrounding areas (Figure 29).

Climate warming is extending the growing season for many plants and expanding the range of many species. Native pine bark beetles can be kept in check where winter temperatures remain cold enough for longer periods. Warmer than usual winters have enabled pine bark beetle infestations in places like British Columbia (Figure 30).

Other applications:

- ◇ Remotely sensed satellite imagery has been applied to map white pine mortality in Yellowstone National Park, where warming and drier conditions have increased mortality. White pine is a major food source for the endangered grizzly bear, and wildlife managers can work to lessen threats using information derived from satellite-based studies.
- ◇ The effects of climate variability on water supplies are being monitored in Nebraska reservoirs that provide flood control, irrigation water resources, and habitat for many forms of wildlife.
- ◇ North Dakota is in a period of increased rainfall and expansion of lakes and wetlands with accompanying flooding, now monitored by using remotely sensed images.

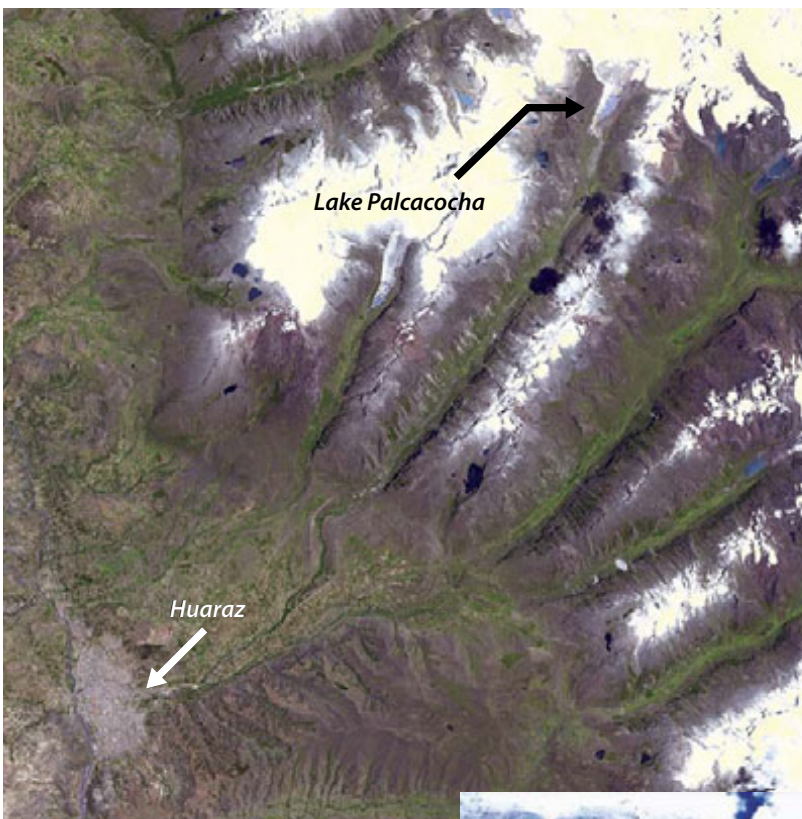


Figure 29a. An ASTER image taken in November of 2001 shows Lake Palcacocha situated at the head of a valley above the Peruvian city of Huaraz. Collapse of the front of the Hualcan glacier filling the valley above the lake appeared imminent, threatening to rapidly displace the water from the lake downstream to flood Huaraz and its 60,000 inhabitants.



Figure 29b. Lake Palcacocha in 2006. In April of 2010 a large chunk of the glacier fell into the lake, generating a 23-meter high surge of water that killed four people and destroyed property in the valley downstream.

Figure 30c. A Mountain Pine Beetle.



Figure 30b. (above) Damage caused by the Mountain Pine Beetle in E. C. Manning Provincial Park, British Columbia.



Figure 30a. An ASTER image from October of 2006 shows healthy forests in bright green and damaged forests in brown tones. Clear cuts where trees have been logged appear in pink, along with treeless floodplains.

Resource Development

Resource development —the extraction of natural resources such as metals, sand and gravel, and fossil fuels — contributes to many kinds of change, including land use and cover changes and changes in water quality and availability. The extraction of these resources may impact human developments and ecosystems. Where surface mining and agriculture compete, contaminated waters can affect water quality and agricultural productivity, while the mining can compete for acreage with valuable soil resources (Figure 31).

Figure 31. Bauxite and asbestos extraction from open-pit mines in Kazakhstan encroaches into wheat farmland, as seen in an astronaut hand-held photograph taken from the Space Shuttle by the crew of STS 112 in October of 2002.



Deforestation accompanies surface mining in mountainous parts of Brazil, with accompanying loss of habitat and effects on water resources (Figure 32). Tree removal in mountainous regions also increases the risk of landslides.

Runoff from deforested slopes and ore-processing waste water is captured in artificial reservoirs, failure of which can result in flooding and contamination of downstream drainages with toxic waters.

Monitoring resource development with remotely sensed images is useful in many ways. Much of modern development is taking place in geographically remote regions best observed by satellite.

Environmental Restoration

Environmental mitigation, remediation and rehabilitation efforts are an expanding application of remotely sensed image applications.

Imagery is typically used to plan and monitor remediation following the effects of one of the many types of environmental change described above. Extreme drought, a serious meteorological hazard, can predispose the natural landscape to wildfires. In 2007, extreme drought conditions in southern California led to the second-largest wildfire in California history, an over-two-month burn that charred more than 240,000 acres of forested hillsides. The fire (Figure 33), which began when a power tool sparked accidentally during a repair effort, began on July 4 and was not contained until September 2; it was finally extinguished on October 29, 2007, at a cost of over \$100 million. The exposed, steep hillslopes now pose not only an extreme risk of flooding, but also are far more susceptible to future landslides.

Other Applications:

- ◇ Fossil fuel production from underground reservoirs of oil or gas can also bring produced waters to the surface. The surface storage of these waters, which may be enriched in dissolved metals and other impurities, can contaminate groundwater.
- ◇ Surface mining that changes land cover and land use can be monitored to assess impacts on ecosystems and water resources.

Figure 32. An ALI image from July of 2009 shows the Carajas Mine, being developed as an open-pit operation in the Carajas Mountains in northeastern Brazil. The iron mine site, including the open pit with terraced layers as well as deforested slopes yet to be excavated, appears rust-red. Still-forested slopes blanket the mountains, and agricultural fields appear as geometric patterns to the north.





Figure 33a. The 2007 active fire front races through the Los Padres National Forest.



Figure 33b. Soils exposed on deforested hillslopes following the fire are at risk of moving downslope when rains resume. Streams and reservoirs may choke with sediment, affecting water quality and availability.

During the fire the MODIS satellite sensor provided firefighters with remotely sensed imagery twice daily. Firefighters used the imagery to plan their response in near real time (Figure 34) and emergency planners used the imagery to plan evacuations. Others used the post-event imagery to map the extent of the affected habitats and assess the impacts, to model and predict potential soil and sediment loss that will impact streams and reservoirs (Figure 35), to design remediation efforts, and to monitor the recovery of vegetation in the affected area.

Diversions of water resources for human use can generate artificial drought conditions. Owens Lake occupies a valley on the eastern margin of California's Sierra Nevada Mountains. Following diversion of the Owens River into the Los Angeles Aqueduct in 1913, Owens Lake dried up; heavy rainfall filled it temporarily but evaporation quickly returned it to a

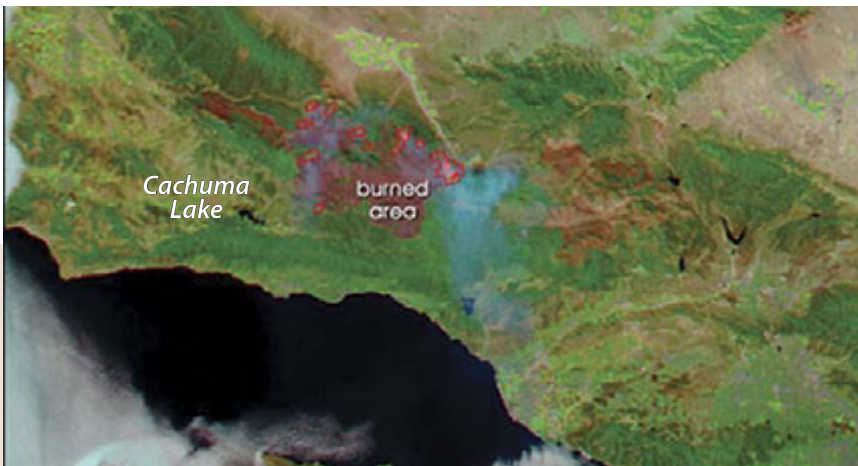


Figure 34. Taken midway through the 2 1/2 -month time during which the fire was active, this August 21 MODIS image shows the burned area in reddish-orange and the active fire front in bright pink (outlined in red).

Figure 35. Detailed ASTER imagery clearly shows the extent of the deforestation and enables accurate identification and mapping of individual drainages and wildlife habitats within the affected area.





Figure 36a. Astronaut photograph of the Owens Lake bed in 2003. The outline of the former lake is delineated by white evaporative salt deposits. Standing, highly saline water is deep red along the western edge of the lake (north is toward the right). The red coloration in this water is the result of colonies of salt-loving bacteria.

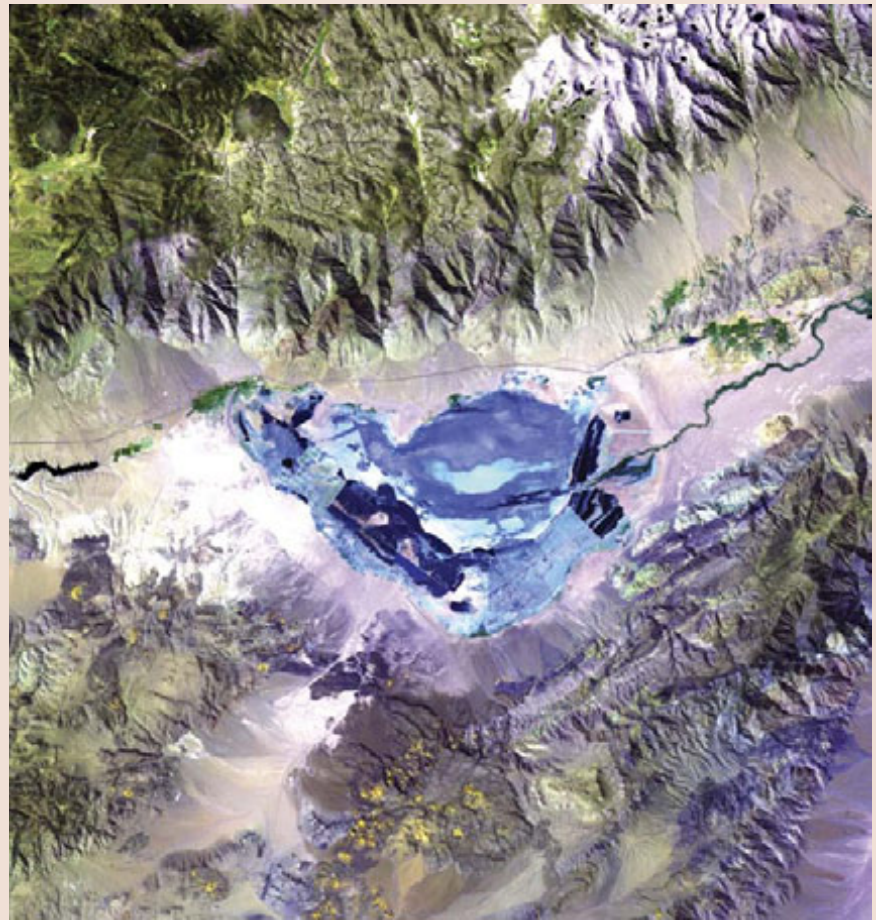


Figure 36b. Landsat imagery taken in 2010 shows flooding of the former lake bed; deep blue indicates deeper water.

dry lake bed (Figure 36). This lake bed became the largest source of airborne dust in the western United States. The lake had previously served as an important stopover for migrating waterfowl and shore birds, and in 2006 efforts were begun to restore the lake. The Los Angeles Department of Water and Power began releasing water into the Owens River again, allowing controlled flooding of constructed pond compartments on the lake floor to deliver water to the lake. Approximately 30% of the former lake bed is now covered with these ponds. Recent bird counts in 2011 indicated over 100 species numbering in the tens of thousands have returned to the restored ecosystem. Satellite imagery will continue to be used to monitor the recovery of this ecosystem (Figure 37).

Other applications:

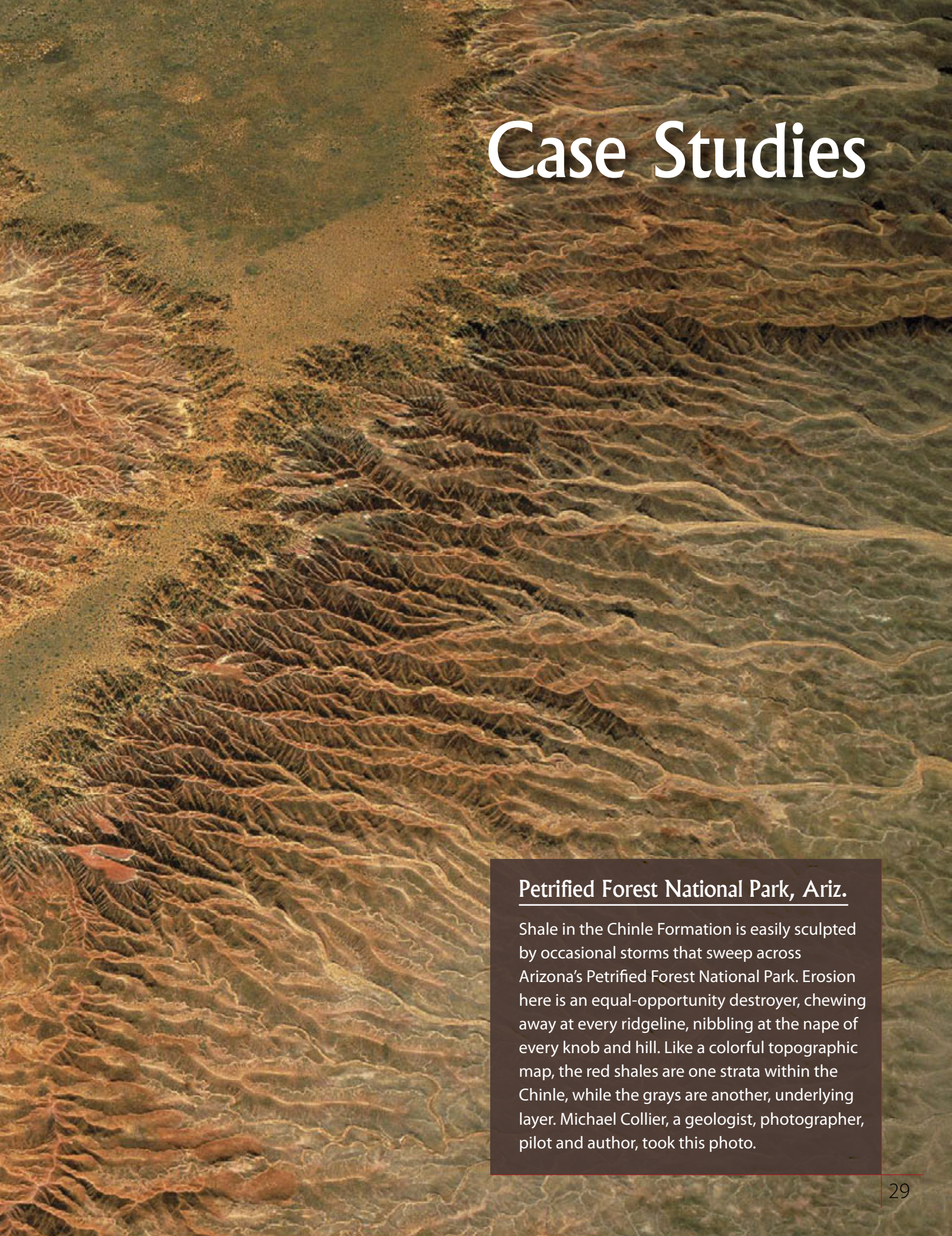
- ◇ Identifying environmental impacts and developing restoration plans involve government, industry, non-governmental organizations and private citizens. In northwest Georgia, communities monitor how development can result in soil being lost into drinking water reservoirs.
- ◇ Forest ecosystems in Kentucky are being damaged by invasive plants and animal species, and remote sensing is enabling identification and mapping of both the affected species and the offenders.



Figure 37. View looking southwest across the southern end of Owens Lake valley. Shallow ponds now cover approximately 30% of the lake bed.



Case Studies



Petrified Forest National Park, Ariz.

Shale in the Chinle Formation is easily sculpted by occasional storms that sweep across Arizona's Petrified Forest National Park. Erosion here is an equal-opportunity destroyer, chewing away at every ridgeline, nibbling at the nape of every knob and hill. Like a colorful topographic map, the red shales are one strata within the Chinle, while the grays are another, underlying layer. Michael Collier, a geologist, photographer, pilot and author, took this photo.

Remote Sensing Enables Assessing Hurricane Damage

Rebecca L. Dodge (Midwestern State University)

Figure 1a. Before and after photographs reveal shoreline retreat and sustained flooding surrounding a resort hotel on the northeast tip of Galveston Island following Hurricane Ike. Arrows mark matching features.



Figure 1b. The Bolivar Peninsula was also unprotected and the storm surge impact on residential development was devastating. Coastal areas inland from the peninsula remained flooded for weeks afterwards. Two-meter high dunes between the residential development and the shoreline were overtopped and flattened by the 5-meter high storm surge. The storm surge passed over the entire peninsula and affected the mainland beyond.

Defining the Problem

Hurricanes bring not only intense rainfall, but also high winds and flooding. This flooding is powered by the hurricane storm surge: the rise in coastal sea level caused by lowered barometric pressure and by wind blowing the ocean onto the land. The result is that waves and currents affect areas that seawater does not normally access. The turbulent surge devastates the landscape twice: first, as it rushes inland, and then again as it flows back to the ocean. Low areas often remain flooded for weeks or months, and saltwater kills vegetation and impacts water wells. Coastlines frequented by hurricanes can retreat significantly during just a single storm event, taking development literally “off the map.”

When Hurricane Ike made landfall along the Texas Gulf Coast on September 13, 2008, Galveston Island and the Bolivar Peninsula were directly in its path. Storm surge reached 3 meters over much of Galveston Island, and 5 meters along the Bolivar Peninsula. While the city of Galveston was protected by a 5- to 6-meter high seawall, the northeast end of Galveston Island had unprotected development immediately landward of the beach (Figures 1 and 2).

Selecting the Imagery

Photographs taken from aircraft immediately after the storm supported real-time rescue response and also enabled aide to those left stranded where storm-surge debris had blocked roads. Remote sensing imagery from the Advanced Spaceborne Thermal Emission and Reflection Radiometer, or ASTER, supplied data for mapping environmental changes at local scales; cloud-free imagery of the hurricane impact area became available two weeks after the event.

Figure 2. Before and after photographs of the Bolivar Peninsula show how the developed area was stripped of vegetation and homes were severely damaged or destroyed. Galveston Bay in the background was brown because storm waves picked up sediments from the peninsula and then carried the suspended sediments into the Bay. Arrows mark matching features in the two photographs.



Applying the Imagery

Before and after images from the ASTER system (Figure 3) clearly show the *extent* of the storm surge impact, including vegetation damage and flooding. The red colors in these false-color images indicate vegetation; the pre-Ike image (Figure 3a) shows healthy vegetation across the whole area. In the post-Ike image taken two weeks later (Figure 3b), areas where vegetation died or was removed because of seawater appear brown. Dark blue and black areas on the mainland north of the Bolivar Peninsula indicate standing water (Figure 3a). Many more areas appear dark blue and black in the post-Ike image showing that, even two weeks after the hurricane, flooding persisted on significant parts of the mainland. Remote sensing images such as these can also be used to re-map affected areas and monitor vegetation regrowth and habitat recovery.

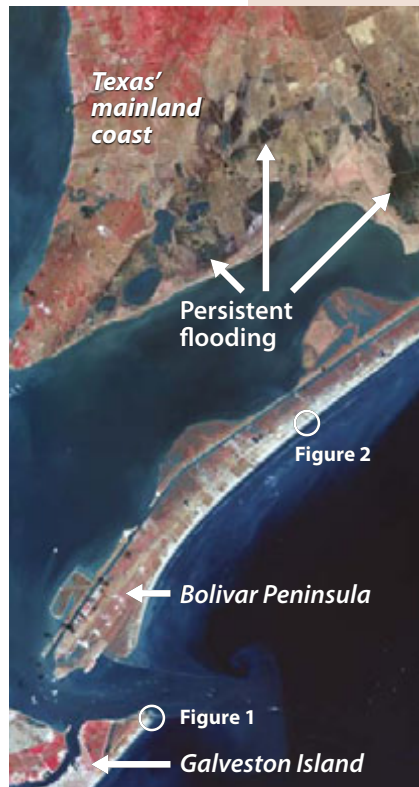


Figure 3a. (left) Pre-Ike ASTER image shows healthy vegetation (red) on Galveston Island, the Bolívar Peninsula, and the mainland in August of 2006. Black and dark blue areas are lakes on land and the waters of Galveston Bay and the Gulf of Mexico offshore.

Figure 3b. (right) Post-Ike ASTER imagery shows dead vegetation in brown, marking the extent of storm surge inundation. The mainland coast shows not only damaged vegetation but also persistent flooding.



Remote Sensing Supports Emergency Management Response to Tornadoes

Sam Batzli (University of Wisconsin–Madison)

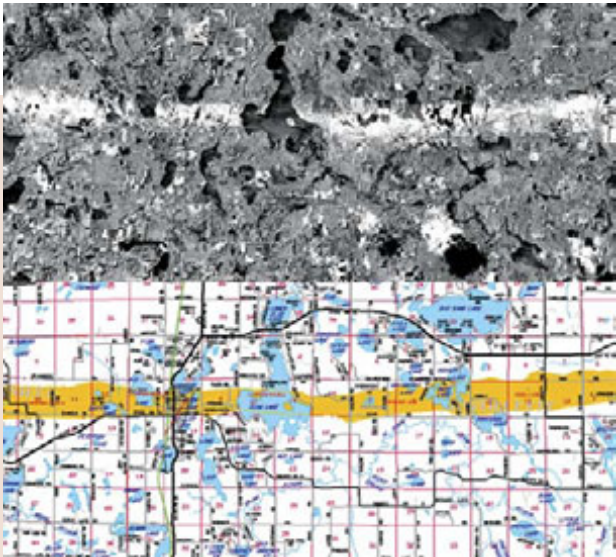


Figure 1. Image map (top) derived from Landsat TM/ETM+ imagery captured before and after the F3 tornado that hit Siren, Wisconsin, on June 18, 2001. The damage swath is plotted on a cartographic map (bottom) that was used by disaster response personnel.

Defining the Problem

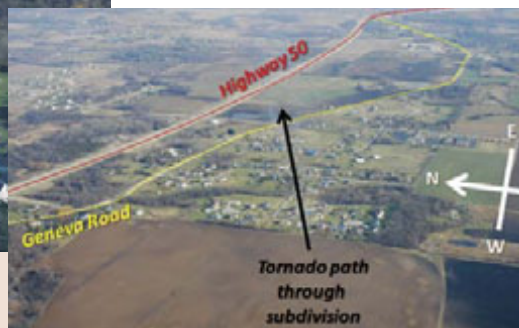
Following a tornado, first responders need maps of the width and location (swath) of the damage area. The biggest challenge when integrating remote sensing into disaster response is timeliness. To be most useful, remote sensing imagery maps must reach emergency management personnel within the first 100 hours after an event. These 100 hours are the most critical for response decisions. For example, first responders need to decide what houses, schools, hospitals, and nursing homes to search first for survivors. After this period, most of the important deployment decisions, such as where and how to get fire engines around blocked streets, have been made with or without the benefit of remote sensing imagery. After the response phase, emergency operations enter the recovery phase. This includes clean-up, victim support, and infrastructure repair. Here too, remote sensing imagery and maps are useful.



Figure 2. Aerial photo of tornado path damage near Wheatland, Wisconsin from a January 7, 2008 storm.

Selecting the Imagery

Researchers at the University of Wisconsin–Madison have developed techniques for using satellite imagery collected by the Landsat TM sensor and the ASTER sensor to measure and map the path of destruction left by tornadoes. Both sensors supply moderate-resolution imagery suitable for such damage analysis, including both before and after images to enable change detection. The type of imagery selected is determined by which sensor recorded the most

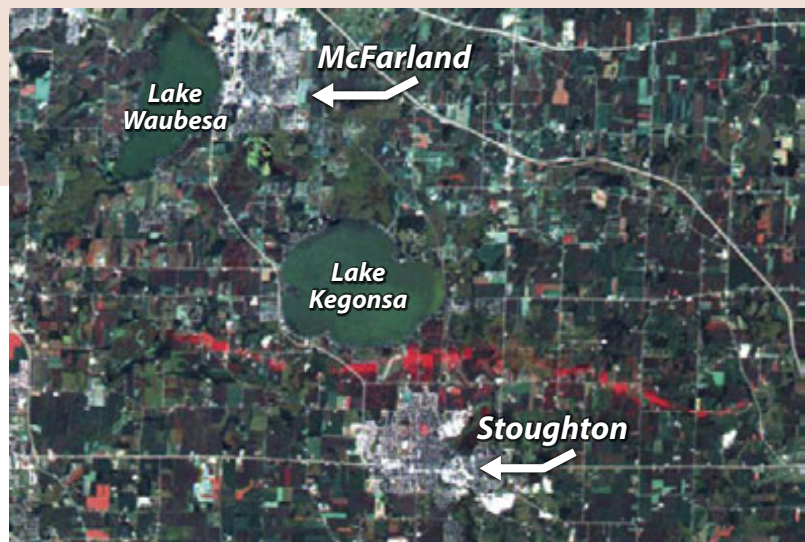


recent, relatively cloud-free imagery before the storm, and by how soon after a storm a satellite with one of these sensors passes over a damaged area during relatively cloud-free conditions.

Figure 3. Landsat TM imagery showing the Stoughton, Wisconsin area on July 19, 2005. This image uses blue, green, and red EM radiation bands in a natural color image.



Figure 4. This image shows the ground trace of an F3 tornado that touched down August 18, 2005, on the north side of Stoughton, Wisconsin. It uses the blue and green spectral bands of a Landsat 5 TM image acquired one month before the storm and the red band of a Terra ASTER image acquired 10 days after the storm.



Applying the Imagery

Researchers at the University of Wisconsin–Madison have worked with Wisconsin Emergency Management personnel to integrate satellite remote sensing imagery into the early response system for tornadoes. This integration has enabled disaster response personnel to use the imagery and resulting maps to support recovery efforts. The first use of remote sensing imagery in response to a tornado in Wisconsin occurred when an F3 tornado touched down in Siren, Wisconsin on June 18, 2001. The Landsat TM/ETM+ imagery acquired before and after the tornado clearly identified the affected area and was used to produce image and cartographic maps of the damage swath (Figure 1). Landsat-7 captured imagery on May 18, 2001, one month before the storm and on June 19, 2001, the morning after the storm of June 18. The tornado tore across the landscape and left a 25-million dollar swath of destruction more than 40 kilometers long through a heavily forested area. This storm resulted in three deaths, eight serious injuries, complete destruction of 180 homes and businesses, and damage to 270 others. The University of Wisconsin–Madison team processed the Landsat imagery from both dates, calculated the change-detection data visible in the Landsat image map (Figure 1), and quickly distributed the imagery and information to emergency management staff onsite via the Internet.

Four years later, this approach was also helpful when another F3 hit Stoughton, Wisconsin, on August 18, 2005. It was one of 28 tornadoes that ripped through southern Wisconsin that day.

Figure 3 is a Landsat TM image of the Stoughton area about one month before the August 18 tornado. Clouds interfered with the timing for acquiring a post-event Landsat image, but 10 days after the storm the ASTER sensor on the Terra satellite captured an image covering the damage area. Figure 4 shows a change detection image that combines data from the earlier TM image with information from the post-tornado ASTER image. This change detection image highlighted the swath of the tornado very well. Even though cloud cover prevented researchers from producing damage swath maps within the first 100-hour response time, Wisconsin Emergency Management found the images helpful in recovery operations for weeks after the storm.

Remote Sensing Enables Forest Ice Storm Damage Detection

Christine E. Emrich (Morehead State University)
and Jeffrey L. Lewis (U.S. Forest Service)



Figure 1. Ice storm damage in the study area.



Defining the Problem

A catastrophic ice storm occurred in eastern Kentucky in mid-February, 2003, depositing up to two inches of ice on tree limbs across the region - damaging stems and branches and completely uprooting some trees (Figure 1). Over \$61 million worth of damage was done to buildings, roadways and other infrastructure across the region, approximately 146,000 residents lost power for 4-8 days, and one person lost his life after being struck by a falling ice-covered branch. This study applied remote sensing to detect changes in the Daniel Boone National Forest following the storm.

Selecting the Imagery

A pair of Landsat 5 Thematic Mapper (TM) images (Figure 2) provides information on changes in forest condition following the ice storm. These images are shown in a 'Color Infrared' display, which is commonly used to highlight changes in forest vegetation health and density due to the high reflectance of near-infrared energy, and low reflectance of red energy, by green vegetation. In a Color Infrared display, healthy green vegetation looks bright red because the reflected near-infrared energy is shown in the color red. For both "before" and "after" of vegetation health, TM imagery was obtained for the mid-summer period to coincide with peak vegetation growth.



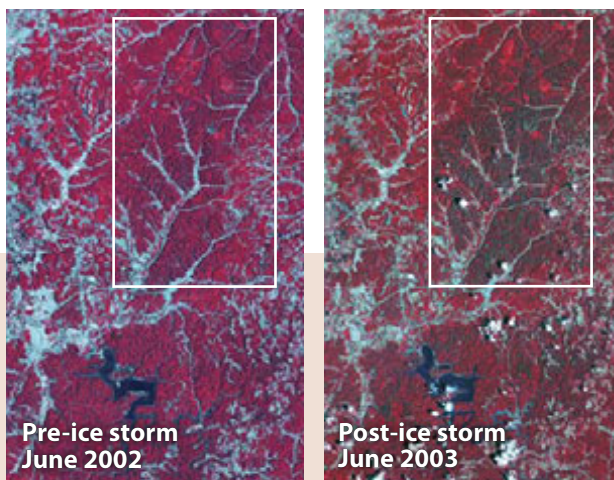


Figure 2. The Landsat 5 Thematic Mapper image pair shown in *Color Infrared* format: red = healthy forest cover, brown = damaged forest cover, pink = agriculture, dark blue = water, light blue = urban areas and bare areas, white = clouds, black = cloud shadows. The area of the forest experiencing the most overall damage is contained within the white box.

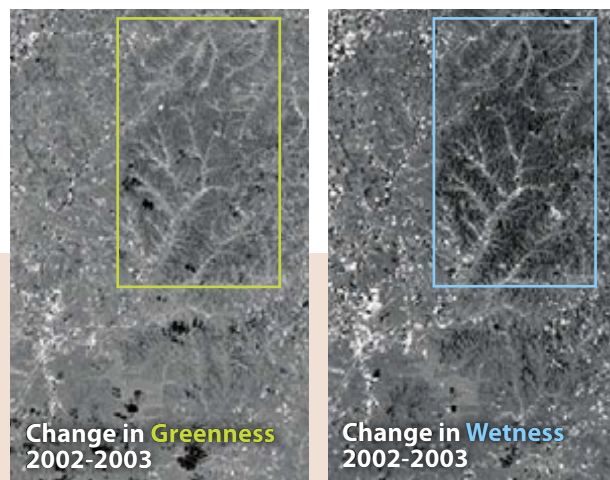


Figure 3. The transformed TM imagery. Change in Greenness image: darker areas correspond to larger decreases in greenness between image dates. Change in Wetness image: darker areas indicate greater declines in wetness between image dates. The area of the forest experiencing the most overall damage is contained within the colored box. (Small black areas correspond to cloud shadows).

Applying the Imagery

Changes in forest condition following the ice storm were examined for stands that experienced different levels of damage: heavy, moderate, and light. The original TM image pair was transformed using a set of mathematical equations in order to highlight changes in forest 'greenness' and 'wetness' conditions (Figures 3 and 4). Changes in greenness are primarily associated with an increase or decrease in tree leaves, while changes in wetness generally correspond to an increase or decrease in the water content of tree leaves. Declines in forest greenness and wetness are indicators of potential ice storm damage.

Decreases in forest greenness and wetness between image dates were greatest for the most heavily damaged forest stands and smallest for stands experiencing the least damage. Moreover, declines in greenness and wetness were generally larger on south and east facing slopes. This information will be used to facilitate forest rehabilitation and planning efforts on private and public lands in this region.

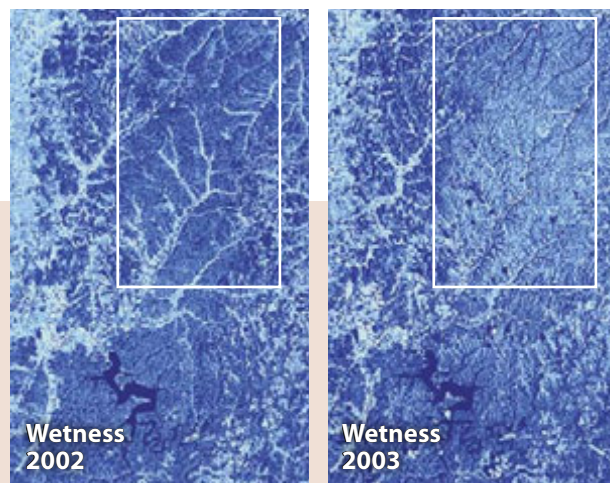


Figure 4. The transformed TM imagery: Wetness 2002 and Wetness 2003: darker blue areas indicate moister surface conditions while lighter blue areas correspond to dryer conditions. The area of the forest experiencing the most overall ice storm damage is contained within the colored box. (Figure 3 shows the change in surface wetness conditions between 2002 and 2003.)



Remote Sensing Identifies Hail Damage to Crops

Cheryl Reese, Mary O'Neill, Pravara Thanapura (South Dakota State University) and Ryan Patterson (Farmer in Britton, South Dakota)

Defining the Problem

Hailstorms destroy about 3 percent of crops grown in the Prairie States each year. These devastating storms can move quickly across a field, destroying all crops and vegetation in their path. Because of the prospect of hail impacting their farms, many farmers carry hail insurance. Hail insurance coverage varies, but in the event of a severe hailstorm the insurance enables the farmer to recover some of the economic loss even though the crop may be completely destroyed. One particularly severe hail storm struck near Britton, South Dakota on July 3, 2003, causing many thousands of dollars of damage to the soybean crop.



Figure 1. Healthy soybean crops.

Applying the Imagery

Landsat imagery of soybean and wheat fields is shown in Figure 2 for three dates in 2003: May 21, July 8 and July 16. On May 21, before the hail event, the plants were just beginning to emerge from the soil. The two July dates are five and 13 days after the hail event. All three dates of imagery are shown as the red, green and blue band combinations 4-3-2 (near-infrared, red, green) and 5-4-3 (short wavelength-infrared, near-infrared, red) and also as a Normalized Difference Vegetation Index (NDVI) image. Figure 2 shows the same dates of imagery and band combinations for the hail-affected area and for another soybean field that was not hail-damaged, located approximately four miles southeast of the destroyed fields.

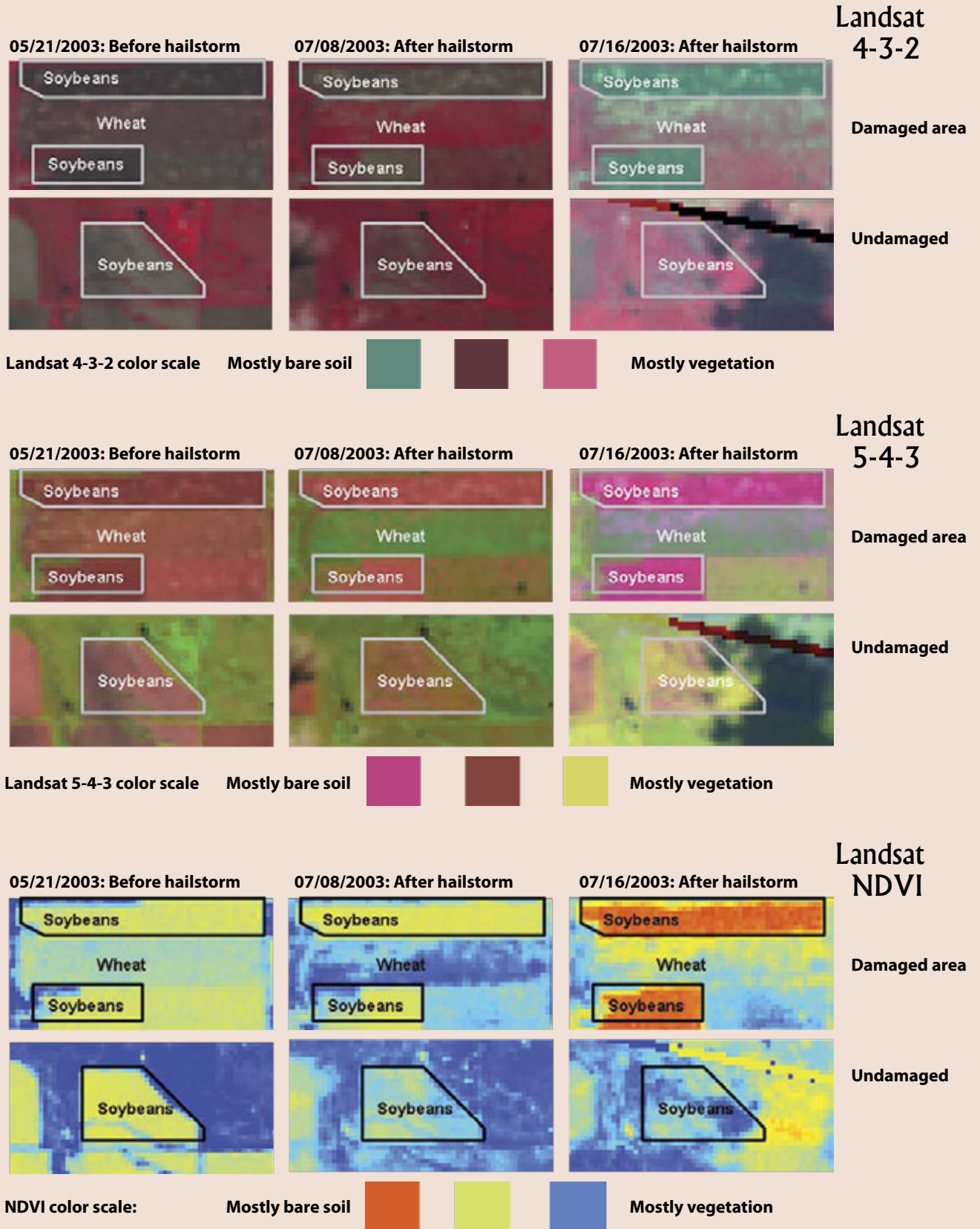
The normal progression of color in the Landsat band 4-3-2 imagery during a growing season is from grayish tones (mostly bare soil) early in the season to reds (mostly vegetation) as the season continues. For Landsat band 5-4-3 imagery, the normal progression is from pinkish tones to increasing amounts of green. In Figure 2, the lack of the red tones in the July 4-3-2 imagery and the lack of the green tones in the July 5-4-3 imagery are evidence of the crop damage caused by the hail event. Compare these colors to those in the undamaged fields, which show the normal color progressions for the growing season.

Selecting the Imagery

Landsat Thematic Mapper (TM) imagery is a good source of before and after hailstorm imagery because of its 30 x 30 meter pixel size and because of its synoptic view of the affected fields. The imagery enables farmers to document the fact that, before the storm, the crops were growing well. It also helps determine the number of acres damaged by the hail. Using Landsat imagery to document crop damage is not limited to hail, but can be used to document crop damage from other natural disasters such as heavy rain events and flooding.

The evidence is even more clearly shown in the NDVI imagery, where the normal sequence of colors over the growing season is from orange to yellow to blue (least to most vegetation). The hail-affected soybean fields in Figure 2 are orange in the July 16 image, indicating little to no vegetation. The soybean field that was not hail-damaged is blue for July 16, indicating that it is highly vegetated.

Figure 2. Landsat imagery sets of hail-damaged and nearby undamaged areas before and after the hail event near Britton, SD.



Remote Sensing Identifies Hazards at Anatahan Volcano, Northern Mariana Islands

Rebecca L. Dodge (Midwestern State University)

Defining the Problem

Anatahan Island is one of the 15 volcanic islands in the western Pacific Ocean that make up the Northern Mariana Islands, a Commonwealth of the United States. The island was evacuated in 1990 because of earthquake activity, but it wasn't until April 2003 the island experienced a volcanic eruption, the first in recorded history for Anatahan Volcano. The island remains off-limits to people today.

Anatahan Volcano also lies along the flight paths of many international flights. Eruptions of volcanic ash into the atmosphere along these flight paths could be devastating to aircraft. During the 2003 eruption, remote sensing imagery was the key to monitoring ash eruptions from Anatahan Volcano, making it possible to reroute aircraft to safe flight paths.

Selecting the Imagery

On May 10, 2003, around 5:00 p.m., Anatahan Volcano began erupting from its east crater. On May 11, 2003, Astronaut



Figure 1a. (left) Photographic image of the 9-km-long volcanic island taken on November 21, 1996, from the Space Shuttle Columbia shows Anatahan Volcano prior to the 2003 eruption. The island is covered by a green blanket of healthy vegetation.

Figure 1b. (right) Photographic image of Anatahan Volcano taken on May 11, 2003, from the International Space Station documents the first eruption of Anatahan Volcano in recorded history. The entire volcano is obscured by ash.

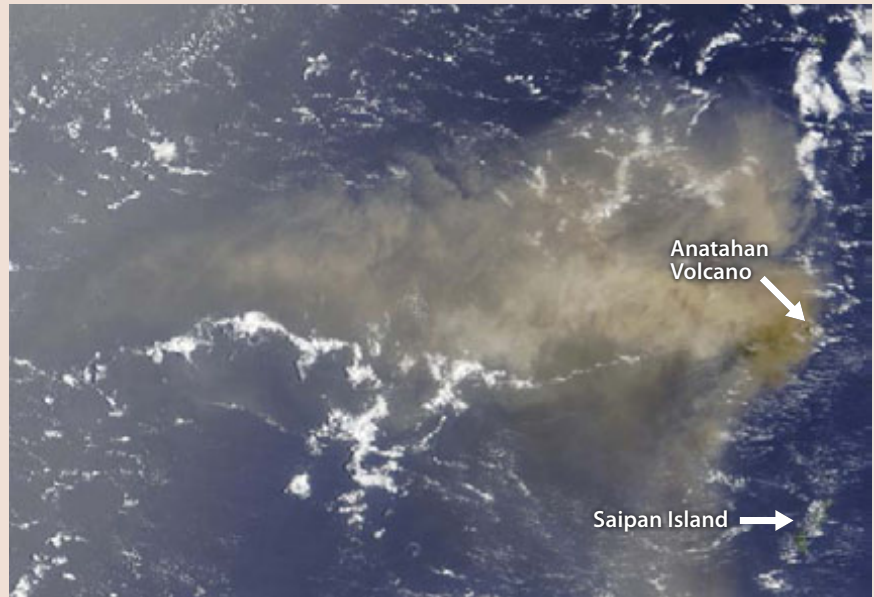
Ed Lu, aboard the International Space Station (ISS), identified a broad plume of ash in the atmosphere beneath him as the ISS passed over the Pacific Ocean. Camera in hand, Lu recorded an image (Figure 1b) of what was the volcano's first eruption in recorded history.

Approximately one hour later, the MODIS remote sensing instrument on NASA's unmanned Terra satellite acquired an image of a much larger geographic area (Figure 2). MODIS sensors orbiting the Earth on two unmanned satellites (Terra and Aqua) provide remote sensing imagery for the entire Earth once every 24 hours, and provide baseline image data for tracking volcanic ash. The broad geographic extent of MODIS imagery highlights another important capability of remote sensing imagery — that of “zooming out” to cover broader geographic areas when necessary (Figure 2). An April 2005 image from the ASTER satellite (Figure 3) shows the “zoom-in” capability of this data; this image has a much higher resolution than either the MODIS image or the photographic images from the ISS and Space Shuttle (Figure 1). Although the broad geographic coverage of MODIS is critical for tracking the extent and orientation of the plume, the ASTER data's higher resolution is critical for monitoring changes in land cover on the tiny island. The Terra MODIS satellite also has the ability to sense wavelengths beyond the visible range, including emitted thermal wavelengths related to hot objects (Figure 4). These wavelengths are especially valuable for monitoring volcanic activity.

Applying the Imagery

International airline traffic was diverted in response to the 2003 eruption of Anatahan; more than 25,000 aircraft pass through the affected airspace each year and cannot safely fly through volcanic ash. A daily, steady stream of remotely sensed images from MODIS and other unmanned satellites allowed scientists to monitor the changing trajectory of

Figure 2. Terra MODIS image showing the geographic distribution of the ash cloud streaming westward from Anatahan Volcano on May 11, 2003. The island is outlined in black on the right side of the image. An ash plume extends over 600 kilometers toward the west. Saipan Island, where the Territorial capitol is located, is in the lower right corner of the image.



the ash plume as it shifted over time as the plume changed orientation when the prevailing east winds were affected by changing weather patterns. Anatahan Island had been uninhabited since 1990, but the shift directed ash and sulfur pollution toward islands to the north and south that were still inhabited.

Satellite monitoring also allowed government emergency management personnel to model and predict the plume's movements and respond with air quality advisories. MODIS data enabled continuous volcanic ash and air-quality advisories throughout the five-year eruption activity of the Anatahan Volcano.

The ASTER color infrared composite image (Figure 3), taken in 2005, shows healthy vegetation in red (instead of green as in the Space Shuttle photograph, Figure 1a). The central part of the island appears to be completely devoid of vegetation, and in the western part vegetation appears to be heavily blanketed with ash.

Figure 4 is a thermal image from 2008, taken at night as the Terra satellite passed over Anatahan. The bright white spot in this image is in fact a hot spot centered on the volcano summit, which was still actively erupting in February 2008. The purple signature of the ash cloud in this nighttime image provided scientists with the capability to monitor the ash plumes 24 hours per day. Eruptions prevented all but scientific observers from returning to the island. They ceased in 2008. If residents are allowed to reoccupy the island, new imagery will be needed to plan recovery and remediation efforts and monitor their progress.



Figure 3. ASTER imagery taken in April of 2005 documents the devastating effects of the eruptions that continued from Anatahan Volcano.

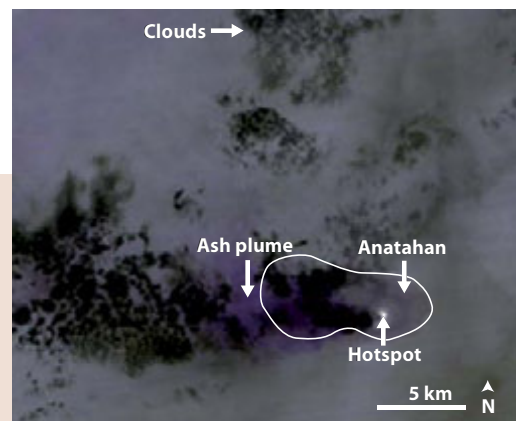


Figure 4. Terra ASTER image of Anatahan taken during nighttime on February 7, 2008. Dark features are clouds at high altitude. Purple indicates volcanic ash in the atmosphere.



Remote Sensing Enables Lava Flow Hazard Assessment

Robert Wright (University of Hawaii at Manoa)

Figure 1a. Photograph of an active aa lava flow near the summit of Italy's Mount Etna. The lava channel is narrow at this position near the vent, which is only a couple of meters wide.

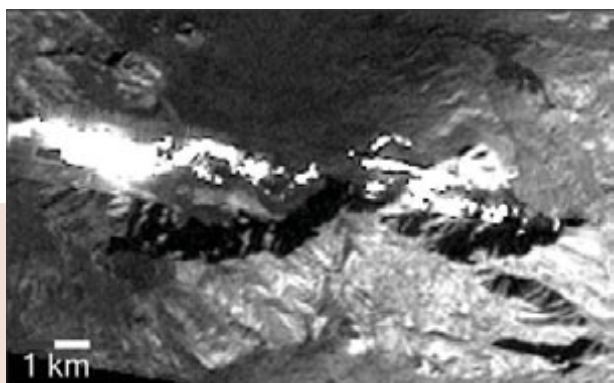


Figure 1b. Landsat TM band 5 (1.65 micrometers) image of Etna acquired on January 2, 1992. White pixels running from top left to lower right denote the hot, active lava flow surface.

Figure 1c. The same lava flow that can be seen in Figure 2 was imaged only one day later by a different satellite sensor, the European Space Agency's ERS-1 Along-Track Scanning Radiometer, at the same shortwave infrared wavelength. This image (shown) was acquired at night, so thermal emission from only the active lava is apparent (the ground beside the flow is too cool to radiate at this short wavelength). In contrast, the Landsat image in Figure 2 was acquired during the day. Ground adjacent to the active lava is visible in that image because it is reflecting sunlight, not because it is hot. Lava reflects very little light at this wavelength, it is bright because it is very hot.



Defining the Problem

Active lava flows are a potential hazard to property and, in some cases, even to humans and wildlife. When a volcanic eruption begins, lava flows downhill from the vent, cooling as it advances. Eventually it cools and stiffens sufficiently to stop flowing. Predicting where on a volcano lava may flow during an eruption depends on answering two questions: Along which paths from the vent could the lava possibly flow, and how far along those paths can it advance before it stops? Satellite remote sensing can help answer these questions.

Selecting the Imagery

The estimate of the volume of lava coming from the eruptive vent, in cubic meters per second, is the volumetric lava effusion rate. The higher this effusion rate, the greater the area the lava can cover. Thermal infrared satellite data can be used to identify and quantify the active lava flow area. High resolution Landsat Thematic Mapper images are useful for this purpose because active lava flows are hot enough to radiate substantial amounts of energy in the short-wave (TM bands 5 and 7) and long-wave infrared (TM band 6).

Effusion rates can also be estimated using low-resolution images acquired by sensors such as MODIS, AVHRR, and ATSR (Figure 1). Although the spatial resolution is much coarser (1 kilometer versus 30 to 120 meters) the increased temporal resolution (i.e. about one image each day) allows many more observations of the flow to be made as the eruption progresses. Because effusion rates can vary substantially during an eruption, and because lava flow predictions rely on accurate estimates of effusion rate, the combination of both high- and low-resolution data sets is ideal for monitoring lava flows.

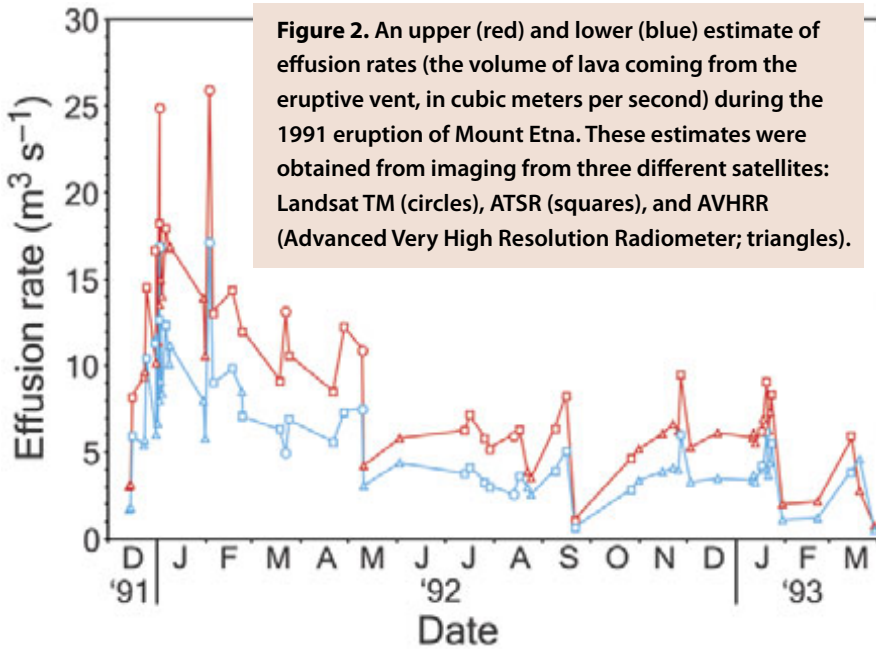
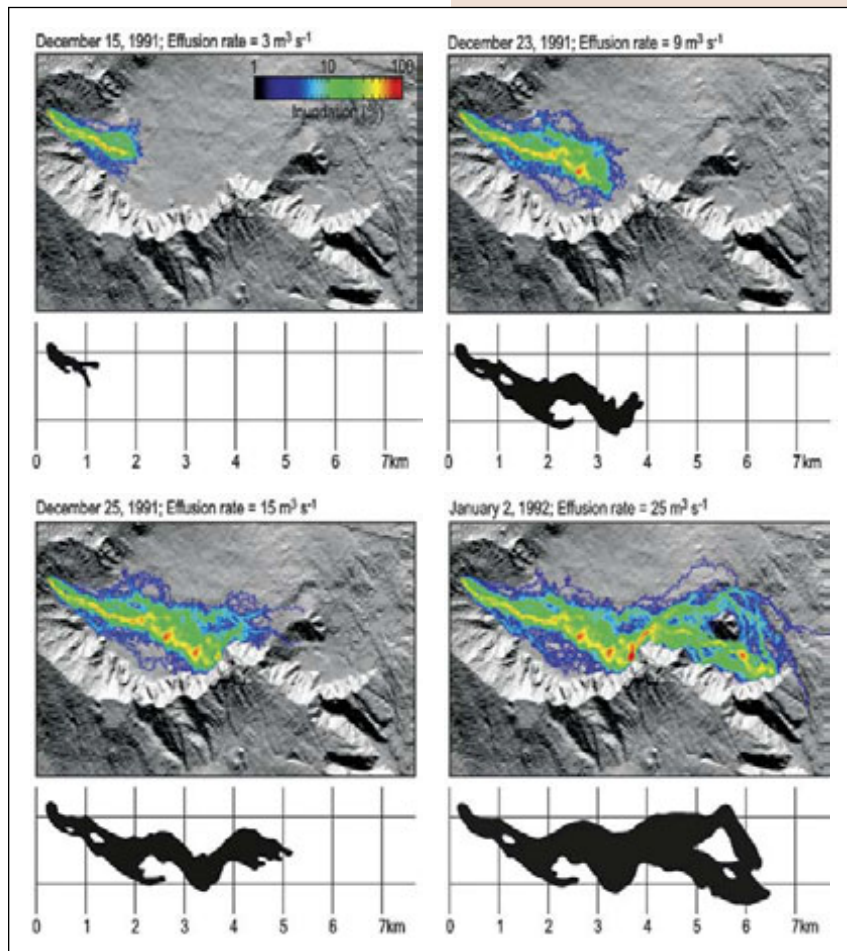


Figure 3. Color images show the predicted flow dimensions of the 1991–1993 Etna lava flow on four dates during the eruption. These predictions were obtained by using satellite derived effusion rates to drive a numerical lava flow model. Sketch maps beneath show the actual flow dimensions on the same dates. The color scale indicates the number of times a location on the volcano was predicted to be inundated with lava, after running the model 10,000 times. The length of each line is determined by the satellite-derived effusion rate, the physical model that describes how the lava cools, and the underlying ground slope.

Applying the Imagery

By assuming the minimum and maximum temperatures of the lava, the area of lava required to produce the spectral radiance measured by the sensor can be calculated from each image. This area (in square meters, or m^2) can then be converted to an estimate of the lava effusion rate (in cubic meters per second or m^3/s) by using a field-derived empirical relationship. Results obtained from analysis of images acquired during the 1991–1993 eruption of Mount Etna are shown in Figure 2.

The estimated lava effusion rate provides a prediction for the lava’s path over time. By using time-varying, satellite-derived effusion rates (Figure 3) in a numerical lava flow simulation model, the satellite data can be used to predict which areas might be inundated with lava. The prediction combines the most probable downhill path of the lava from the vent, an estimate of how quickly the lava solidifies, and the satellite-derived effusion rates to predict distances from the vent at which solidification occurs. Given that data from sensors such as MODIS can be obtained within hours of satellite overpass, this approach



allows for near-real-time predictions of lava flow hazards. This information makes it easier to determine whether, for example, a specific town may be in a lava flow’s path.



Remote Sensing Reveals Vertical Coastline Displacements Caused by Earthquakes

Rebecca L. Dodge (Midwestern State University)

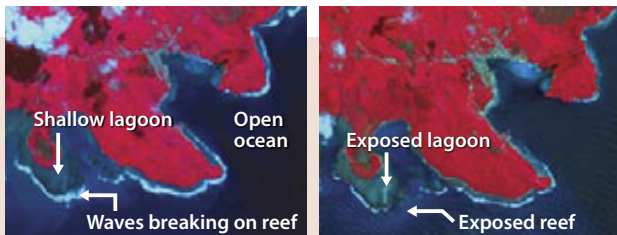


Figure 1a. (left) ASTER image showing the southeastern coast of Nias Island, located 80 miles (125 kilometers) west of Sumatra, on July 13, 2000. **Figure 1b.** (right) ASTER image taken on April 6, 2005.

Defining the Problem

The December 26, 2004 and March 28, 2005 earthquakes in the Indian Ocean near Sumatra, Indonesia, generated tsunamis that devastated coastal communities. The earthquakes also caused vertical displacements, both uplift and subsidence, along the coast. These displacements affected ecosystems vital to coastline stability and ocean productivity. Uplift killed coral reefs that had protected the coastline from erosion and had provided safe spawning grounds for marine life. Subsidence, or downward displacement, killed mangroves that had been vital in coastal stabilization and as spawning grounds. Remote sensing identified the extent of these ecosystem impacts.

Selecting the Imagery

ASTER (Advanced Spaceborne Thermal Emission and Reflection Radiometer) imagery is a high-resolution data source designed for land-cover analysis. Detecting changes in land cover and coastal configuration, including changes in water depth, is supported by several imaging wavelength bands (green, red, and near infrared). The ASTER imagery also provides 15-meter spatial resolution, which is sufficient for many land-change studies. These data are freely available and new acquisitions can be requested for studies of specific natural disasters.

Figure 2. Uplifted lagoon floor and exposed coral reef following the March 2005 earthquake.

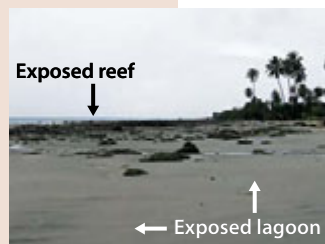
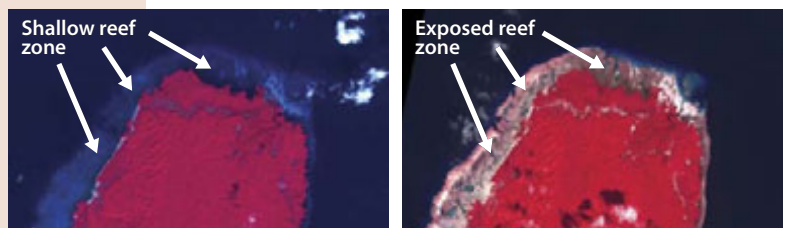


Figure 3a. December 2, 2004, ASTER image of Interview Island in the Andaman Island chain; submerged reefs ring the island in a pale blue.

Figure 3b. February 4, 2005, ASTER image shows brown ring of exposed reef surrounding the island. Vertical uplift of up to one meter exposed the reef.



Flood in Karawang, Indonesia, March 25, 2010.



Applying the Imagery

Coastal damage following the earthquakes was widely distributed and vast geographic areas needed to be surveyed. Satellite imagery was first applied to delineate tsunami damage onshore in populated areas. Observations were later extended to map areas of ecosystem devastation that could impact coastal stability and productivity in the long term.

Figure 1 shows the coastline along the southern side of Nias Island, which is 90 miles (150 kilometers) southeast of the March earthquake's epicenter. Submerged reefs in the pre-earthquake image (Figure 1a) are separated from deep, dark-blue open ocean waters by bright, breaking waves. The protected, shallow lagoons behind the reefs are a brighter blue; these reefs protected the shoreline and were productive fish nurseries. In the post-earthquake image (Figure 1b) these lagoons are exposed, and the coral reefs are above water (Figure 2).

In the Andaman Islands northwest of Sumatra, specifically on Interview Island, reef uplift was even more dramatic. Figure 3 shows ASTER images acquired before and after the quakes. The comparison reveals extensive exposure of reefs (Figure 4) caused by tectonic uplift.

Areas near Banda Aceh, on the island of Sumatra, were tectonically submerged; subsidence caused shorelines to shift landward, flooding coastal ecosystems. In a Landsat image from August of 2001 (Figure 5a), sandy barrier islands line the coast on the northern side, and coral reefs are highlighted by bright breaking waves on the west side of the scene. An ASTER image (Figure 5b) from June of 2005 shows a significant southward shift of the northern coastline and submergence of the barrier islands. The coral reefs, left more submerged by the subsidence, no longer break incoming waves. The image also shows the western coastline dramatically robbed of vegetation by tsunami waves; many trees were destroyed and remaining tree roots are now submerged by up to 1 to 2 meters of salt water.



Figure 4. Dead coral exposed by tectonic uplift on Palua Karang, Banyak Region, Indonesia.

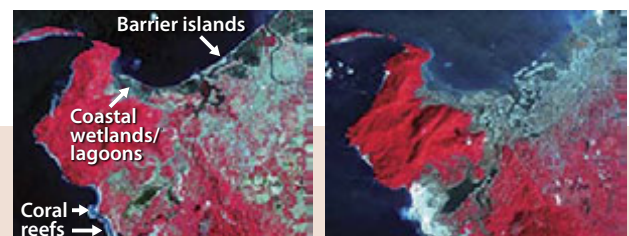


Figure 5a. (left) Landsat imagery of northwestern Banda Aceh Province, Indonesia shows vegetation in red. Developed areas are light gray-blue; deep water is blue, and shallow water is light blue.

Figure 5b. (right) Post-tsunami ASTER image; water along the northern and western coastline encroached landward and barrier islands along the northern coastline were breached and severely eroded.



Remote Sensing Determines Urban Heat Island Effects

Kevin Czajkowski, Teresa Benko and Timothy Ault
(University of Toledo)

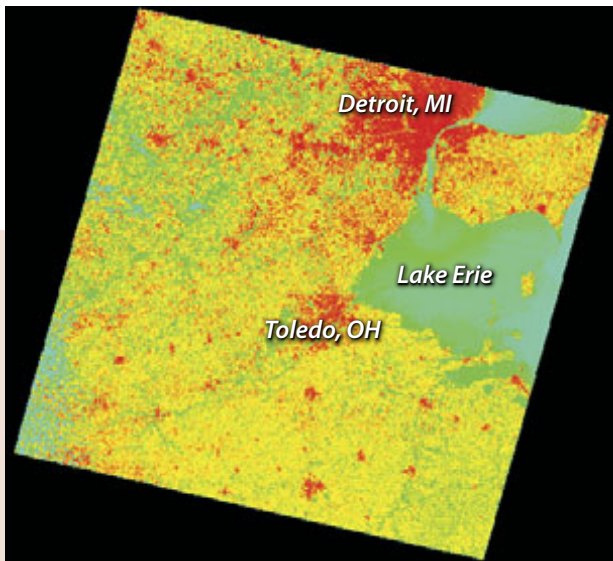


Figure 1. Landsat 5 image from June 24, 2006, using the thermal band 6. Red is warmer and yellow and green are colder. Cities are warmer than the surrounding landscape.

Defining the Problem

Land-surface temperature is defined as the temperature at a particular location on Earth's surface. It is affected by land use and land cover, and as cities grow with more paving and construction, the surface temperatures increase. Roads, parking lots, sidewalks, and buildings tend to be warmer than vegetation. Houses and other buildings as well as parking lots and other paved surfaces retain less moisture than vegetated areas. Where moisture is less, a smaller portion of the energy from the sun goes into evaporation, leaving more energy to heat the land surface, therefore producing a higher surface temperature. This effect contributes to health hazards in cities during heat waves and also drives up energy demand in the summer as air conditioning is used to cool buildings. Remote sensing is used to study how the growth of urban areas affects land-surface temperature. Knowledge of where and how land use and land cover are changing is important for decision makers address these problems.

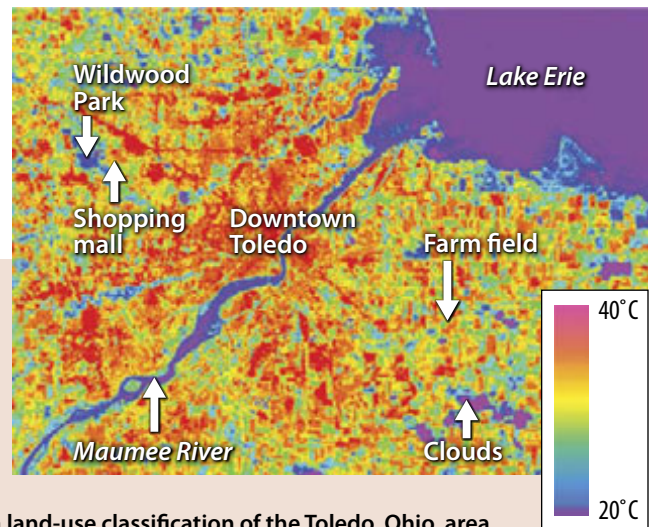
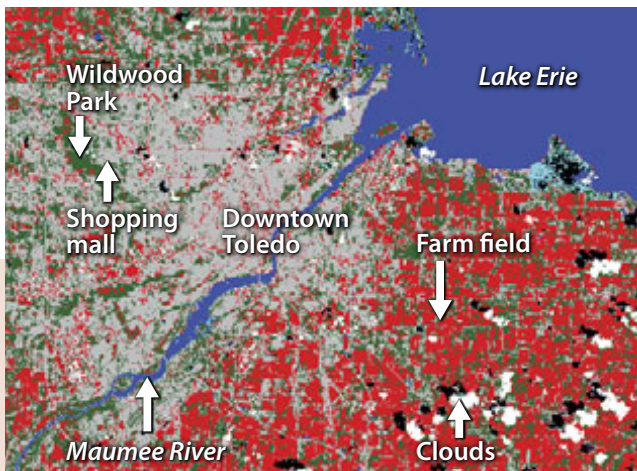


Figure 2. Landsat 7 image from July 1, 2000. The left side shows a land-use classification of the Toledo, Ohio, area (gray is urban, green is forest, blue is water, red is agriculture, and white is clouds). At right, the same area is seen as a thermal image created from band 6. The built environment of roads, parking lots of the mall, and downtown area of Toledo are warmer than a forested park and warmer than the water in the Maumee River and Lake Erie.

Selecting the Imagery

The emission of electromagnetic radiation from Earth's surface can be used to study surface temperatures. Every object emits electromagnetic radiation, and the wavelength of the emitted radiation depends on the object's temperature. Hot objects emit energy that peaks at shorter wavelengths, while cooler objects emit energy that peaks at longer (thermal) wavelengths. Satellite sensors that observe in the thermal infrared wavelength region of the electromagnetic spectrum can be used to study surface temperature.



Figure 3. New development on the outskirts of Toledo, Ohio, contribute to urban sprawl and change the land-surface temperature.

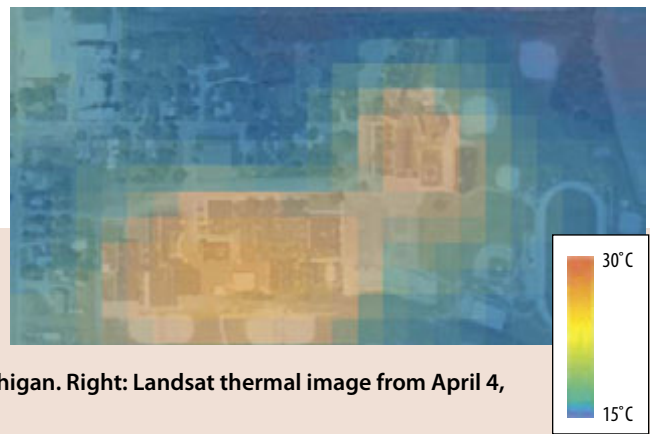


Figure 4. Left: aerial photograph of Ida School District, Ida, Michigan. Right: Landsat thermal image from April 4, 2005, superimposed on the aerial photograph.

Figure 4b shows surface temperatures around Ida, Michigan. Temperatures were determined using thermal infrared imagery from the Landsat satellite. Landsat is often used to study the way that land cover and land use affect the input and output of energy and surface temperature; its 120-meter resolution in the thermal infrared band combined with its geographic coverage of a single scene are useful for studying thermal effects at the scale of an individual city. Its 16-day return cycle also allows for seasonal monitoring of thermal emissions in cities and surrounding rural landscapes. Landsat 5 also has a very long collection record, spanning from 1983 to 2012, which allows analysis of long-term effects of urban expansion.

Applying the Imagery

The satellite images in Figures 1 and 2 show very clearly that cities and their built environment warm the surface. A parking lot can be up to 20° Celsius warmer than a forested

area or grassy field (Figure 2). As cities continue to expand outward, surface temperatures are expected to continue to go up (Figure 3). Not only are cities warmer than the surrounding rural areas, as evident in these satellite images, some agricultural fields are warm as well. Bare agricultural fields tend to have warmer temperatures than actively growing fields. Also, fields that have been harvested tend to be warmer than fields where living vegetation is present. These changes to the landscape by humans change the energy budget of the Earth's surface and affect local climate.

Greenhouse gases in the atmosphere interfere with the thermal signal emitted by the surface before that radiation reaches the satellite. There are many ways to correct for this effect including using surface observations. Citizen scientists (in this case, middle-school students involved in the GLOBE program) have gathered ground-based data that have been used to calibrate the satellite observations and correct for atmospheric interference. Figure 4 shows Landsat surface temperature was warmer over the school buildings than the surrounding sports fields and ponds.

Remote Sensing is Essential for Suppressing Alaska Wildfires

Thomas Heinrichs (University of Alaska Fairbanks)



Defining the Problem

Wildfires occur regularly in Alaska — over 11 million acres burned between 2004 and 2005. Smoke is often so thick that airborne surveillance is impossible (Figure 1). Satellite imagery, on the other hand, can detect infrared wavelengths that locate the actively burning perimeter of the fires. Knowing these perimeters, firefighters can respond to the correct locations.

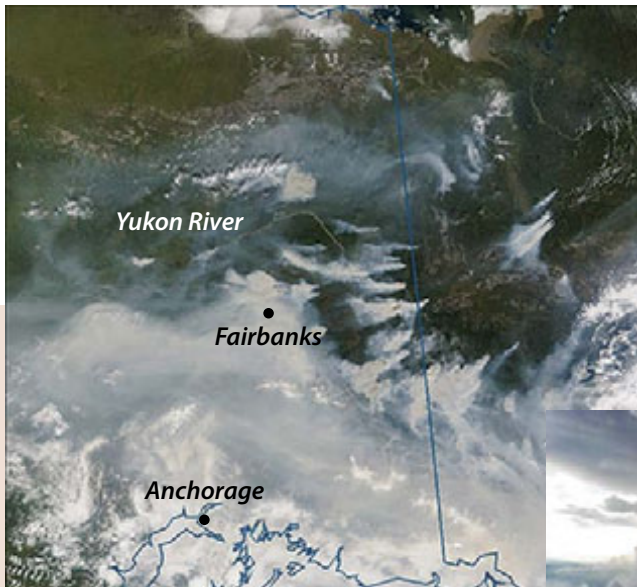


Figure 1. MODIS 250-meter resolution imagery of fires on June 28, 2005. Smoke obscures many of the fire perimeters and limits visibility for flight operations, hampering response efforts. Satellite imagery is a better tool.



Selecting the Imagery

Near real-time satellite imagery, available from the MODIS sensor, is captured and processed by GINA and transmitted in near-real-time to the Bureau of Land Management (BLM) Alaska Fire Service multiple times each day. Landsat imagery is readily available and can be delivered to the BLM firefighters in less than 24 hours by the Geographic Information Network of Alaska (GINA). Both MODIS and Landsat record infrared wavelengths that penetrate the smoke and reveal the actively burning fire perimeter (Figures 2 and 3). Fire fronts can move quickly, so it requires image acquisitions from multiple sensors to keep firefighters updated and improve response efforts.

Applying the Imagery

The “hot spot” mapping capability provided by near real-time remote sensing dramatically improves decision-making capabilities and resources available to fire managers. In the vast expanse of Alaska, satellite imagery is often the best — and only — information available for locating and mapping fires.

Figure 2. The red points plotted on this June 29, 2004, image map show the actively burning perimeter.

A June 29, 2004, infrared (Figure 2) image penetrates the wildfire smoke that obscured several fire fronts; images like this deliver real-time fire detection “hot spot” points to the BLM Alaska Fire Service. The smoke was so thick that aircraft tasked to identify fire front locations were grounded for more than a week, meaning the only reliable information for many fire locations was remote sensing imagery from satellites.

When the Sheenjek River fire threatened Fort Yukon, Alaska, in June of 2005, the capability for 24-hour delivery of Landsat imagery from the USGS and GINA (Figure 3) had been operational for less than two weeks. With firefighters battling a convoluted fire front that had become more than 20 miles long by June 21, fast access to the higher-resolution Landsat imagery helped to direct firefighting efforts effectively. Firefighters were especially interested in keeping the fire from crossing the Sheenjek River.

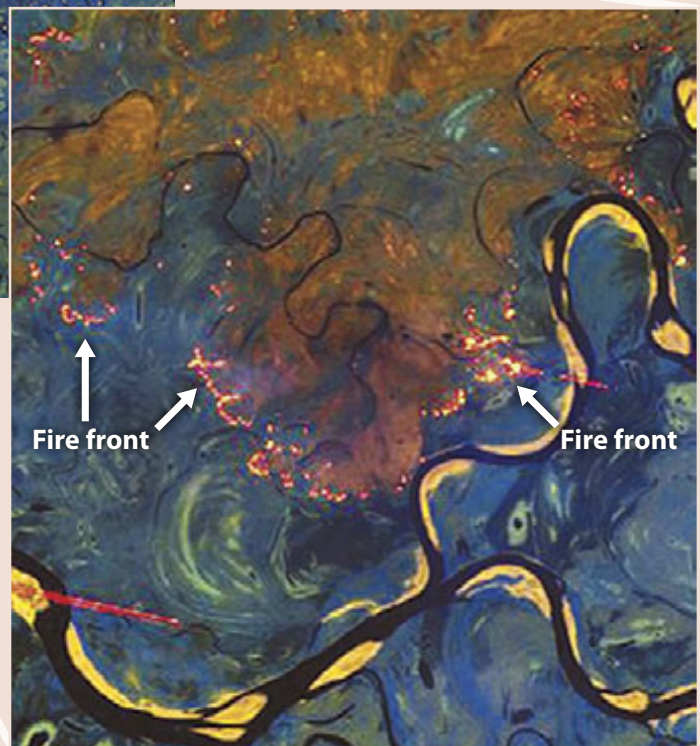
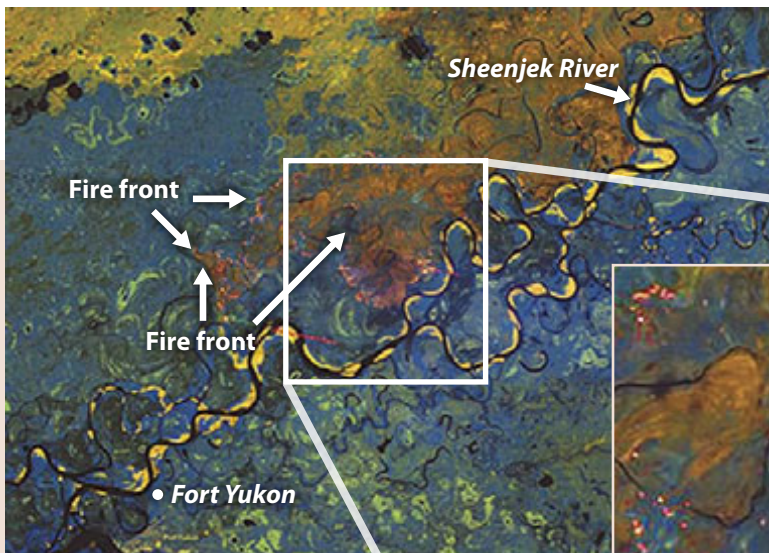
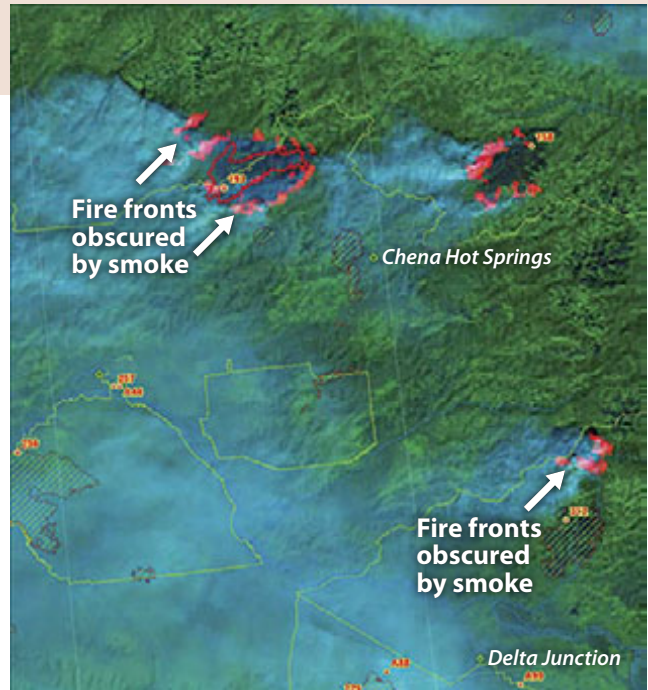


Figure 3. Landsat imagery of the Sheenjek River fire enabled firefighters to direct efforts toward stopping the fire from crossing the river, preventing its access to Fort Yukon. The burn scar from the Sheenjek River fire is dark orange, and burn scars from the previous year are orange. Bright points are actively burning (see inset).



Remote Sensing identifies Agricultural Problem Areas

Cheryl Reese, Sharon Clay, David Clay, and Gregg Carlson
(South Dakota State University)

Defining the Problem

In agriculture, walking the fields is one way to locate weed, disease, or insect problems. This method can be very time consuming and, depending on the stage of crop growth, difficult or even impossible to spot crop problems. Farmers are now using remote sensing to evaluate crop health. With remotely sensed images, they can identify areas where crops do not appear healthy and then visit each site to determine the cause of the abnormality.

Remote sensing can detect problem areas because spectral reflectance is influenced by total plant material and plant health. Healthy plants reflect more near infrared (NIR) and less blue and green radiation than unhealthy plants. Factors that influence plant health are nutrient deficiencies, water stress, disease, and insect damage. For a given pixel, the

reflectance value is the average of the reflectance values for all objects within the pixel. If a pixel contains 40 percent weeds with a reflectance value of 20, and also contains 60 percent crop cover with a reflectance value of 60, the reflectance value for the pixel is 44. The variance from 60 (the reflectance for complete crop cover in this example) identifies areas containing weeds. A key factor in using remote sensing to identify weed patches or diseased areas is to know the reflectance characteristics of the different components within a pixel.

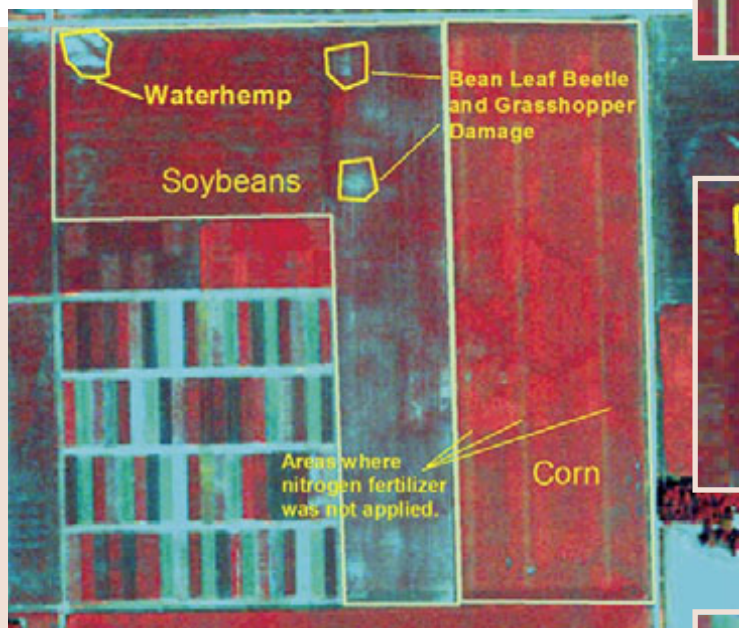


Figure 1. IKONOS false color image showing several problem areas. Field work later confirmed the exact cause of damage to vegetation.

Figure 6. Close-up view of areas (strips) within a corn field where nitrogen fertilizer had not been applied.



Figure 3. Close-up view of the waterhemp weed patch.



Figure 2. Close-up view of the bean leaf beetle and grasshopper damage areas.



Figure 4. (left) Ground photo of the bean leaf beetle and grasshopper damage area (light area in center).



Figure 5. (right) Ground photo of the waterhemp weed patch.



Selecting the Imagery

In one example of the application of remote sensing to crop health, imagery from the IKONOS satellite was selected for a farm in southeast South Dakota. The four-meter spatial resolution of IKONOS multispectral data makes it possible to detect relatively small areas within a field that are affected by weeds and/or disease. The near-infrared band that is part of the IKONOS multispectral image data is especially useful for agricultural applications because of the high infrared reflectance that is characteristic of healthy vegetation. False color composites of the July 17, 2002, imagery were prepared using IKONOS bands 4 (near-infrared), 2 (red) and 1 (blue).

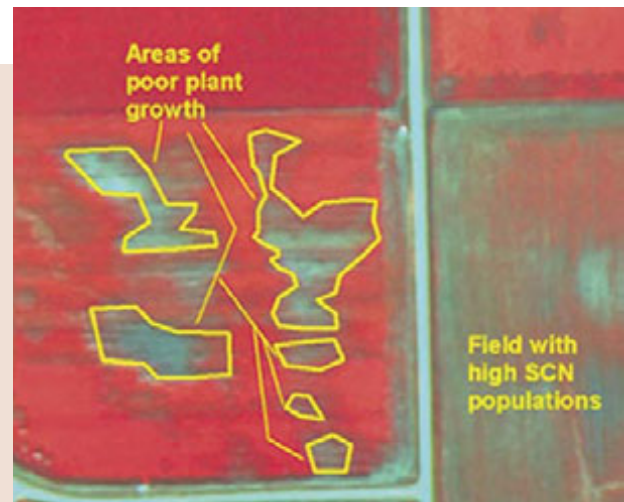


Figure 7. Soybean cyst nematode (SCN) infestation in a soybean field.

Applying the Imagery

In one IKONOS image (Figure 1), several abnormalities were observed within the fields. Within a soybean field, insect (bean leaf beetle and grasshopper) damage was detected (Figure 2) and a waterhemp weed patch was apparent (Figure 3). On-the-ground photos of the insect damage area and the waterhemp weed patch are shown in Figures 4 and 5, respectively. In an adjacent cornfield, areas where nitrogen fertilizer was not applied could be distinguished (Figure 6). In a second IKONOS image (Figure 7), areas of poor plant growth due to soybean cyst nematode (SCN), which attack the roots of soybeans, causing the plants to be stunted, yellowed and less vigorous, were identified.

The images assisted the land manager to find these problem areas in a timely manner. The economic advantage to the land manager is the reduced cost of pesticides and herbicides, because they are applied only to those areas where the imagery showed insect or weed problems.

Without the advantage of remotely-sensed imagery, the pesticides and herbicides would be applied to the entire field. The environment also benefits because of the reduced amount of pesticide and herbicide on the landscape.

Remote sensing is becoming increasingly important for farmers, ranchers, crop consultants, and university researchers. As this example shows, near real-time imagery is important for applications that require timely in-field intervention. Such applications include the detection of diseased areas, insect and weed infestations, and nutrient deficiencies. However, historical imagery is also of value to land managers and researchers. Current-year imagery in combination with imagery of the same area from previous years can be used for year-to-year comparisons, such as the movement and/or spread of weeds or disease. Adding other layers of information such as soil type, elevation, and crop yield is valuable for field management purposes — for example, identifying which areas require more fertilizer for the next growing season.



Remote Sensing Enables Census of Lake Water Quality

Marvin Bauer and Leif Olmanson
(University of Minnesota)

Figure 1. Measurement of lake water clarity with a Secchi disk and examples of varying lake clarity from high (left) to low (right).



Defining the Problem

Minnesota, known as the “Land of 10,000 Lakes,” actually has about 12,000 lakes larger than 10 acres in size. They are a critical component of the state’s economic, environmental and natural resources with many ecological, aesthetic and recreational benefits. Protecting the quality of Minnesota lakes is a priority for state and local agencies. The Minnesota Pollution Control Agency (MPCA) has been assessing lake water quality since 1973 and its lake monitoring activities accelerated with passage of the Clean Water Legacy Act in 2006. While effective management and protection require both current and historical information on the condition of lakes, conventional observations and measurements are made yearly on only about 1,000 lakes. This number is a relatively small proportion given the lakes’ importance to the environment, quality of life and economic vitality of the state.

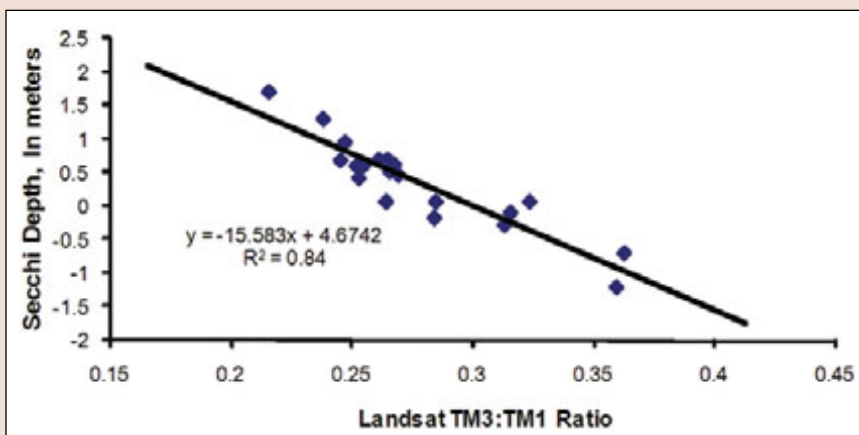


Figure 2. Relationship between Secchi depth measurements of water clarity and Landsat spectral response.

An important measurement made by the MPCA, along with the local agencies and the Citizen Lake Monitoring Program that the MPCA coordinates, is Secchi depth (Figure 1). Secchi depth is the distance light penetrates water; it is a measure of water clarity and a key indicator of water quality. In Minnesota, lake clarity is primarily determined by the amount of phytoplankton (algae) present, although in some lakes soil particles and humic matter may also contribute to decreasing clarity. Lake clarity is a useful measure because it is directly related to human perceptions of quality (especially for swimming) and to the abundance of algae. With Secchi depth information, the lakes' trophic state or nutrient concentrations and biological productivity can be determined.

Selecting Satellite Imagery

There is a strong relationship between water clarity, measured by Secchi depth (Figure 2), and the reflectance of water in the red and blue spectral bands of satellite imagery. Sunlight penetrates clear water, but is reflected from waters with sediment or algal growth (Figure 3). This relationship, particularly the ratio of the red and blue spectral bands of Landsat, makes it possible to estimate lake clarity using remote sensing. Landsat data are particularly well suited for monitoring lake water clarity because: (a) the relationship between water clarity and spectral-radiometric response is strong, (b) the image coverage of about 12,000 square miles enables surveying of thousands of lakes over large areas, (c) the 30-meter resolution is suitable for practically all lakes and can provide information about variability within a single lake, (d) imagery has been regularly collected since 1972, and (e) acquiring the imagery is very cost effective for making state and regional assessments.

Figure 3a. True color Landsat image of Lake Minnetonka, Minnesota, and surrounding area. The clearest water appears black; water reflecting more light contains more algae or sediment, and appears green to blue-green in this image.

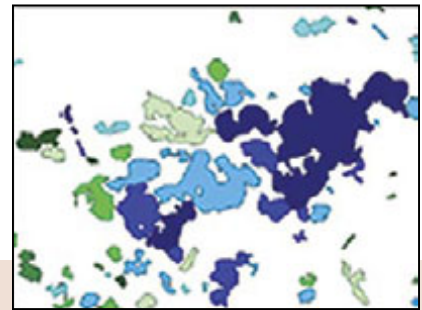
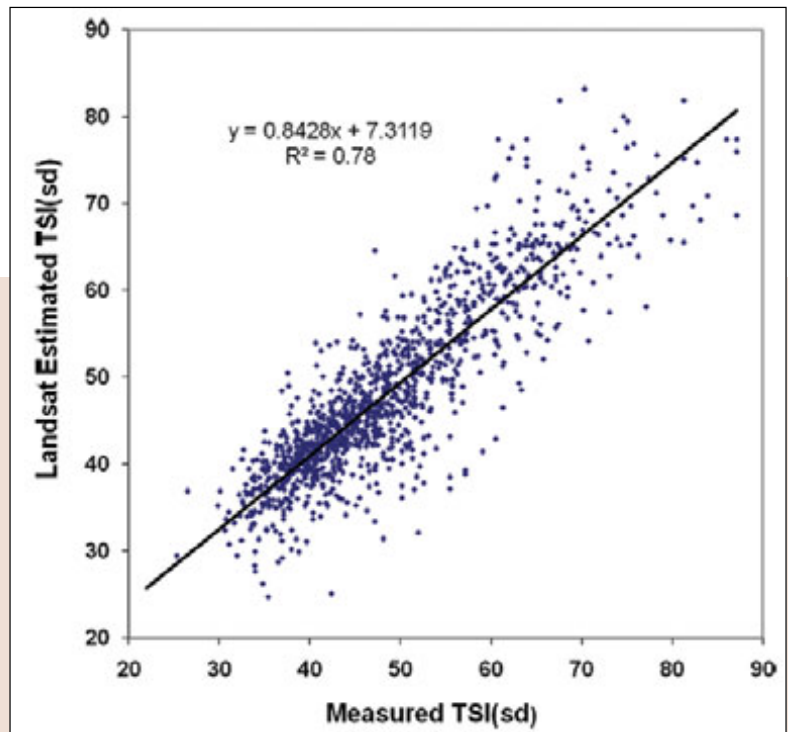


Figure 3b. Lake clarity classification map. The highest clarity is dark blue, moderate clarity lakes are light blue and light green and low clarity is dark green.

Figure 4. Comparison of estimates of lake clarity from in-situ observations and from Landsat images. TSI(sd) is trophic state index (Secchi depth).



Applying the Satellite Imagery

Landsat images selected to determine lake clarity must be clear (cloud-free) and acquired within three days of Secchi depth observations during mid-July to early September when the amount of algae and chlorophyll are at a maximum and lake clarity is at its seasonal minimum and quite stable. Following geometric correction, an unsupervised classification is performed to generate a “water only” image. Using a representative sample of lakes with Secchi data and a range of clarities from low to high, a multiple regression model relating Secchi depth to the Landsat spectral responses is developed (Figure 2). Models are developed for each path of Landsat images and then applied to the Landsat digital numbers for each lake, providing estimates of the water clarity for all lakes greater than 20 acres in size. An example of the agreement between in-situ observations and Landsat estimates of lake clarity is shown in Figure 4.

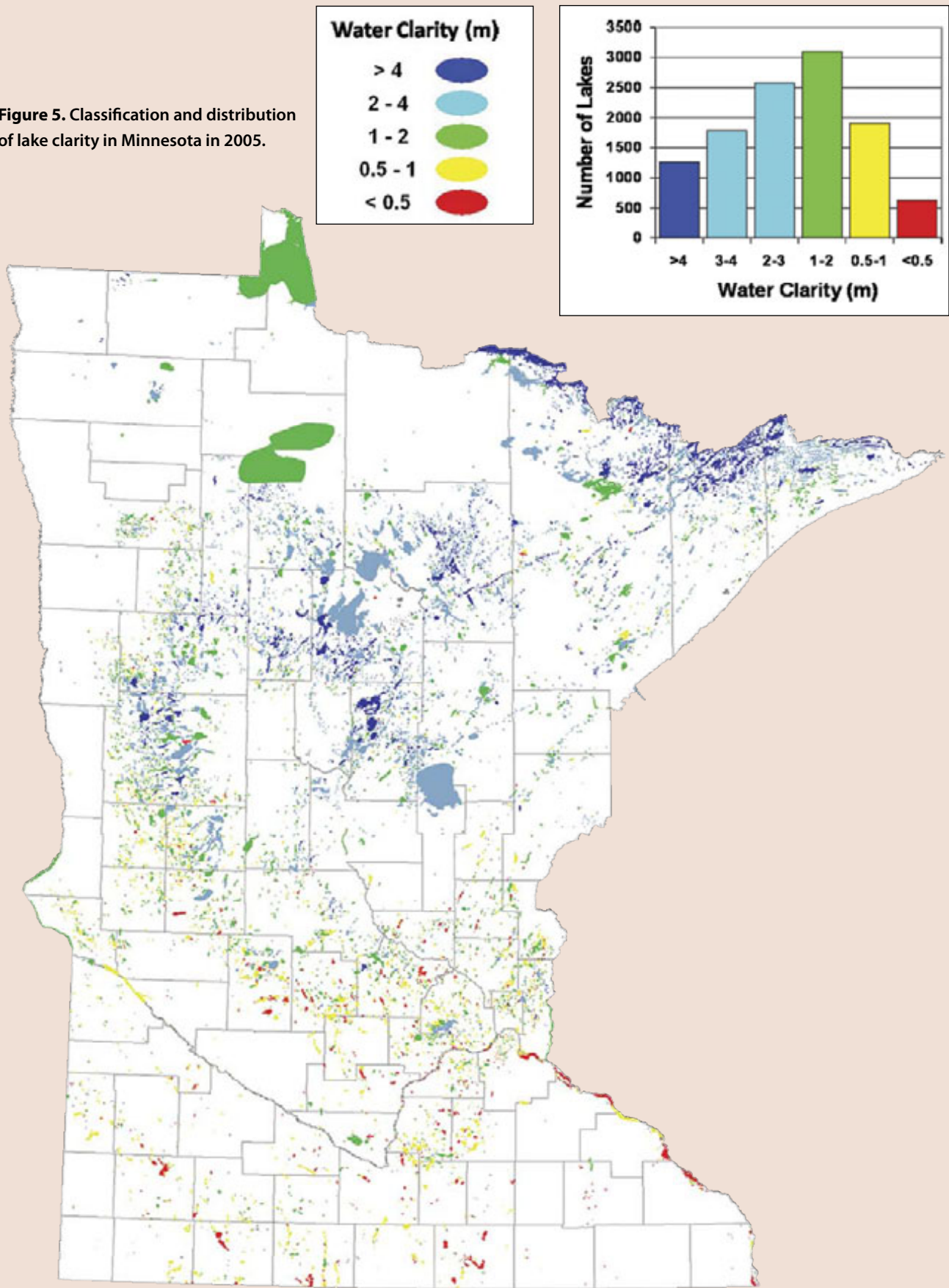
Landsat images acquired at approximately five-year intervals over a 33-year period — 1975, 1985, 1990, 1995, 2000, 2005 (shown in Figure 5) and 2008 — for the

entire state of Minnesota have been classified. More than 10,500 lakes are included, providing an unprecedented assessment of lake water quality in terms of number of lakes and geographic and temporal extent. The data have been analyzed for temporal and geographic patterns and trends, as well as for relationships to land use and other factors that may cause changes in lake quality. The analysis indicates relatively stable conditions statewide, but there are significant variations among ecological regions and watersheds, as well as for individual lakes. Water clarity is strongly related to lake depth, with deep lakes generally having higher clarity than shallow lakes. Agriculture and urban land uses are correlated with lower water clarity, while an increasing proportion of forest cover (up to about 45 percent) is correlated with higher water clarity.

The data are being used by the MPCA and other agencies to identify problem lakes needing management and protection activities. Data for all lakes and years are available in the LakeBrowser, a web-based mapping tool that enables search and display of results for individual lakes: water.umn.edu.



Figure 5. Classification and distribution of lake clarity in Minnesota in 2005.





Remote Sensing Enables Modeling of Groundwater Pollution Risk

James W. Merchant (University of Nebraska–Lincoln) and Patti R. Dappen (New Mexico Highlands University)

The acronym, DRASTIC, is derived from the seven factors used: **D**epth to water table, **R**echarge (net), **A**quifer media, **S**oil media (texture), **T**opography (slope), **I**mpact of the vadose zone and **C**onductivity (hydraulic) of the aquifer. The model, which is formulated as a weighted linear combination ($D_{RW} + R_{RW} + A_{RW} + S_{RW} + T_{RW} + I_{RW} + C_{RW} = \text{Index of Pollution Potential}$), is implemented as shown in Figure 1 (r_r is a rating value and w_w is a weight applied to each factor [Table 1]). The index computed is dimensionless and must be interpreted within a particular geohydrologic setting; however, higher index values generally indicate higher risks of groundwater pollution.

Defining the Problem

Groundwater is the principal source of drinking water for nearly 2 billion people around the world. In the United States, approximately 40 percent of the public water supply, serving over 74 million people, is derived from groundwater. In many locales, increasing attention is being directed toward groundwater pollution as both nitrate and pesticide concentrations in excess of national health standards have been found. Concerns about human health effects stemming from use of contaminated water have heightened pressure on public agencies to better manage and protect public water supplies. However, protection strategies need to be targeted so that limited staff and financial resources can be focused on those areas most threatened.

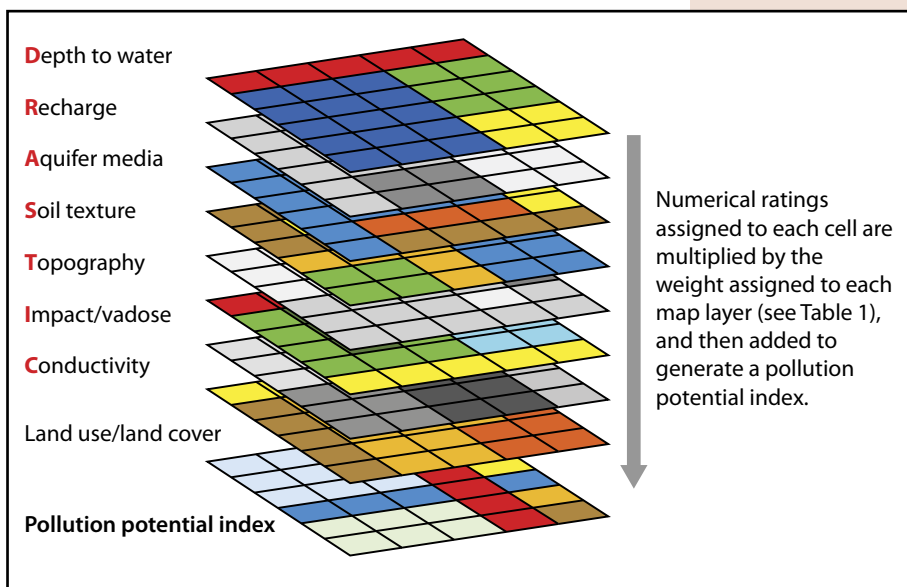


Figure 1. The DRASTIC model is implemented by overlaying in GIS gridded maps that portray Depth to water, Recharge, Aquifer geology, Soil texture, Topographic slope, Impact of the vadose zone and Conductivity (hydraulic) of the aquifer. A numerical “pollution potential” index is computed for each grid cell using ratings and weights that reflect the importance of each variable in determining groundwater pollution risk (e.g., Table 1). In this study, land use derived from remote sensing, was added as an additional map layer.



Figure 2. Nearly 45 percent of the land in York County is typically used to grow irrigated corn.

DRASTIC, a model designed to evaluate the potential for a groundwater resource to become polluted, has been widely used to identify what areas are at risk and to what degree (Figure 1).

A shortcoming of the DRASTIC model is that it does not account for the influence that land use has on groundwater quality. It is, however, well known that areas characterized by intensive row-crop production are especially vulnerable to groundwater pollution. Fields of irrigated crops are particularly important because rain and irrigation water can accelerate transport of nutrients into groundwater. Work in York County, Nebraska (Figure 2), a county dominated by irrigated agriculture, demonstrates that the DRASTIC model can be enhanced by incorporating information on land cover and land use provided by remote sensing.

Table 1. Ratings and weights for DRASTIC factors, including land cover. Land cover ratings were determined by the average amount of nitrogen fertilizer typically applied to various crop types.

FACTOR	WEIGHT	CLASS	RATING
Depth to water	19%	0–5 feet	10
		5–15 feet	9
		15–30 feet	7
		30–50 feet	5
		50–75 feet	3
		75–100 feet	2
		100+ feet	1
Aquifer recharge	12%	2+ inches	3
		0–2 inches	1
Aquifer media	7%	Sand and gravel	8
		Glacial till	5
Soil media	19%	Sand	10
		Silty loam	4
		Clay loam	3
		Nonaggregated clay	1
Percent slope	7%	0–2%	10
		2–6%	9
		6–12%	5
		12–18%	3
		18+%	1
Vadose zone	12%	Silt/clay	3
		Sand and gravel with silt and clay	7
Hydraulic conductivity	5%	300–100 gdp/ft ²	2
		100–1 gdp/ft ²	1
Land cover	19%	Irrigated corn	9
		Dryland corn	8
		Irrigated sorghum	6
		Dryland sorghum	5
		Irrigated small grains	5
		Dryland small grains	4
		Urban	4
		Other agricultural lands	4
		Irrigated alfalfa	3
		Irrigated soybeans	3
		Dryland soybeans	2
		Dryland alfalfa	2
		Roads	2
		Summer fallow	1
		Bare fields	1
Trees	1		
Water	1		
Wetlands	1		

Figure 3. Classification of land use and land cover from Landsat ETM+ data, York County, Nebraska. Center-pivot (circular) and rectangular agricultural field patterns, representing diverse crop types that contribute differing levels of risk, predominate across the map; urbanized areas appear in grey.



- | | |
|---|---|
|  Corn |  Open Water |
|  Soybeans |  Riparian Forest and Woodlands |
|  Sorghum |  Wetlands |
|  Alfalfa |  Other Ag. Lands |
|  Small Grains |  Irrigated Areas |
|  Range/Pasture/Grass |  Rivers and Streams |
|  Urban Land | |

Selecting the Imagery

For York County, Nebraska, land cover types and irrigation status were mapped at 30-meter spatial resolution using Landsat-7 Enhanced Thematic Mapper+ (ETM+) imagery; resolution and repeat coverage availability made this data the appropriate choice (Figure 3). Three dates of imagery obtained during the growing season (e.g., May, July, and September) were selected and used together in a hybrid classification strategy that employed both supervised and unsupervised methods. Field data, supplied by the USDA Farm Service Agency (FSA), were used to assess classification accuracy. The overall accuracy of mapping was determined to be 82.7 percent. Data for each of the seven DRASTIC factors, plus remote sensing-derived land cover, were reclassified using the rating system proposed by EPA researchers in 1987. Land cover ratings were determined by the average amount of nitrogen fertilizer typically applied to various crop types.

Applying the Imagery

The DRASTIC pollution potential index was calculated both with and without consideration of land cover. Rescaled index values above 5 were mapped (Figures 4 and 5). Areas that exceeded the national health standard of greater than 10 parts per million nitrate-nitrogen were identified from 237 water wells and mapped along with the results of DRASTIC calculations. When land cover was used to compute the DRASTIC index, the area predicted to be at risk was better correlated with regions observed to have nitrate contamination in excess of national health standards (Figure 5). The area of York County predicted to be at high risk for groundwater pollution was substantially larger when land cover was considered than when it was not (Table 2).

Models such as DRASTIC, when modified to include land cover, can be helpful tools for targeting areas requiring protection of groundwater. Moderate resolution satellite imagery, such as Landsat ETM+, enables the frequent updating of land cover maps and repeat modeling of risk factors.

**York County, Nebraska
(same area as Figure 3)
Map Explanation
(Figures 4 and 5)**

DRASTIC index



Nitrate exceeding national health standards

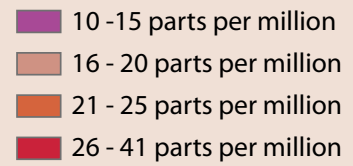


Figure 4. DRASTIC index and excess nitrate correlation without land cover data.

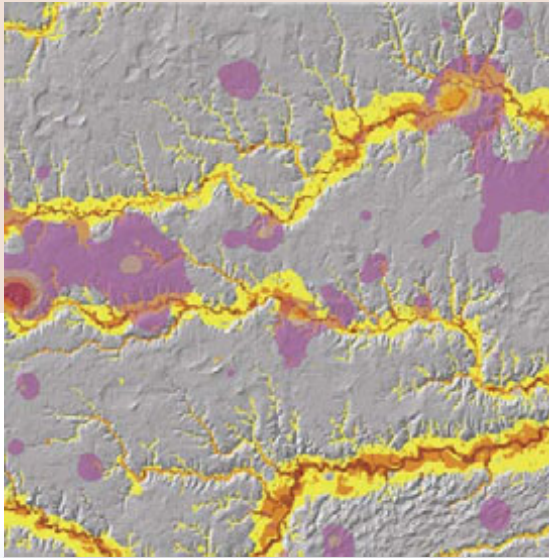
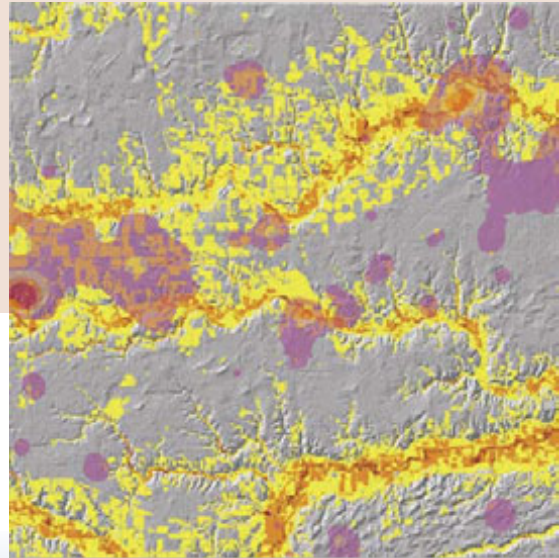


Figure 5. DRASTIC index and excess nitrate correlation with land cover data.



NITRATE CONTAMINATION RATES	DRASTIC WITHOUT LAND COVER (acres)	DRASTIC WITH LAND COVER (acres)
10-15 ppm	8,424.95	14,661.32
16-20 ppm	1,725.55	1,827.19
21-25 ppm	822.64	723.67
26-41 ppm	127.88	96.07

Table 2. Areas predicted to be at risk following modeling.



Remote Sensing Monitors Vegetation Changes Over Time

Demetrio P. Zourarakis (Kentucky Division of Geographic Information)

Defining the Problem

Kentucky's complex and rich landscapes and ecosystems are constantly changing as a result of human disturbances such as logging, mining and urbanization or through natural influences such as climate change and weather events. As much of the state's land area is not readily accessible for field investigations, monitoring landscape change using remote sensing is ideal. Results from two NASA-funded projects, the Kentucky Landscape Snapshot and Kentucky Landscape Census (Kentucky Geography Network Geoportal: <http://kygisserver.ky.gov/geoportal/catalog/main/home.page>) provided statewide estimates of rates of net forest loss in excess of 100 acres per day (41 hectares per day) from 2001 to 2005. The census also accounted for similar gains in compact areas of scrub/shrub and grassland/herbaceous land covers. Mining activities result in deforestation, and reclamation activities result in new growth, such as shrubs. Recent inquiries from agencies monitoring these activities in the state's Eastern Coal Field physiographic region prompted this exploratory search for imagery and methods to quantify the degree to which trends from previous years persist.

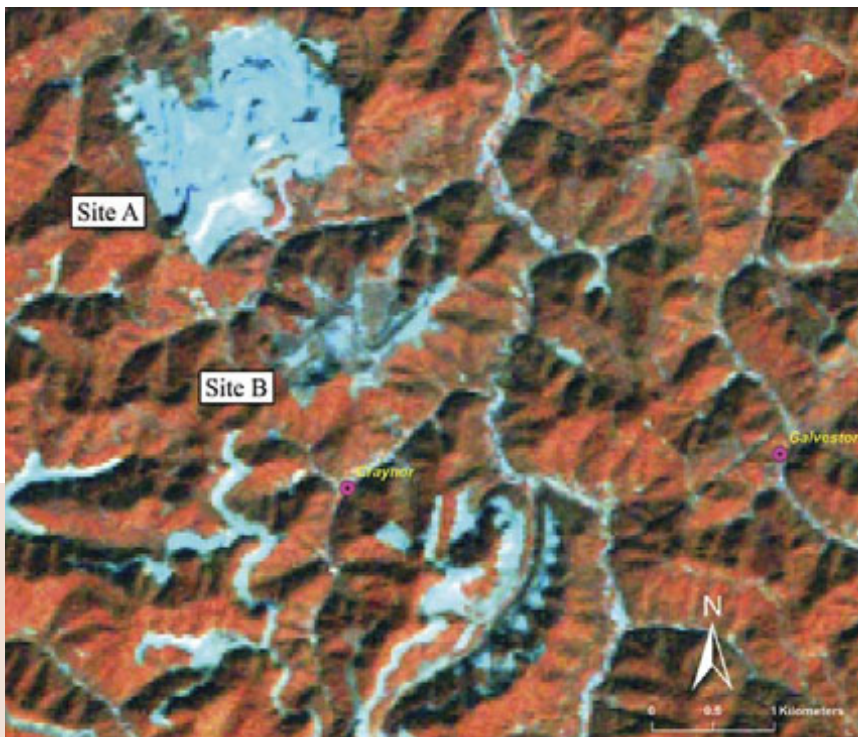
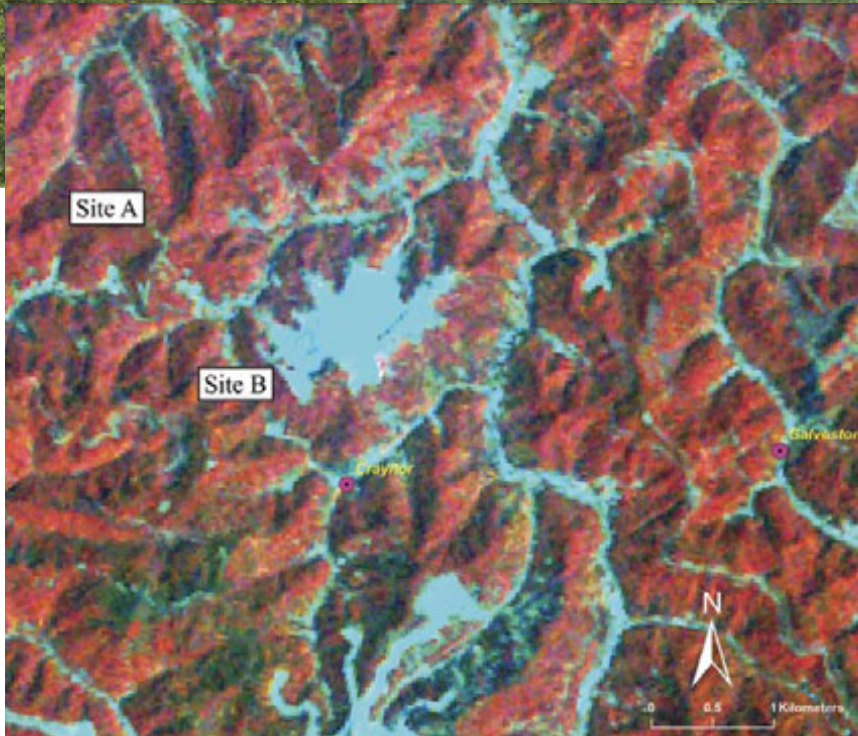


Figure 1. (top) 2005 Epoch Landsat 5 TM scene (R, G, B= bands 4, 2, and 1) of Floyd County, Kentucky

Figure 2. (bottom) 2008 Epoch Landsat 5 TM scene (R, G, B= bands 4, 2, and 1) of Floyd County, Kentucky

Figure 3. (top) 2006 NAIP Orthoimage (0.61 meter ground resolution; natural color) of Floyd County, Kentucky

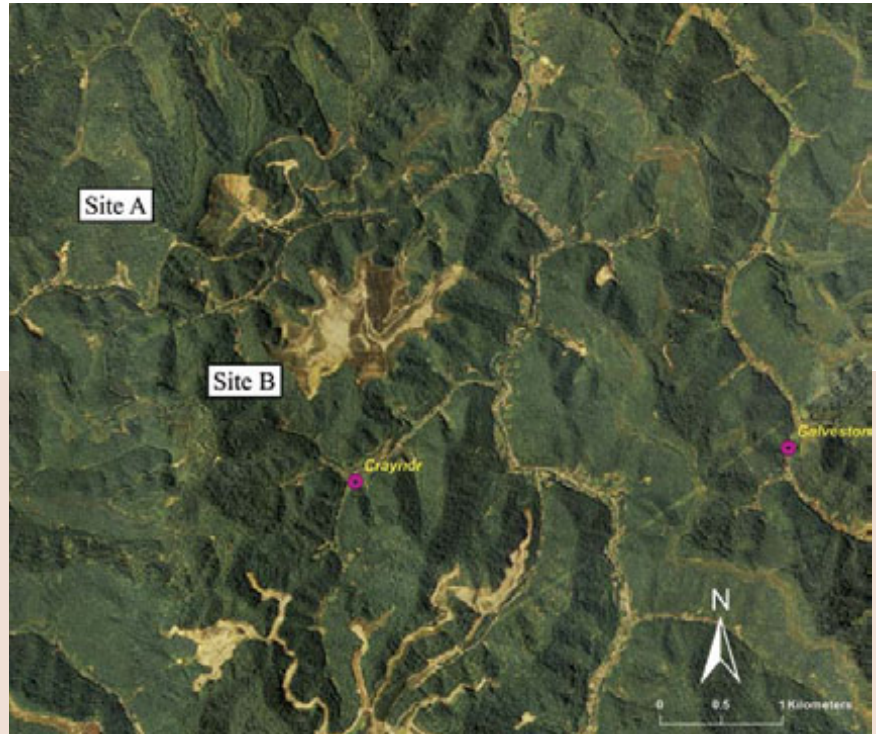


Figure 4. (bottom) 2008 NAIP Orthoimage (1 meter ground resolution; natural color) of Floyd County, Kentucky



Selecting the Imagery

The geographic area selected for a pilot study of the dynamics of vegetation change is located in Floyd County, a part of the state where forest constitutes the original, dominant land cover. The communities of Craynor and Galveston are within the study area. This region has experienced cyclic episodes of mining and deforestation and related land cover changes in recent years. Landsat 5, Thematic Mapper (TM) scenes from 2005 and 2008 (30 meters ground resolution) and true color, National Agricultural Imagery Program (NAIP) aerial photographs (0.61 meter and 1 meter ground resolution, respectively) taken in 2006 and 2008 were used to explore ways to quantify the vegetation changes happening over time (Figures 1, 2, 3 and 4). The satellite and aerial images chosen were from the mid-growing season time frame — when plants have leaves on — to provide evidence of both the presence and absence of vegetative covers.

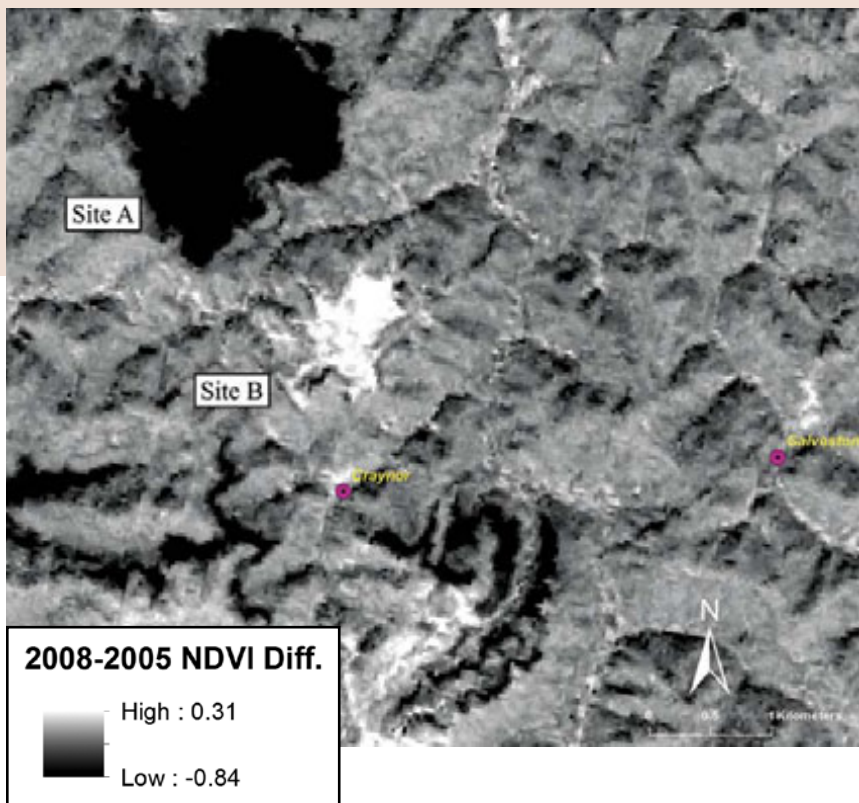


Figure 5. 2008-2005 NDVI difference image of Floyd County, Kentucky

Applying the Imagery

To reveal areas of potential forest loss, potential gain in vegetative cover, and potential for no change, the NDVI (Normalized Difference Vegetation Index) difference for the Landsat 5 TM, 2008–2005 image pair, and the second principal component (PC2) difference for the NAIP 2008–2006 image pair were calculated (Figures 5 and 6).

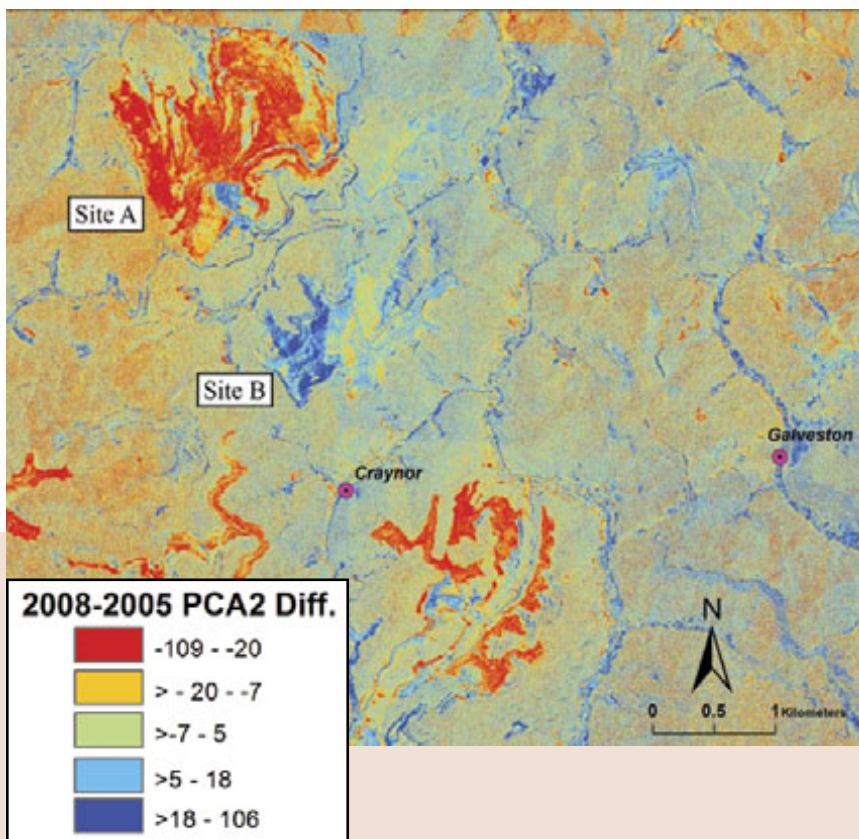


Figure 6. 2008-2006 PCA2 difference image of Floyd County, Kentucky

New deforestation from mining activities is visible in 2008 with re-vegetation due to reclamation of 2005 barren land occurring at the same time, as exemplified by site locations A and B, respectively. Clear patterns of deforestation and re-vegetation emerged in the time series imagery, visible in the false color infrared Landsat images and when photointerpreted from the 2006 and 2008 aerial images. Re-vegetated areas were associated with increases in NDVI and PC2.

Previously deforested areas that were experiencing new vegetative growth in 2005 were being denuded again by 2008 (Site A; Figure 7). In 2008, reclamation was ongoing and vegetation was being re-established on mined areas from 2005 (Site B; Figure 8). Results from this pilot study seem promising for the ability to construct a time series for land cover change detection that is based on archival imagery.

Figure 7. Oblique aerial photograph of site "A" taken in 2008.



Figure 8. Oblique aerial photograph of site "B" in 2008.



Remote Sensing Enables Watershed Analysis for Land Use Assessment and Planning

Brian D. Lee, Ph.D. and Corey L. Wilson (University of Kentucky),
 Angela Schörgendorfer, Ph.D. (IBM T.J. Watson Research Center)

Defining the Problem

The availability of water is a limiting resource for economic development in many parts of the world. Watershed boundaries, rather than political boundaries, increasingly make sense as better spatial definitions for addressing water resource issues, but not all watersheds are the same in their form and function. Given this variability, the specific similarities and differences need to be determined to inform on-the-ground management decisions to improve environmental and economic activity.

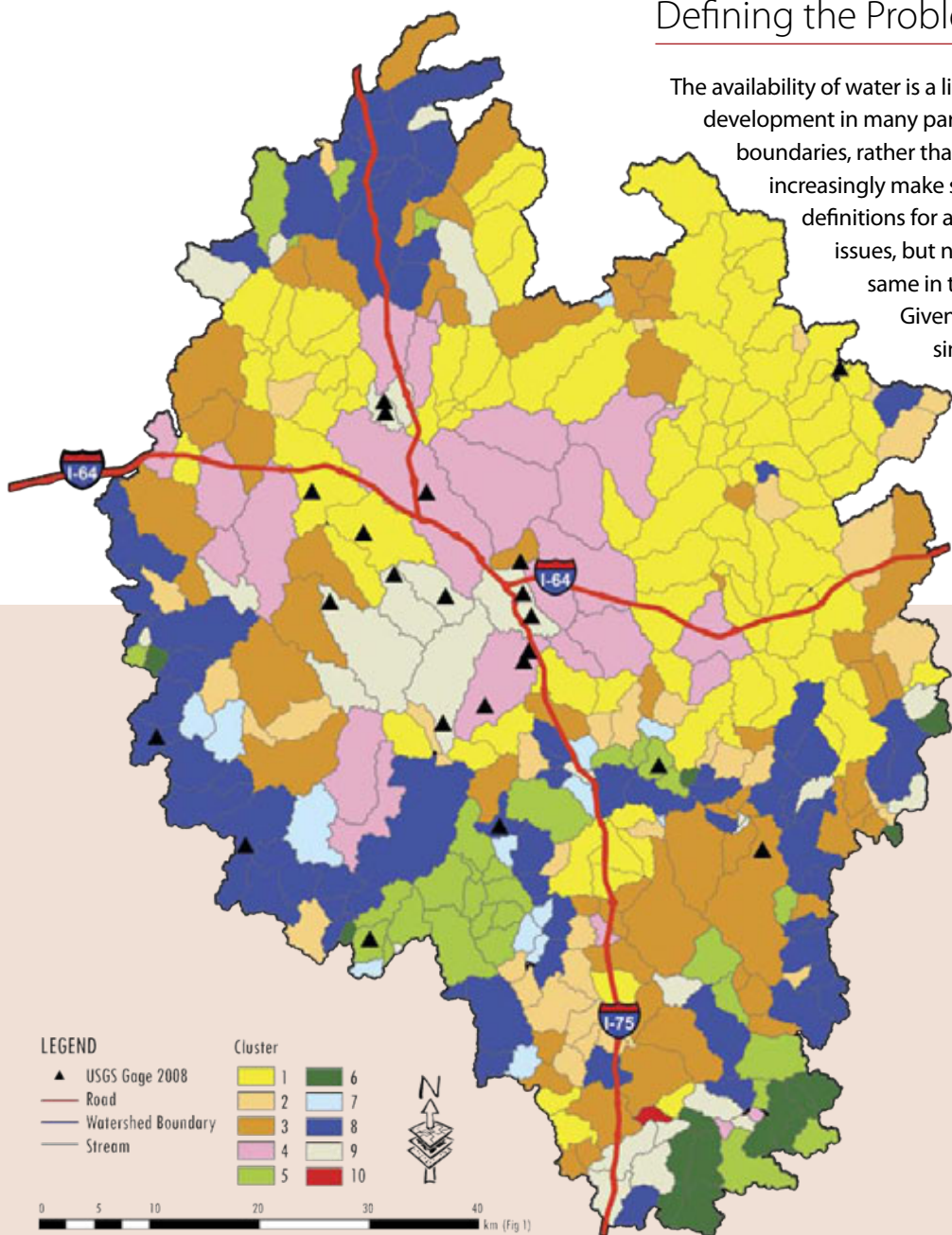


Figure 1. A map of watersheds in Central Kentucky.

Figure 2. Group 9 — This group represents more urbanized watersheds. Road density is greater, as is the number of river bank roads in this cluster. The average impervious cover for all scenes in this cluster is nearly 10 percent, but one watershed has as much as 45 percent impervious cover. The amount of forest cover, tree canopy cover, and pasture/hay land cover in these watersheds is highly variable.

Several types of remote sensing imagery and related data can identify watershed characteristics and be used to cluster watersheds by geomorphic and human-influenced factors such as proximity of agriculture and roads to streams, percentage of impervious (paved) surfaces, slope of land surface, and land cover (trees, agriculture, pasture). All of these factors affect the quality and availability of water.

Selecting the Imagery

This project explores the opportunities for describing over 350 subwatersheds across an urban-rural continuum in central Kentucky. Over 50 landscape-scale factors have been used to describe watershed conditions, and several of these are derived from Landsat data. The Landsat data can be used to describe the proportion and spatial configuration of urbanization and imperviousness, as well as agriculture and forest-cover characteristics. These data are available for most of the United States from the Multi-Resolution Land Characteristics Consortium (MRLC). More specifically, National Land Cover Database 2001 (NLCD2001) data based on Landsat Enhanced Thematic Mapper+ (ETM+) were used in this project. These data help to group watersheds having similar characteristics.





Topographic data are also valuable data for this work. In particular, Digital Elevation Model (DEM) data and Shuttle Radar Topography Mission (STRM) 2000 data are used to describe landforms for determining surface flow characteristics and slope. These topographic data are combined with Landsat-based land cover data to identify watersheds that have large amounts of agricultural crops growing on relatively steep topographic slopes. By identifying this confluence of factors, areas at increased risk of erosion can then be identified.

Applying the Imagery

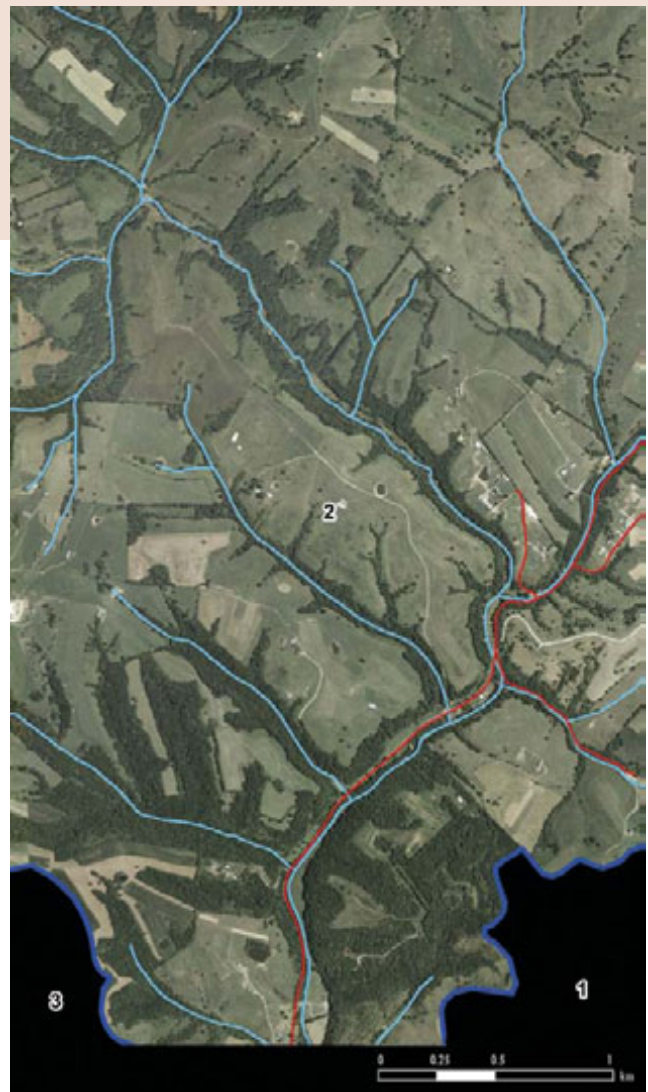
Using multiple indicators such as impervious cover, tree canopy cover, other land cover classes, and geographic features, the watersheds are statistically separated into groupings. In this example, 10 groups (statistical clusters) were identified for the Central Kentucky study area. Although 10 groups

Figure 3. Group 1 — Topographically these are some of the most gently sloping watersheds with some of the smallest percentages of tree canopy cover and interior forest. These watersheds also have the highest percentage of pasture/hay land cover as crops on slopes 3% or greater, and also have some of the lowest proportions of riparian forest and relatively higher percentages of riparian agriculture.



Figure 4. Group 6 — These watersheds are found generally in the south and east of the study area and are among the highest, smallest, topographically roughest, and steepest watersheds. On average, these watersheds have almost 75 percent forest cover. This cluster also has some of the lowest percentages of pasture/hay land cover. It also has a little more than 50 percent of its riparian area in forest cover and some of the steepest stream valleys on average.

Figure 5. Group 2 – These watersheds have a greater than average percentage of riparian forest than some of the other clusters and less than average impervious cover. They have relatively higher percentages of pasture/hay land cover as well as pasture/hay on slopes 3% or greater. These watersheds are generally found distributed across the study area individually or in small geographic groupings.



were identified in this study, four groups are shown and described here in order to demonstrate the characteristics used to define the groups.

The clustering process is intended to improve watershed categorization for prioritization when identifying rehabilitation and protection, identifying effective field-based monitoring strategies, and developing and implementing action plans for watershed management. The analysis used geomorphic and human-influenced variables to categorize watersheds and relied on readily-available imagery that could serve as the basis for a network that would monitor nonpoint sources affecting water quantity and quality. Efforts are underway to expand this work to the rest of Kentucky with additional sources of data such as the 2006 National Land Cover Data and the revised 2001 National Land Cover Data.



Remote Sensing Reveals Relationships Among Whitebark Pine, Bark Beetles and Climate Variability

Rick L. Lawrence and Jeffrey Jewett (Montana State University)



Figure 1a. The Landsat image is an infrared false color composite of Big Sky ski resort.



Figure 1b. A true color high-resolution image of the region around Avalanche Peak from Google Earth. Both areas shown in Figure 1a and 1b have experienced significant forest mortality. To the unaided eye, forest mortality is evidenced by the reddish trees, but difficult to see in the Landsat image. Through transformations of the Landsat image, however, forest mortality was mapped reasonably well.

Defining the Problem

Whitebark pine (*Pinus albicaulis*) serves as a subalpine keystone tree species that regulates snowmelt runoff, reducing soil erosion, facilitating the growth of other plants, and providing food for wildlife. Its seeds are also a key food source for grizzly bears, a species listed under the Endangered Species Act. Mountain pine beetle (*Dendroctonus ponderosae*) is an ideal bio-indicator of climate change, as its life cycle is temperature sensitive. Western North America is currently experiencing the largest outbreak of mountain pine beetles on record, and evidence suggests that a changing climate has accelerated the life-cycle of this bark beetle. The mountain pine beetle poses a threat to the health of whitebark pine in the Greater Yellowstone Ecosystem and has been a key factor in keeping the grizzly bear on the endangered species list in this area. Remote sensing images, combined with historical climate data, are well suited to studying these relationships because they can efficiently cover large areas that cannot practically be covered on the ground, while at the same time providing the regular coverage needed to address the changing conditions that have occurred.

Selecting the Imagery

Landsat imagery provided key advantages for addressing this problem compared with other sources of data. First, a single Landsat scene encompasses the entirety of Yellowstone National Park, making scene-to-scene corrections unnecessary. Second, the unprecedented Landsat archive meant that quality data are available from before the mountain pine beetle infestation became epidemic to today. Third, the broad spectral range covered by Landsat imagery has been shown to be important in detecting beetle infestations. Finally, the provision by the

USGS of Landsat imagery at no additional cost meant that yearly imagery could be obtained easily for every year from 1999 to 2008 (except 2000, when persistent smoke from fires was present) for our analysis. High resolution time series imagery was available for some parts of Yellowstone National Park and provided key reference data for calibrating the Landsat imagery.

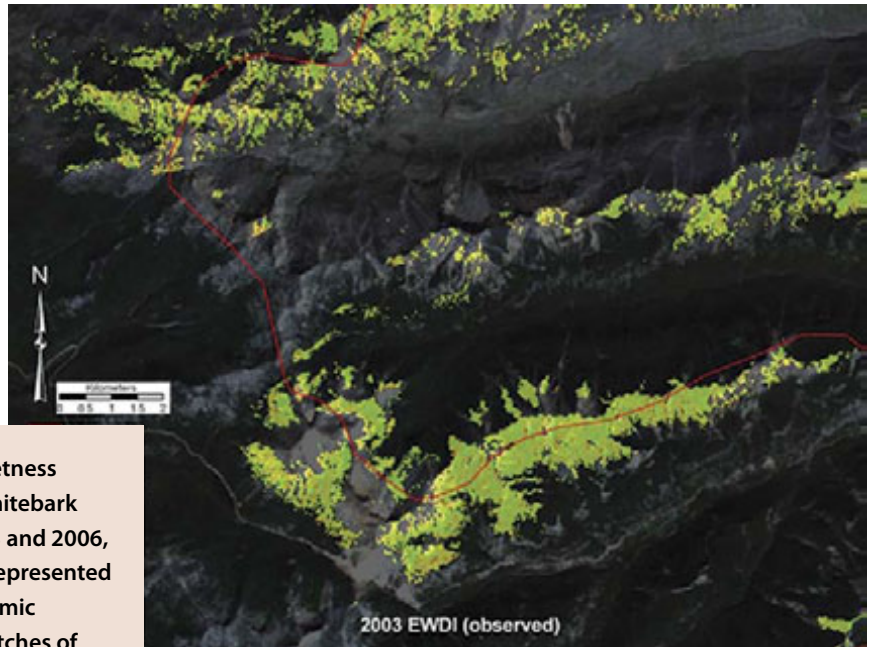


Figure 2. The difference in the Landsat wetness index (EWDI) was a strong predictor of whitebark pine mortality. In these images from 2003 and 2006, we see how a minor infestation in 2003 (represented by warm colored pixels) became an epidemic infestation by 2006. One can see small patches of yellow, orange, and red in the top, 2003, image, indicating limited whitebark pine mortality. These small patches have grown to extensive areas of orange and red in the 2006, image, indicating that the infestation has become extensive.



Applying the Imagery

Differences in forest canopy wetness, as determined from each of our Landsat images, was a strong predictor of whitebark pine mortality from mountain pine beetle. This measure of tree mortality was then compared to climate variability, including where conditions were warmer, colder, wetter, or drier than normal. Other factors that might be related to forest mortality were topography and whether there was nearby mortality, and therefore a beetle outbreak, within the prior three years. This last factor was important in the analysis because beetles in the whitebark pine zone have historically had a three-year life cycle, but it has been hypothesized that the life cycle might be getting shorter with increasing warmer temperatures.

Climate variability was strongly correlated with Landsat-based measures of whitebark pine mortality. Warmer and drier conditions were related to increased mortality. It is believed that warmer conditions favor beetle survival, while drier conditions decrease trees' ability to produce sap, which is their primary defense mechanism against beetle attack. Previous presence of beetles in an area was also related to forest mortality, as beetle attack nearby provides a population for future infestations, while beetle attack at a given location results in host tree depletion. This was the first study showing a link between climate variability and whitebark pine mortality across the Greater Yellowstone Ecosystem.



Remote Sensing Identifies Impacts of Climate Variability on Reservoirs

James W. Merchant (University of Nebraska–Lincoln) and Milda R. Vaitkus (University of Nebraska–Lincoln)

Defining the Problem

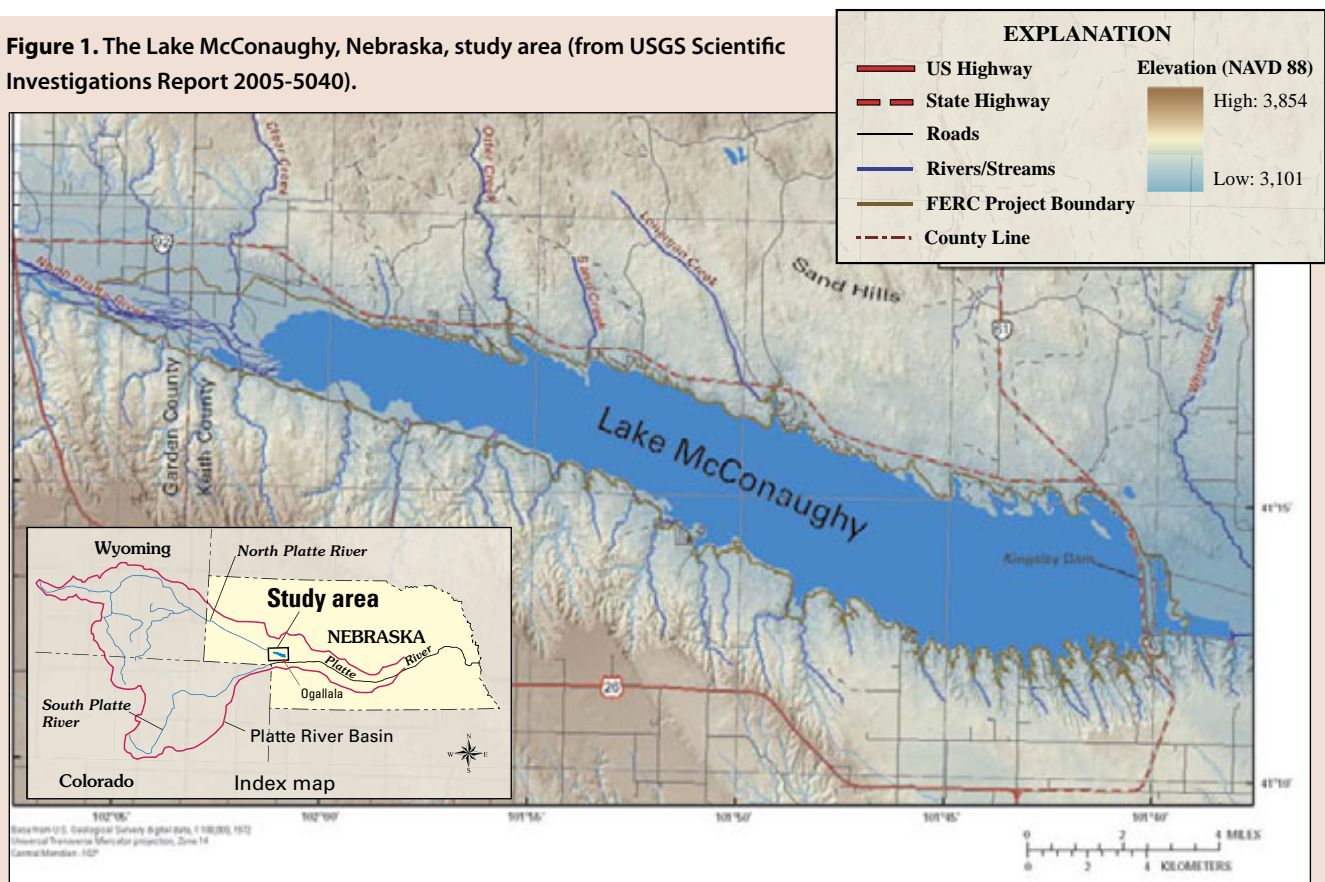
Reservoirs in the semiarid western United States are usually constructed to serve multiple functions such as flood control, recreation, irrigation and, in some cases, hydroelectric power generation. The water supply for most reservoirs is highly dependent on runoff from rainfall and snowmelt in their drainage basins. However, precipitation in the western United States is highly variable. Prolonged periods of drought are often interspersed with episodes of higher-than-normal rain and snowfall. Climate variability, therefore, greatly affects both water supplied to the reservoirs and their character. This study illustrates how satellite remote sensing has been used to monitor such impacts at Lake McConaughy, Nebraska. Understanding the way variations in climate affect

a major lake helps natural resources managers monitor the connections between climate and water resources.

Lake McConaughy (“Big Mac”), constructed over 70 years ago, is the largest body of water in Nebraska (Figure 1). Located on the North Platte River west of Ogallala, Nebraska, the reservoir is normally 22 miles long and 3 miles wide, covering an area of about 30,500 acres when filled to its maximum storage capacity of 1,900,000 acre-feet. Lake McConaughy has a drainage basin of some 28,000 square miles, encompassing parts of northern Colorado, southern and central Wyoming and western Nebraska.

Mean annual precipitation within Lake McConaughy’s drainage area varies from approximately 10 inches in the

Figure 1. The Lake McConaughy, Nebraska, study area (from USGS Scientific Investigations Report 2005-5040).



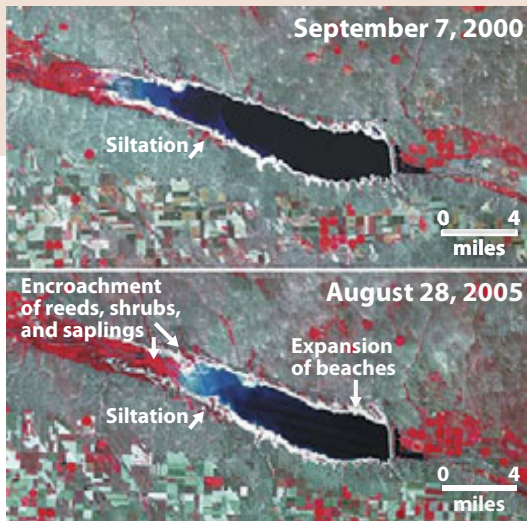


Figure 2. Landsat-5 Thematic Mapper images of Lake McConaughy, Nebraska, acquired in 2000 and 2005. The 2005 image clearly portrays the diminished lake extent and the encroachment of reeds, shrubs and saplings into the shallow western reach of the lake.



Figure 3. Landsat-7 Enhanced Thematic Mapper+ image of Lake McConaughy from August 2010. Note that the lake is filled to about 80 percent of its capacity, having risen 14 feet from the previous year. The white area shows the extent of the lake at its lowest level.

extreme western reaches to about 18 inches at Ogallala. Precipitation (including rain and snowfall) can, however, vary greatly from year to year. From 2000 to 2006 the basin experienced extreme drought. As water inflow to the reservoir diminished and lake levels dropped, irrigation releases were curtailed. Large expanses of sand and mud were exposed around the lake's periphery.

Beginning in 2007, the environment became wet again, with annual precipitation often exceeding the long-term average. Inflows into the lake in 2010 were near record levels as the lake approached full storage volume. In 2011, snowpack exceeded the average, producing even higher levels of runoff. Water was released from Lake McConaughy to keep the lake within its approved capacity. Excess water creates new problems for natural resources managers who must deal with potential flooding and threats to wildlife habitats downstream.

Selecting the Imagery

Landsat provides coverage of Lake McConaughy, its drainage basin and downstream environs approximately every 16 days, increasing the opportunities for images to be acquired in critical late spring and mid-autumn time periods each year. These times are important because of the high runoff that typically follows snowmelt in spring and lake drawdown in fall following the irrigation season. Exact dates of coverage are, of course, dictated by cloud cover. Comparison of images taken in different years allows analysts to observe many of the impacts of climate variability on the reservoir (Figures 2 and 3).

Applying the Imagery

The effects of the 2000–2006 drought and the pace of refilling the lake during wetter periods are clearly seen in Figure 3. As water inflow to the reservoir diminished, lake levels dropped. By 2005 the lake surface area was reduced to about 13 square miles, about half of normal. Extensive tracts of sand and mud were exposed by the dropping water levels. Vegetation invaded the shallow delta at the western end of the reservoir where most water enters the lake, and siltation was occurring much farther into the lake than is usually evident.

In 2007, the region entered a wetter period, and the lake was replenished in just four years (Figure 3). By 2010, the lake surface elevation stood at 3,263 feet above mean sea level, nearly 65 feet higher than the lake's lowest elevation in 2004. The lake surface area expanded to over 48 square miles, and sand and mud flats exposed during the drought were again covered by water.

Images acquired by Earth-observing satellites, such as Landsat, provide important information about the impacts of long-term precipitation variability on reservoirs in semiarid areas. Landsat imagery of Lake McConaughy shows that both the effects of prolonged drought and the consequences of above-normal rain and snowfall are evident. Such imagery can be used by natural resources managers to help mitigate effects of abnormally low or high inflows to reservoirs, and can be employed in public education to improve understanding of the complex relationships between climate and water resources.



Remote Sensing Assesses Flooding at Devils Lake, North Dakota

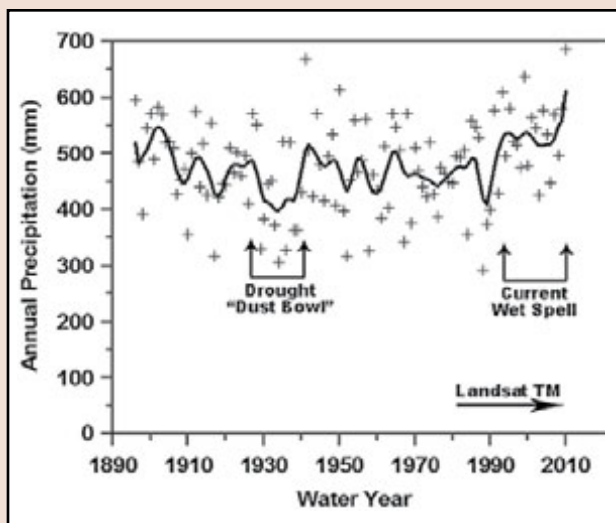
Bradley C. Rundquist and Paul E. Todhunter
(University of North Dakota)

Defining the Problem

The natural variability of climate affects water resources and hazards experienced in a region (Figure 1). The variability of annual precipitation between an upper and lower threshold provides the basis for the water resources available to sustain the regional economy. For northeastern North Dakota, this economy includes rain fed agriculture (a mix of grain crops and row crops), livestock production (pasturage and hay production), recreation and tourism (on streams and lakes), and waterfowl feeding and breeding grounds provided by prairie pothole wetlands.

Years with annual precipitation amounts above and below a critical threshold create climatic hazards such as drought and floods. When precipitation levels are outside this critical zone, climatic disasters, such as the Dust Bowl drought of the 1930s (Figure 1) are likely outcomes.

Figure 1. Annual precipitation time series (plus signs) for Climate Division 3 (northeastern North Dakota) for water years 1896–2010. A nine-year moving average for the series is also shown (bold line). Peaks along the bold line indicate wet periods while troughs represent dry periods. The 1930s Dust Bowl and the current wet cycle are labeled, as is the range of availability for Landsat TM remote sensing data.



Since 1993, increased annual precipitation has produced riverine, wetland and lake flooding at Devils Lake, a terminal lake in the closed Devils Lake Basin of North Dakota. Remote sensing enables quantitative assessment of all three types of flood disasters.

Selecting the Imagery

Landsat Thematic Mapper's spatial resolution (30 x 30 meters) and spectral capabilities, in particular the reflected infrared bands, make it ideal for monitoring the impact of changes around Devils Lake. The U.S. Geological Survey's archive of Landsat TM data for the study area extends back into 1982 and spans the region's most recent drought-to-flooding cycle (Figure 1). This study uses Landsat TM scenes (Figure 2) corresponding to times when the level of the lake was extremely low (1991) and very high (2010). Also included are images illustrating changes in wetland extent (Figure 3) which, in the current flooding cycle, has had measurable impact on the region's agricultural economy.

Applying the Satellite Imagery

Researchers at the University of North Dakota's Department of Geography, and at North DakotaView at the University of North Dakota in Grand Forks, have developed an archive of data for the Devils Lake Basin, including Landsat TM imagery. The data are used to monitor changes in lake and wetland extent over time, and to assess the impact those changes have on the region's infrastructure and on its land use and land cover patterns.

The Landsat TM imagery shows that the water surface elevation of Devils Lake rose by 8.74 meters (28.67 feet) between August 31, 1991, and August 3, 2010 (Figure 2). Lake area increased by 354 percent, and lake volume grew by 520 percent during the same period. The lake expansion

Figure 2a. This image was acquired by Landsat 5 on Aug. 31, 1991, near the end of an extended dry cycle, when the water surface elevation of Devils Lake was 433.80 meters (1,423.22 feet) above mean sea level. To delineate the land/water interface, the band combination used is Red = TM Band 5, Green = TM Band 4 and Blue = TM Band 3. Labeled on this image are: (1) the City of Devils Lake; (2) Devils Lake; (3) Stump Lake, which was two separate lakes in 1993 (East Stump Lake and West Stump Lake); and (4) the City of Minnewaukan, which was about 13 kilometers from the shoreline in 1991.



Figure 2b. This image was acquired by Landsat 5 on August 3, 2010, when the water surface elevation of Devils Lake (labeled 2) was 442.54 meters (1,451.89 feet) above mean sea level. Note that Stump Lake (3), now a single lake, merged with Devils Lake in recent years. The City of Minnewaukan (4) now sits on the lakeshore. Also note the change in the number and size of wetland ponds north of Devils and Stump lakes (5).



has resulted in more than \$1 billion in direct damages. This amount includes: money to raise federal, state, county and rural township roads and bridges, to construct levees for protecting the City of Devils Lake, to pay for relocation and buyouts for over 500 buildings, to repair damage to state park and recreational infrastructure, and to make repairs to utility and water-line infrastructure.

The direct cost of lost agricultural production to prime farmland within the basin, and the cost of associated secondary and tertiary activities, is substantial, but undetermined. Remote sensing is critical to monitoring changes in the surface water extent of Devils Lake and wetlands in the Devils Lake Basin. It is the only economically viable way to get timely information about changes in surface water extent over such a large area and to predict and assess the impact of

rising water on local communities, transportation networks and agricultural land use.

A tremendous expansion in the total number, average depth and permanence of prairie wetlands has also accompanied the flooding cycle, as shown in Figure 3. This expansion has significantly threatened the rural transportation network, caused economic hardship for the region's agricultural producers because of inundated agricultural land, and delayed farming and the increased fragmentation of the agricultural landscape. The dramatic increases in waterfowl and game fish associated with the lake rise and wetland expansion have offset only a small portion of the regional agricultural losses.

Figure 3. Figure 3a (left) was acquired by Landsat 5 on August 31, 1991, and Figure 3b (right) on August 3, 2010. Note the overall increases in wetland area, which has reduced cropland area significantly, especially in the vicinity of label 1.





Remote Sensing Maps Co-Produced Water from Natural Gas Extraction

Ramesh Sivanpillai and Scott N. Miller
(University of Wyoming)



Figure 1. Waters produced from the extraction of Coal Bed Natural Gas flow into an ephemeral stream in the Powder River Basin of Wyoming.



Defining the Problem

Water produced during the extraction of Coal Bed Natural Gas (CBNG) has been discharged into ephemeral streams (Figure 1) or small retention ponds (Figure 2) throughout the Powder River Basin in Wyoming. Land management agencies are tasked with the monitoring of these water bodies, as constituents present in the co-produced water can degrade the quality of surface water.

However, collecting information about these changes through field investigations is expensive and time consuming. Remotely sensed satellite data can be used to locate and monitor these water bodies, and link them to environmental indicators for land management. For example, the risk of West Nile Virus is increased in the region due to the presence of ponds and drainage waters. The primary risk is that waters adjacent to the ponds form habitats for the primary vector of West Nile Virus, the mosquito *Culex tarsalis*. Mapping and monitoring can identify target areas for treatment to minimize virus exposure risk.

Figure 2. Retention ponds impound produced waters in the Powder River Basin of Wyoming.

Selecting the Imagery

Satellite images, such as those collected by Landsat or ASTER satellites, measure the amount of light reflected from various features on the ground. Differences in the reflected values between images can be associated with the type and magnitude of changes occurring on Earth's surface. Landsat images are collected every 14 (Landsat 7) or 16 (Landsat 5) days, enabling periodic monitoring of earth surface features. Satellite images serve as a relatively inexpensive source for monitoring features across large geographic areas.

Landsat 5 Thematic Mapper (TM), Landsat 7 Enhanced Thematic Mapper Plus (ETM+) and Advanced Spaceborne Thermal Emission and Reflection Radiometer (ASTER) data were used to map water bodies in the Powder River basin of Wyoming. Landsat TM and ETM+ multispectral data are acquired in 30 meter spatial resolution across six spectral bands, while 3 bands of the ASTER data are acquired in 15 meter spatial resolution. The utility of higher spatial resolution data for detecting water bodies, ranging in size from relatively small to quite large, was tested. The lower resolution Landsat results were compared with the higher resolution ASTER data and with pan-sharpened Landsat data, which is created by merging ETM+ multispectral data (30 meters) with ETM+ panchromatic data (15 meters).

Applying the Imagery

TM (Figure 3) and ETM+ images were digitally processed for mapping water bodies based on the amount and pattern of light reflected by these features. Clear water bodies appear dark in infrared bands because they effectively absorb light, while turbid water bodies appear in lighter colors. The accuracy of mapping water bodies with pan-sharpened ETM imagery, in which the 15-meter panchromatic band was used to provide higher spatial resolution, combined with the 30-meter data for spectral information, was significantly higher than the original Landsat data for small water bodies. Large reservoirs were very accurately mapped, with both image types producing identical results (96 percent accuracy).

Figure 3. Retention ponds appear in differing shades of blue, and vegetation appears green in this Landsat TM image. The presence of sediments and floating vegetation in these ponds alter their appearance in the satellite image.



Figure 4. Retention ponds and other Earth surface features are shown in more detail in the higher resolution ASTER image.



ASTER images distinguish numerous small water bodies throughout the basin. The ASTER (Figure. 4) image had significantly higher accuracies for detecting clear and green-colored water bodies, but did not demonstrate significant improvement for detecting turbid water bodies. ASTER also showed significant improvements in detecting small water bodies. However, this improved performance was somewhat offset because other landscape elements in the ASTER image were easily misclassified as water. Overall, when compared to Landsat TM image, ASTER images accurately detected more water bodies but both images produced similar results for larger water bodies.

Pan-sharpened Landsat or ASTER data are useful for monitoring and mapping water bodies in the Powder River Basin and elsewhere. Periodically updated information derived from satellite images is used for identifying water bodies that require treatment.



Remote Sensing Enables Modeling of Soil Loss Susceptibility

Jackie Reed, John Congleton (University of West Georgia);
Rebecca L. Dodge (Midwestern State University)

Defining the Problem

Snake Creek Reservoir is a 650-acre reservoir located in Carroll County, Georgia. Nearly 30,000 people rely on the reservoir for drinking water. Erosion of soil from the surrounding landscape is a serious issue for the Carroll County Water Authority (CCWA) in managing the reservoir and preserving the quality of the water supply. Major known sources of erosion include new development construction sites, rural commercial operations, forestry, unpermitted roads (Figure 1) and off-road vehicle trails. Satellite images were used to identify where erosion was greatest. CCWA is now using this information to implement improved strategies for managing and preventing erosion.

Selecting the Imagery

Landsat Thematic Mapper (TM) imagery (Figure 2) provides current information about land cover and land use within the Snake Creek watershed, through digital image classification and field-based accuracy assessment. The imagery was chosen from the early growing season time frame, when plants still have their leaves, to enable mapping of diverse vegetation types and to highlight the occurrence of cleared ground.



Figure 1. One road 10 feet wide and 150 feet long can potentially deposit 4.6 tons of sediment into the reservoir annually. This illegal road trends directly down slope to the reservoir. It creates a direct “soil chute” feeding soil into the reservoir.

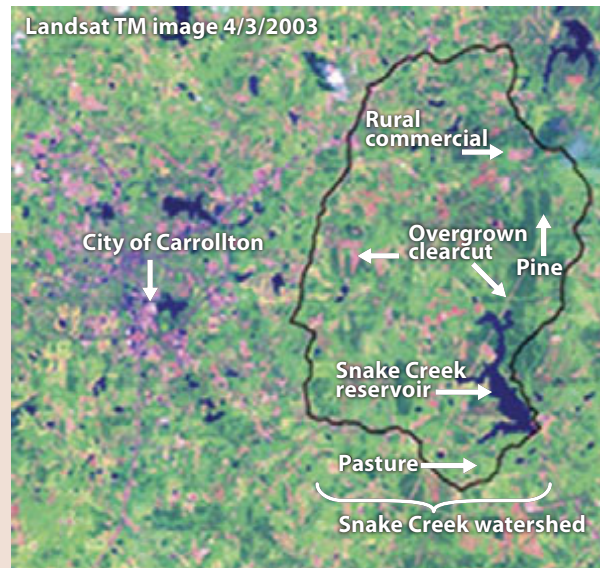


Figure 2. Landsat TM image of the Snake Creek watershed.

Applying the Imagery

Soil loss susceptibility was modeled using the Revised Universal Soil Loss Equation (RUSLE), which is based on a set of parameters that includes soil classification (taken from the digitized Soil Survey for Carroll and Haralson Counties), slope angle and slope length (generated from USGS Digital Elevation Models using ARCInfo), rainfall, and land cover. The only parameter that had no recent data available was land cover; a new land cover map (Figure 3) was interpreted from recent Landsat TM imagery. The RUSLE modeling produced a map of Predicted Annual Soil Loss in tons per acre per year (Figure 4).

CCWA used the results to identify specific areas with high potential erosion rates that will potentially deliver sediment to the reservoir; these areas are targeted for restoration, remediation, or restrictions on further development. High-risk activities adjacent to the reservoir include new subdivision construction sites, rural commercial operations, forestry operations, four-wheeler and off-road vehicle trails,

and power line rights-of-way. Any activity that disturbs the land cover without installing conservation measures can increase the rate of erosion.

Factors that CANNOT be controlled:

- ◇ Rainfall
- ◇ Soil characteristics
- ◇ Slope angle and length

Factors that CAN be controlled:

- ◇ Type of land cover
- ◇ Conservation practices

Figure 3. Land cover map in the Snake Creek watershed.

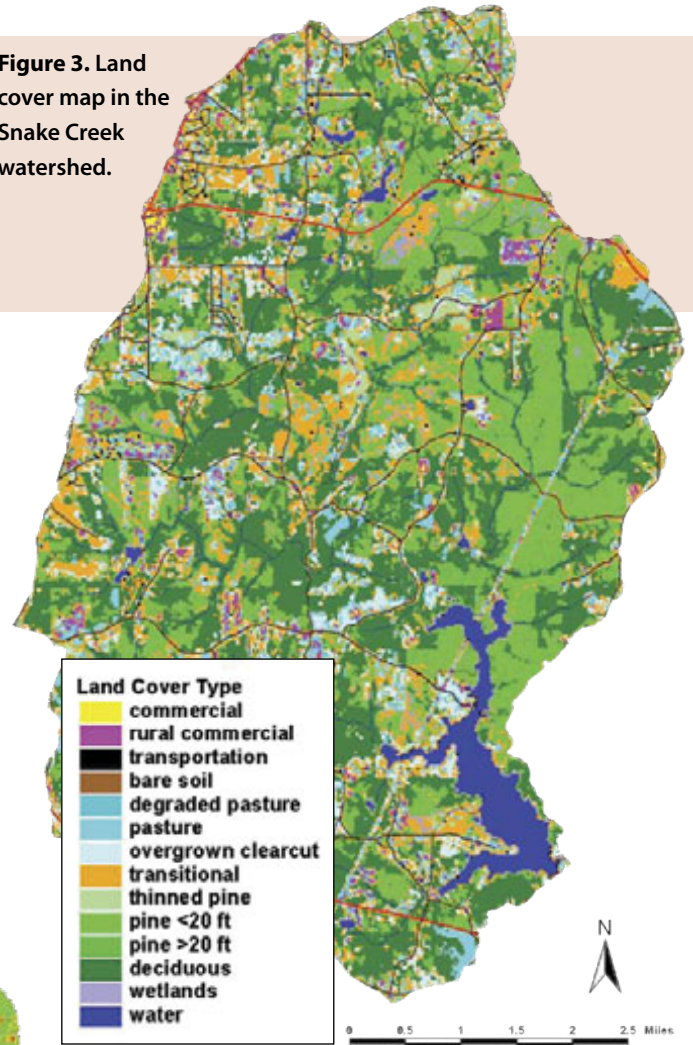
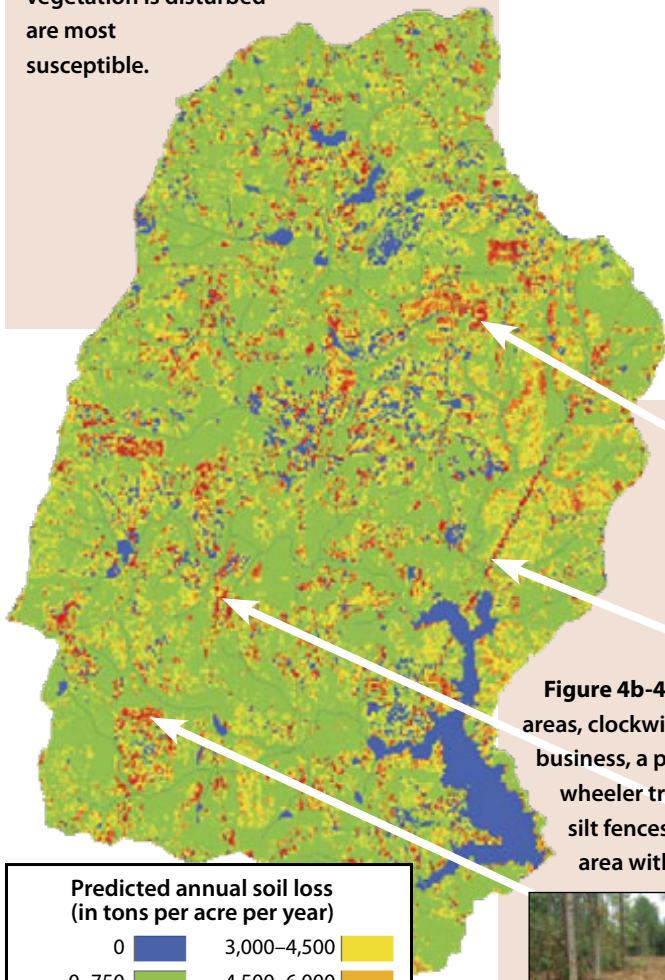


Figure 4a. Erosion-prone areas in the Snake Creek watershed. Areas where vegetation is disturbed are most susceptible.



Predicted annual soil loss (in tons per acre per year)	
0	3,000–4,500
0–750	4,500–6,000
750–1,500	6,000–9,000
1,500–2,200	9,000–17,000
2,200–3,000	>17,000

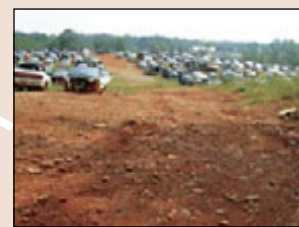


Figure 4b-4e. Examples of erosion prone areas, clockwise from top: an auto salvage business, a power line clearing with four-wheeler tracks, a subdivision with failing silt fences, a selectively-harvested timber area with access roads.





Remote Sensing Enables Mapping of Understory Invasive Plants

Songlin Fei (Purdue University) and Michael Shouse (University of Kentucky)

Defining the Problem

Invasions of exotic species are a significant ecological and economic problem. The health and longevity of many of our ecosystems are at risk due to significant invasion by exotic plants. Bush honeysuckle (*Lonicera maackii*), an invasive shrub species, has a significant impact on many important ecosystems by forming dense patches with thick canopies that choke off native species (Figure 1). Not only does it eliminate native species, but it also alters nutrient cycling and degrades the habitat for wildlife. Our ability to prevent and/or mitigate the invasion of exotic species is in part hindered by the lack of precise spatial information about the forest ecosystems that are challenged by this invasive species. Remote sensing addresses this challenge by providing detailed spatial distribution of invasive species across a large geographic extent.



Figure 1. A monocultural *L.maackii* system.

Selecting the Imagery

Bush honeysuckle is a deciduous understory species that cannot be remotely sensed during the overstory leaf-on season. However, bush honeysuckle begins its growing season before native vegetation leaf bud and continues to produce chlorophyll after native vegetation leaf fall. This characteristic is a key trait that enables it to be invasive, but also provides an opportunity for it to be remotely sensed during the beginning or end of leaf-on conditions of the native plants. High-resolution aerial photography is an ideal candidate because it not only provides rapid turnaround with flexible collection times for bush honeysuckle mapping, but also allows identification of detailed features such as distribution patterns that are important for invasive species management (Figure 2).





Figure 2. Mapping *L. maackii* with high resolution aerial photos: (a) overview of Cherokee park with *L. maackii* classification; (b) aerial photo shows extensive *L. maackii* distribution; (c) aerial photo shows limited *L. maackii* ; (d) photo of understory with *L. maackii*; (e) photo of understory *L. maackii* removal

Applying the Imagery

Traditional, standard per-pixel classifiers for remote sensing imagery have proven ineffective for extracting information from imagery having high spatial resolution. Recently developed, feature-based classification programs are especially well-suited for use with high-resolution imagery. Feature-based classification uses multiple spatial attributes (size, shape, texture, pattern, spatial association and shadow) as well as spectral information to identify geospatial features. These programs can also be trained by users to fine-tune the classification process based on initial error analysis of the results. As shown in Figure 2, this project successfully classified the distribution of bush honeysuckle using 0.3 meter resolution aerial photos in Cherokee Park, Louisville, Kentucky. Mapping accuracy is over 90 percent and has been used to guide Louisville Metro Parks in removing bush honeysuckle.

Mapping understory invasive plant species is proven to be feasible and effective with high-resolution aerial photography. The imagery needs to be acquired during a time window when invasive species are leaf-on and native species are leaf-off. Feature-based classification methods should be used to improve mapping accuracy and results in information to enable targeted remediation efforts for restoring ecosystem balance.



Remote Sensing Helps Protect Hemlock in an Invasion Crisis

Songlin Fei and Ningning Kong (Purdue University)

Defining the Problem

Eastern hemlock (*Tsuga canadensis*) is an ecologically important tree species in the eastern United States. The invasion of the exotic insect hemlock woolly adelgid (HWA, *Adelges tsugae*), can cause high mortality of eastern hemlock. The loss of hemlock can degrade stream quality, reduce aquatic invertebrate and vertebrate biodiversity, change vegetation composition and structure, and affect wildlife. HWA was first discovered in Kentucky in March 2006, and infestations have been steadily expanding since then. In spite of the ecological importance of eastern hemlock, little is known about its fine-scale distribution in Kentucky. In order to understand the extent of our eastern hemlock resources and the extent to which the invasive HWA will affect these resources, maps must be produced that accurately show areas of hemlock cover. Remote sensing helps because it provides detailed mapping of hemlock in a large geographic area that is time and cost efficient.



Healthy eastern hemlock

Selecting the Imagery

To ensure complete coverage we took advantage of the large scenes offered by the mid-resolution Landsat 7 Enhanced Thematic Mapper Plus (ETM+) satellite imagery. Six Landsat 7 ETM+ satellite images (three winter images and three summer images), covering three geographic sections of eastern Kentucky (Figure 1), were obtained. In the winter images, deciduous foliage was not present to interfere with the vegetative near infrared and red reflectance characteristics. The summer images offer good spectral information for forest classification and have less terrain slope-aspect effect due to a higher sun angle compared to the winter image.

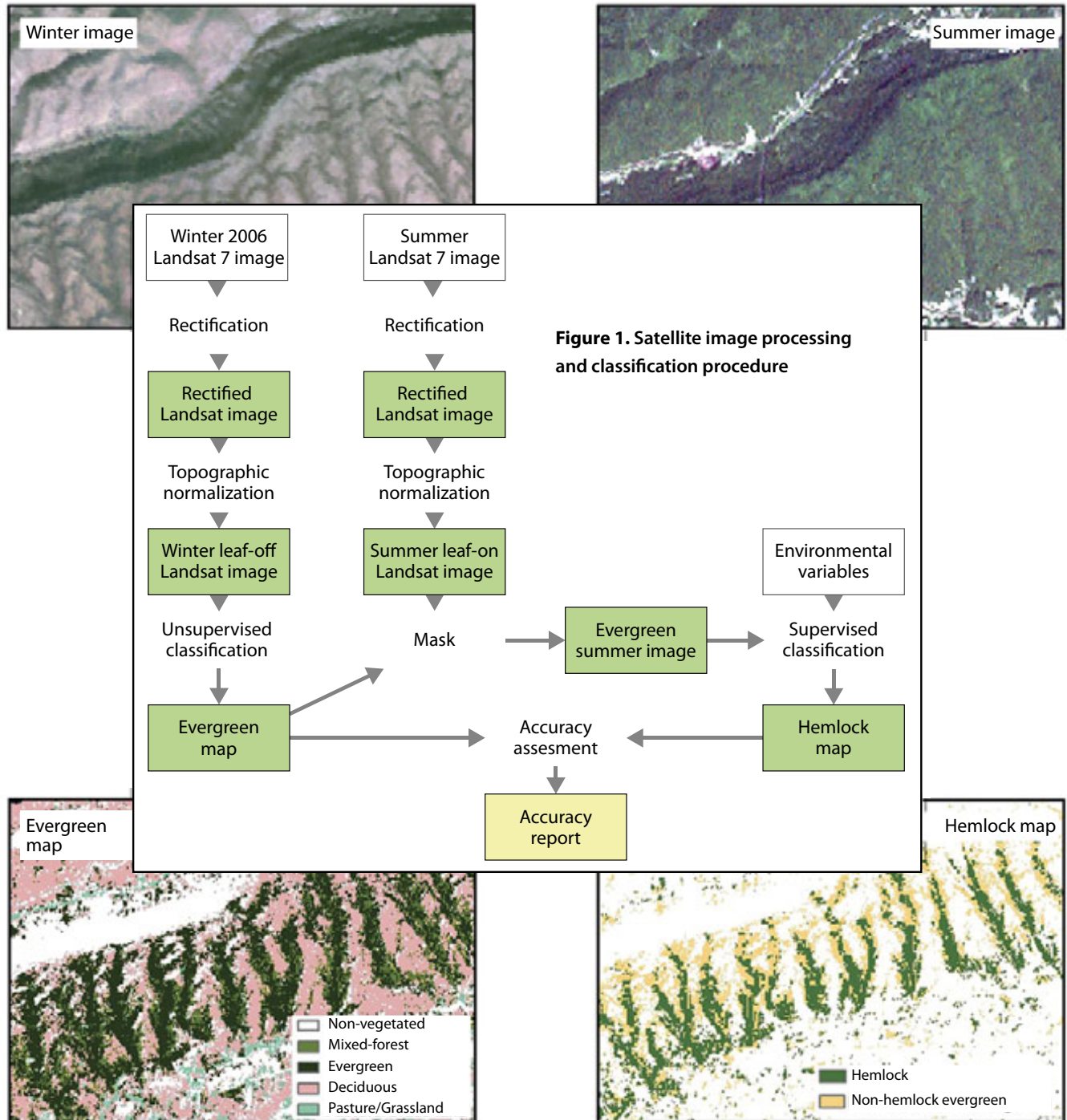
Applying the Imagery

The image processing and classification steps that made it possible to distinguish evergreen forest areas from other land types are shown in Figure 2. First, geometric correction and topographic normalization were applied on the winter and summer images. Images were corrected to align with true geographic points. Topographic normalization was performed using the C-correction method to reduce the variance of sun incidence angles (i.e., the angle between sun beam and earth surface varies with different topographic relief). The evergreen forest areas were separated from the other land types using winter images in a three step process. First, a normalized difference vegetation index (NDVI) was generated to identify areas with green vegetation ($NDVI > 0$), and then a supervised classification was applied on these areas to distinguish evergreen forest from other land use types such as field or pasture. Lastly, using spectral information (spectral bands 1–5 and 7) from summer images, and a set of environmental explanatory variables such as moisture index and soil type that are possibly associated with hemlock distribution, classification and regression tree (CART) analyses were employed in the evergreen forest areas

to classify the presence or absence of eastern hemlock. Two accuracy assessments were conducted. The first assessment was to evaluate the results from a supervised evergreen classification using the winter image. The second was to evaluate accuracy of the final hemlock map.

Landsat 7 ETM+ satellite imagery, along with a set of environmental variables, successfully mapped the detailed

distribution of eastern hemlock in eastern Kentucky with an accuracy rate near 80 percent. Satellite imagery provides a quick, cost-efficient, accurate way to map in detail the distribution of eastern hemlock, resulting in maps that assist natural resource agencies in managing this threatened species by making it possible to identify patterns of hemlock spread. Certain patterns can point to areas that should be targeted for treatment.





Remote Sensing Enables Space Shuttle Columbia Recovery

Paul R. Blackwell (Stephen F. Austin State University)



Figure 1. Pieces of the Space Shuttle *Columbia* land in the streets of Nacogdoches, Texas on February 1, 2003.

Defining the Problem

When the Space Shuttle *Columbia* exploded over East Texas on February 1, 2003, researchers at Stephen F. Austin State University (SFA) in Nacogdoches, Texas, responded along with hundreds of volunteers from across Texas and the nation. Initially, recovery of the remains of the astronauts was the priority. Later, the focus shifted to collecting as much of the lost shuttle as possible (Figure 1) to aid investigation and prevent any possibility of another catastrophe of this nature. Satellite imagery was a critical tool throughout the recovery effort.

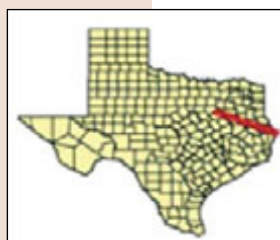


Figure 2. The first map produced by SFA personnel for the recovery effort was this Nacogdoches County locator map based on Landsat 7 ETM+ data.

Selecting the Imagery

As in any emergency response scenario, satellite imagery was selected for the *Columbia* recovery effort more on a basis of availability than suitability, particularly during the first critical days. In fact, many datasets were utilized over the course of the recovery as availability and needs arose. Early on, Landsat 7 ETM+ data were used to orient searchers and provide background images for status maps (Figure 2). Later, higher-resolution satellite data such as those from the French SPOT program were used, either alone or resolution-merged with other imagery to provide greater detail. Subsequently, a post-event, IKONOS satellite acquisition became available and was used extensively for various phases of the response. In addition, high-resolution orthoimagery, aerial photography geometrically corrected to remove distortions and ensure all distance measurements are consistent, was used throughout the effort.

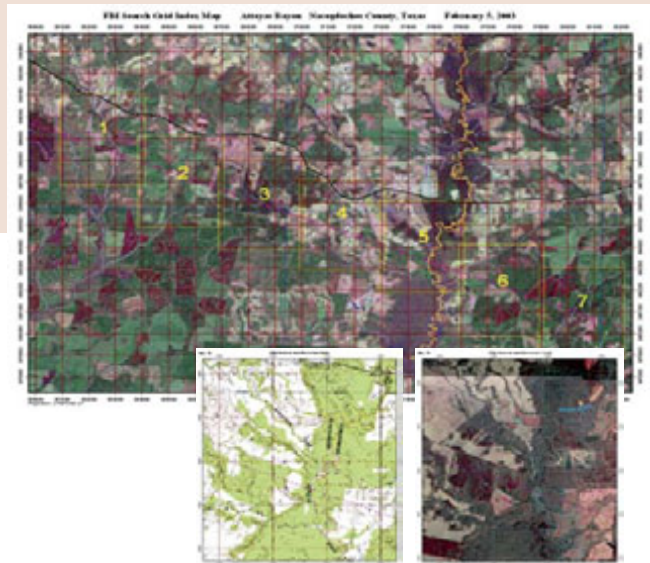
Figure 3. Location of the space shuttle *Columbia* recovery effort in East Texas.



Applying the Imagery

During the course of the response, researchers at Stephen F. Austin State University developed a hierarchy of map products for various groups. Strategic maps were generated to assist in mission planning and assessment. These products were generally small-scale depictions of the overall

Figure 4. Tactical maps such as this set of Search and Rescue (SAR) grid maps were used by various groups during the recovery effort to organize the search operations. Each set consisted of an overview map with accompanying 8 ½" x 11" topographic and image maps for each grid square in the area.



response, or larger-scale representations of specific mission results. Tactical maps were created to assist the search teams with navigation and to establish search patterns. These maps were generally large-scale products showing as much detail as possible and often included overview grid maps to aid in mission organization. Finally, media maps were developed to satisfy the public's intense interest in the effort without revealing specifics that might adversely affect operations. These maps were very small scale and often included obscured data to discourage citizens from visiting sites where the recovery was in progress.

Satellite imagery was used to create all of these products, either as a background for discrete data being displayed or, as in the case of tactical maps (Figures 4 and 5), to provide precise information about the terrain and landforms in the area. Once post-event data became available, analysts began using these data to identify actual debris locations. The IKONOS data collected during the afternoon of February 1, 2003, was used to locate linear patterns of disturbance in the tree canopy (Figure 6). In many cases, these disturbances proved to be caused by large pieces of the shuttle crashing into the forest. Several significant pieces were located and successfully retrieved by this method.

Although satellite imagery is only one aspect of geospatial technology used during the *Columbia* Shuttle recovery, it proved to be an extremely important one, playing a role in strategic, tactical and media mapping. Satellite imagery provided an indication of conditions searchers would face in the field, a backdrop for planning search missions and plotting results, a navigation aid for making way through heavily wooded areas, a reporting tool for satisfying media curiosity and, finally, a direct indication of the locations of large pieces of *Columbia*. The space shuttle *Columbia* recovery was the largest forensic search and rescue effort in history, and satellite imagery was a vital part of it.

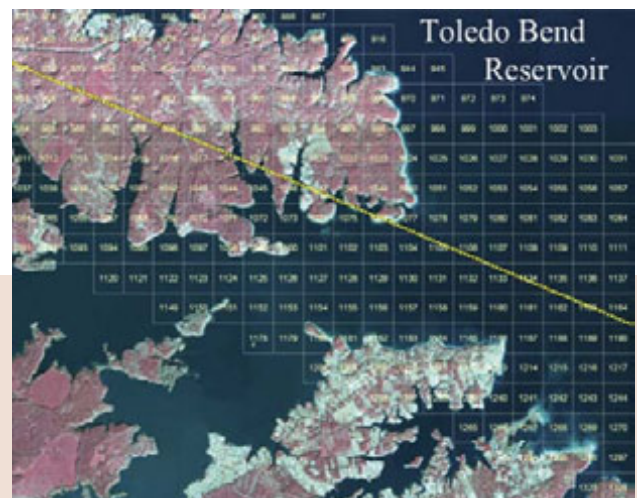


Figure 5. This map is based on high-resolution satellite imagery and was used by the U.S. Navy to delineate search areas over Toledo Bend reservoir. Although fishermen reported seeing debris land in the water, no debris was recovered from the lake, despite an intense effort by Navy divers.

Figure 6. Post event IKONOS satellite imagery was used to identify tree crown damage from large pieces of the shuttle. Here the arrows point to locations where pieces were recovered using this method.



Image Credits

Cover:

Image courtesy of U.S./Japan ASTER Science Team

About the Authors:

Courtesy of Kevin Czajkowski, Teresa Benko, and Timothy Ault

Preface:

Preface page 1: top: Courtesy of Bradley C. Rundquist and Paul Todhunter; bottom: Courtesy of Demetrio P. Zourarakis

Preface page 2: right top and bottom: Courtesy of Brian Lee, Corey Wilson, and Angela Schorgendorfer; middle: Courtesy of Sam Batzli

What is Remote Sensing:

First image: NASA Earth Sciences and Image Analysis Laboratory at Johnson Space Center

Figure 1. U.S. Army

Figure 2, 3. Courtesy of NASA

Figure 4. AGI/Kathleen Cantner

Figure 5. Russell G. Congalton, AGI/Kathleen Cantner

Figure 6 - 16. Rebecca L. Dodge

Figure 17a. and 17b. ©Michael Collier /ESW Image Bank

Figure 18. Jesse Allen, GSFC Visualization Analysis Lab

Figure 19. Robert Simmon, NASA

Figure 20-21. Jesse Allen, Earth Observatory

Figure 22. Goddard Space Flight Center Scientific Visualization Studio

Figure 23a,b. NASA Goddard Space Flight Center

Figure 23c. Shutterstock 13054297: ©Shutterstock.com/ Beth Schroeder

Figure 24. CRUSH Project, NASA Ames Research Center

Figure 25. NASA

Figure 26a. NASA Landsat Program, The Global Land Cover Facility, University of Maryland, College Park

Figure 26b,c. NASA MODIS, The Global Land Cover Facility, University of Maryland, College Park

Figure 27. NASA

Figure 28. Lonnie Thompson, From the Glacier Photograph Collection. Boulder, Colorado USA: National Snow and Ice Data Center/World Data Center for Glaciology. Digital media

Figure 29a. NASA/GSFC/MITI/ERSDAC/JAROS, and U.S./Japan ASTER Science Team

Figure 29b. Georg Kaser, Archiv des Institutes fuer Geographie der Universitaet Innsbruck

Figure 30a. NASA/GSFC/METI/ERSDAC/JAROS

Figure 30b. Jon Hall

Figure 30c. ©iStockphoto.com/ DavidParsons

Figure 31. NASA Earth Sciences and Image Analysis Laboratory at Johnson Space Center

Figure 32. NASA

Figure 33. U.S. Forest Service

Figure 34. NASA MODIS Rapid Response Team

Figure 35. NASA/GSFC/MITI/ERSDAC/JAROS

Figure 36a. NASA Earth Sciences and Image Analysis Laboratory at Johnson Space Center

Figure 36b. NASA Landsat Program

Figure 37. Great Basin Unified Air Pollution Control District

Case Studies start image: ©Michael Collier/ESW Image Bank

Assessing Hurricane Damage:

Corner: Hurricane Isabel: NASA

Figure 1, 2. USGS

Figure 3. Jesse Allen, Earth Observatory

Emergency Management Response to Tornadoes:

Corner: ©Digital Vision

Figure 1, 3, 4. Courtesy of Sam Batzli

Figure 2. NOAA/Civil Air Patrol.

Forest Ice Storm Damage Detection:

Corner: Shutterstock 27580906: ©Shutterstock.com/Allen Lee Lake

Bottom left: ©Digital Vision

Figure 1, 2, 3, 4. Courtesy of Christine E. Emrich and Jeffrey L. Lewis

Figure 1, 2, 3, 4. Courtesy of Christine E. Emrich and Jeffrey L. Lewis

Figure 1, 2, 3, 4. Courtesy of Christine E. Emrich and Jeffrey L. Lewis

Hail Damage to Crops:

Corner: Shutterstock 108218576: ©Shutterstock.com/Roger Wissmann

Figure 1. Shutterstock 125898779: ©Shutterstock.com/Sunny Forest

Figure 2. Courtesy of Cheryl Reese, Mary O'Neill, Pavara Thanapura, and Ryan Patterson

Hazards at Anatahan Volcano, Northern Mariana Islands:

Corner: AGI/Meteor Studios

Figure 1. NASA

Figure 2. NASA MODIS Rapid Response Team

Figure 3, 4. Jesse Allen, Earth Observatory

Lava Flow Hazard Assessment:

Figure 1, 2, 3. Courtesy of Robert Wright

Vertical Coastline Displacements Caused by Earthquakes:

Corner: Shutterstock 99748898: ©Shutterstock.com/PhotoRoman

Figure 1, 2, 3, 4, 5, 6, 7, 8. Courtesy of Demetrio P. Zourarakis

Figure 1, 2, 3, 4, 5, 6, 7, 8. Courtesy of Demetrio P. Zourarakis

Figure 1. Robert Simmon, NASA

Figure 2. Brian Williams/USGS

Figure 3. Jesse Allen, Earth Observatory

Figure 4. Robert Foster, Reef Check

Figure 5. Landsat.org, Global Observatory for Ecosystem Services, Michigan State University

Facing – top right corner: Shutterstock 50038966: © Shutterstock.com/leolintang

Figure 1, 2, 3, 4. Courtesy of Kevin Czajkowski, Teresa Benko, and Timothy Ault

Figure 1, 2, 3, 4. Courtesy of Kevin Czajkowski, Teresa Benko, and Timothy Ault

Figure 1, 2, 3, 4. Courtesy of Kevin Czajkowski, Teresa Benko, and Timothy Ault

Figure 1, 2, 3, 4. Courtesy of Kevin Czajkowski, Teresa Benko, and Timothy Ault

Figure 1, 2, 3, 4. Courtesy of Kevin Czajkowski, Teresa Benko, and Timothy Ault

Figure 1, 2, 3, 4. Courtesy of Kevin Czajkowski, Teresa Benko, and Timothy Ault

Figure 1, 2, 3, 4. Courtesy of Kevin Czajkowski, Teresa Benko, and Timothy Ault

Figure 1, 2, 3, 4. Courtesy of Kevin Czajkowski, Teresa Benko, and Timothy Ault

Figure 1, 2, 3, 4. Courtesy of Kevin Czajkowski, Teresa Benko, and Timothy Ault

Figure 1, 2, 3, 4. Courtesy of Kevin Czajkowski, Teresa Benko, and Timothy Ault

Figure 1, 2, 3, 4. Courtesy of Kevin Czajkowski, Teresa Benko, and Timothy Ault

Figure 1, 2, 3, 4. Courtesy of Kevin Czajkowski, Teresa Benko, and Timothy Ault

Figure 1, 2, 3, 4. Courtesy of Kevin Czajkowski, Teresa Benko, and Timothy Ault

Figure 1, 2, 3, 4. Courtesy of Kevin Czajkowski, Teresa Benko, and Timothy Ault

Figure 1, 2, 3, 4. Courtesy of Kevin Czajkowski, Teresa Benko, and Timothy Ault

Figure 1, 2, 3, 4. Courtesy of Kevin Czajkowski, Teresa Benko, and Timothy Ault

Figure 1, 2, 3, 4. Courtesy of Kevin Czajkowski, Teresa Benko, and Timothy Ault

Figure 1, 2, 3, 4. Courtesy of Kevin Czajkowski, Teresa Benko, and Timothy Ault

Figure 1, 2, 3, 4. Courtesy of Kevin Czajkowski, Teresa Benko, and Timothy Ault

Figure 1, 2, 3, 4. Courtesy of Kevin Czajkowski, Teresa Benko, and Timothy Ault

Figure 1, 2, 3, 4. Courtesy of Kevin Czajkowski, Teresa Benko, and Timothy Ault

Figure 1, 2, 3, 4. Courtesy of Kevin Czajkowski, Teresa Benko, and Timothy Ault

Figure 1, 2, 3, 4. Courtesy of Kevin Czajkowski, Teresa Benko, and Timothy Ault

Figure 1, 2, 3, 4. Courtesy of Kevin Czajkowski, Teresa Benko, and Timothy Ault

Figure 1, 2, 3, 4. Courtesy of Kevin Czajkowski, Teresa Benko, and Timothy Ault

Figure 1, 2, 3, 4. Courtesy of Kevin Czajkowski, Teresa Benko, and Timothy Ault

Figure 1, 2, 3, 4. Courtesy of Kevin Czajkowski, Teresa Benko, and Timothy Ault

Figure 1, 2, 3, 4. Courtesy of Kevin Czajkowski, Teresa Benko, and Timothy Ault

Figure 1, 2, 3, 4. Courtesy of Kevin Czajkowski, Teresa Benko, and Timothy Ault

Figure 1, 2, 3, 4. Courtesy of Kevin Czajkowski, Teresa Benko, and Timothy Ault

Figure 1, 2, 3, 4. Courtesy of Kevin Czajkowski, Teresa Benko, and Timothy Ault

Figure 1, 2, 3, 4. Courtesy of Kevin Czajkowski, Teresa Benko, and Timothy Ault

Figure 1, 2, 3, 4. Courtesy of Kevin Czajkowski, Teresa Benko, and Timothy Ault

Figure 1, 2, 3, 4. Courtesy of Kevin Czajkowski, Teresa Benko, and Timothy Ault

Figure 1, 2, 3, 4. Courtesy of Kevin Czajkowski, Teresa Benko, and Timothy Ault

Figure 1, 2, 3, 4. Courtesy of Kevin Czajkowski, Teresa Benko, and Timothy Ault

Figure 1, 2, 3, 4. Courtesy of Kevin Czajkowski, Teresa Benko, and Timothy Ault

Figure 1, 2, 3, 4. Courtesy of Kevin Czajkowski, Teresa Benko, and Timothy Ault

Figure 1, 2, 3, 4. Courtesy of Kevin Czajkowski, Teresa Benko, and Timothy Ault

Figure 1, 2, 3, 4. Courtesy of Kevin Czajkowski, Teresa Benko, and Timothy Ault

Figure 1, 2, 3, 4. Courtesy of Kevin Czajkowski, Teresa Benko, and Timothy Ault

Figure 1, 2, 3, 4. Courtesy of Kevin Czajkowski, Teresa Benko, and Timothy Ault

Figure 1, 2, 3, 4. Courtesy of Kevin Czajkowski, Teresa Benko, and Timothy Ault

Figure 1, 2, 3, 4. Courtesy of Kevin Czajkowski, Teresa Benko, and Timothy Ault

Figure 1, 2, 3, 4. Courtesy of Kevin Czajkowski, Teresa Benko, and Timothy Ault

Figure 1, 2, 3, 4. Courtesy of Kevin Czajkowski, Teresa Benko, and Timothy Ault

Figure 1, 2, 3, 4. Courtesy of Kevin Czajkowski, Teresa Benko, and Timothy Ault

Figure 1, 2, 3, 4. Courtesy of Kevin Czajkowski, Teresa Benko, and Timothy Ault

Figure 1, 2, 3, 4. Courtesy of Kevin Czajkowski, Teresa Benko, and Timothy Ault

Figure 1, 2, 3, 4. Courtesy of Kevin Czajkowski, Teresa Benko, and Timothy Ault

Figure 1, 2, 3, 4. Courtesy of Kevin Czajkowski, Teresa Benko, and Timothy Ault

Figure 1, 2, 3, 4. Courtesy of Kevin Czajkowski, Teresa Benko, and Timothy Ault

Figure 1, 2, 3, 4. Courtesy of Kevin Czajkowski, Teresa Benko, and Timothy Ault

Figure 1, 2, 3, 4. Courtesy of Kevin Czajkowski, Teresa Benko, and Timothy Ault

Figure 1, 2, 3, 4. Courtesy of Kevin Czajkowski, Teresa Benko, and Timothy Ault

Figure 1, 2, 3, 4. Courtesy of Kevin Czajkowski, Teresa Benko, and Timothy Ault

Figure 1, 2, 3, 4. Courtesy of Kevin Czajkowski, Teresa Benko, and Timothy Ault

Figure 1, 2, 3, 4. Courtesy of Kevin Czajkowski, Teresa Benko, and Timothy Ault

Figure 1, 2, 3, 4. Courtesy of Kevin Czajkowski, Teresa Benko, and Timothy Ault

Figure 1, 2, 3, 4. Courtesy of Kevin Czajkowski, Teresa Benko, and Timothy Ault

Figure 1, 2, 3, 4. Courtesy of Kevin Czajkowski, Teresa Benko, and Timothy Ault

Figure 1, 2, 3, 4. Courtesy of Kevin Czajkowski, Teresa Benko, and Timothy Ault

Figure 1, 2, 3, 4. Courtesy of Kevin Czajkowski, Teresa Benko, and Timothy Ault

Whitebark Pine, Bark Beetles and Climate Variability:

Corner: ©iStockphoto.com/ DavidParsons

Figure 1, 2. Courtesy of Rick L. Lawrence and Jeffrey Jewett

Impacts of Climate Variability on Reservoirs:

Corner: iStockphoto #21819640: ©iStockphoto.com/Phil Augustavo

Figure 1. USGS Scientific Investigations Report 2005-5040

Figure 2, 3. Courtesy James Merchant and Milda R. Vaitkus

Flooding at Devils Lake, North Dakota:

Corner: Shutterstock 81290551: ©Shutterstock.com/MBoe

Figure 1, 2, 3. Courtesy of Bradley C. Rundquist and Paul Todhunter

Co-Produced Water from Natural Gas Extraction:

Corner: Shutterstock 90471127: ©Shutterstock.com/SW_Stock

Figure 1, 2, 3, 4. Courtesy of Ramesh Sivapillai and Scott N. Miller

Soil Loss Susceptibility:

Corner: Shutterstock 11060740: ©Shutterstock.com/Mark Winfrey

Figure 1, 2, 3, 4. Courtesy of Jackie Reed, John Congleton, and Rebecca L. Dodge

Mapping of Understory Invasive Plants:

Corner: Lonicera maackii.jpg: © Matthieu Sontag, License CC-BY-SA, Creative Commons Attribution-Share Alike 3.0 Unported

Figure 1, 2. Courtesy of Songlin Fei and Michael Shouse

Bottom: Shutterstock 37132024: ©Shutterstock.com/Melinda Fawver

Protect Hemlock in an Invasion Crisis:

Corner: Shutterstock 6236737: ©Shutterstock.com/Autumn's Memories

Bottom left: Shutterstock 2608478: ©Shutterstock.com/Andrew Williams

Figure 1 diagram: Courtesy of Songlin Fei and Ningning Kong

Space Shuttle Columbia Recovery:

Corner: NASA

Figure 1, 2, 3, 4, 5, 6. Courtesy of Paul R. Blackwell

Back Cover:

Jacques Desclotres, MODIS Rapid Response Team, NASA/GSFC



American Geosciences Institute
4220 King Street, Alexandria, VA 22302, U.S.A.
(703) 379-2480, www.agiweb.org

The American Geosciences Institute is a nonprofit federation of geoscientific and professional associations that represents more than 250,000 geologists, geophysicists, and other earth scientists. Founded in 1948, AGI provides information services to geoscientists, serves as a voice of shared interests in our profession, plays a major role in strengthening geoscience education, and strives to increase public awareness of the vital role the geosciences play in society's use of resources, resilience to natural hazards, and the health of the environment.

